A Theoretical Study of Brownian Motors with Self-Induced Temperature Gradients

Jack Devine

University of Otago
Physics Department

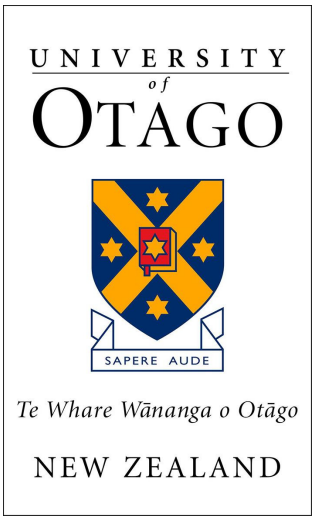

Submitted in partial fulfillment of the requirements for the degree of Master's in Physics at the University of Otago

Supervised by M. W. Jack

Abstract

Brownian motors surmount energy barriers by absorbing and emitting heat to and from their local environment. In most theoretical treatments, the temperature gradients created in these heat exchanges are assumed to dissipate instantaneously. Here we relax this assumption to consider the case where Brownian dynamics can lead to self-induced temperature gradients in the local environment. We explore self-induced temperature gradients by considering an explicit equation of motion for the local temperature field. The equation of motion for the temperature contains a heat source term arising from the Brownian dynamics of the motor. In the same way that externally-imposed temperature gradients can cause directed motion, these self-induced gradients effect the Brownian dynamics of the system. The result is a two-way coupling between the local environment and the Brownian motor. We explore the resulting dynamics and thermodynamics of these novel coupled systems both in the steady state and in the dynamical state. We develop two numerical methods for solving the resulting equations of motion, both methods exploit the physical structure of our model. We check that our numerical methods converge to an analytical solution when available. We also check that the numerical methods converge as the discretization size is reduced. We consider self-induced temperature gradients on potentials that are relevant to Brownian motors. In particular, we show that self-induced temperature gradients can reduce barrier crossing rates in both one and two dimensions. We also implement heat engines and heat pumps based on temperature gradients induced by a Brownian motor on a non-equilibrium potential.

Acknowledgements

I would like acknowledge the kindness and support of the following people:

- My supervisor, Michael Jack, who was always available to answer any of my questions. Michael Jack always pointed me in the right direction as I explored the uncharted territory of self-induced temperature gradients.

- Lucy Patterson, I love you.

Contents

Chapter 1

Introduction

At the macroscopic scale, devices such as heat engines and refrigerators convert energy between different forms. For example, heat engines convert the heat from temperature gradients into work, while refrigerators perform the opposite task. In the 19th century, a thorough understanding of the physical nature of these energy conversion devices led to the industrial revolution. Since the 1960s, futurists have speculated that a "nano revolution" is on the horizon [1]. Manufacturing energy conversion devices at the nanoscale will be a crucial part of the upcoming nano revolution. One logical way to progress the nano revolution is to mimic biological energy conversion devices that have existed in nature for millions of years [2]. Biomolecular motors [3] are a very important class of biological nanoscale devices. One example of a biomolecular motor is a kinesin motor [4]. Kinesin consumes chemical energy in order to transport cargo along filaments in biological cells. The kinesin transports its cargo by walking along the filaments in a "hand over hand" fashion [4]. Another example of a biomolecular motor is ATP synthase [5], located in the mitochondria of cells. Sometimes described as the powerhouse of the cell, ATP synthase uses an electrochemical potential across a membrane to create ATP and vice versa. Researchers are now beginning to synthesize artificial motors at the nanoscale [6]. Some artificial motors convert heat into work against a force [7], while others convert chemical energy into work [6,8]. Examples of artificial devices converting heat into work at the nanoscale include the work of Martinez et al. [9], who implemented a Brownian Carnot engine. On the other hand, Pedro et al. [10] implemented a microscopic steam engine that manipulates a colloidal particle with optical tweezers. Blickle et al. [11], implement a stochastic Stirling cycle. A review of these colloidal heat engines is given in Ref. [7].

Systems at the nanoscale are subject to different laws of motion than macroscopic systems. In particular, at the nanoscale, viscosity dominates inertia and systems are subjected to large thermal fluctuations [3]. One intriguing aspect of nanoscale systems is that they can undergo directed motion while being subjected to a thermal noise that is much larger than the energy available for driving the system. In the case of macroscopic devices, thermal noise is negligible compared to the energy available for driving the system. To put things into perspective, a kinesin motor consumes chemical energy at a rate of 10^{-17}W while thermal noise with a power of 10^{-8}W constantly bombards the motor [12]. In spite of huge thermal fluctuations, kinesin

motors are able to transport cargo in a very efficient manner. Because systems at the nanoscale are subjected to large thermal fluctuations, they are best described as Brownian motion on free energy potentials [13].

This thesis will focus on a particular class of Brownian systems called Brownian motors. For the purpose of the thesis, Brownian motors will be defined as energy converting devices with degrees of freedom that evolve via Brownian motion. The concept of a Brownian motor has had widespread application as a model for biomolecular motors [2–5, 12, 14–20] as well as artificial nanodevices [6,8,10,11,21,22]. The underlying physics of Brownian motors is frequently used as a theoretical tool for understanding how thermodynamics manifests at the nanoscale [23–35]. As with energy conversion devices at the macroscopic scale, the efficiency of a Brownian motor can be quantified mathematically and probed experimentally. Researchers have found that the efficiency characteristics of Brownian motors are quite different to the efficiency characteristics of macroscopic motors [2,3,36]. Just like the evolution of a Brownian motor, the efficiency of a Brownian motor is a stochastic property [36]. In some cases, the efficiency of a Brownian motor can exceed Carnot efficiency for a small number of non equilibrium cycles of the Brownian motor [9].

In this chapter, we will describe a small portion of the vast literature written on Brownian motors. In Sec. 1.1, we will describe some of the already established classes of Brownian motors. Throughout the thesis, we will refer back to the Brownian motors described in Sec. 1.1 to compare the previous results to our own findings. In Sec. 1.2, we will describe some of the techniques that are used to model Brownian motors. In Sec. 1.3, we will use the techniques from Sec. 1.2 to describe the thermodynamics of Brownian motors.

1.1 Classes of Brownian Motors

Here we will list three classes of Brownian motor that are relevant to this thesis. The list is not exhaustive, for a more complete list, we suggest the review [13] and the book [37].

1.1.1 Büttiker-Landauer heat engines

The Büttiker-Landauer heat engine is a Brownian motor that was first described by Büttiker in Ref. [28] and described again by van Kampen in Ref. [29]. Later, Landauer [38] clarified the physical mechanism for the directed motion present in the motor. All three authors discussed the motor as a Brownian particle placed on a nonuniform potential with a nonuniform temperature. To see how a Büttiker-Landauer heat engine works, consider a Brownian particle on a periodic potential with an externally applied periodic temperature as shown in Fig. 1.1. From now on we will refer to the minima of the potential as “wells” and the maxima as “barriers”. For each of the barriers in the potential, the right hand side of the barrier is hotter than the left side. Brownian particles flow out of hot regions more quickly than they do for cold regions, causing a larger flow of Brownian particles to the left than to the right. At a high enough temperature difference we continue to see this net current even against an externally imposed

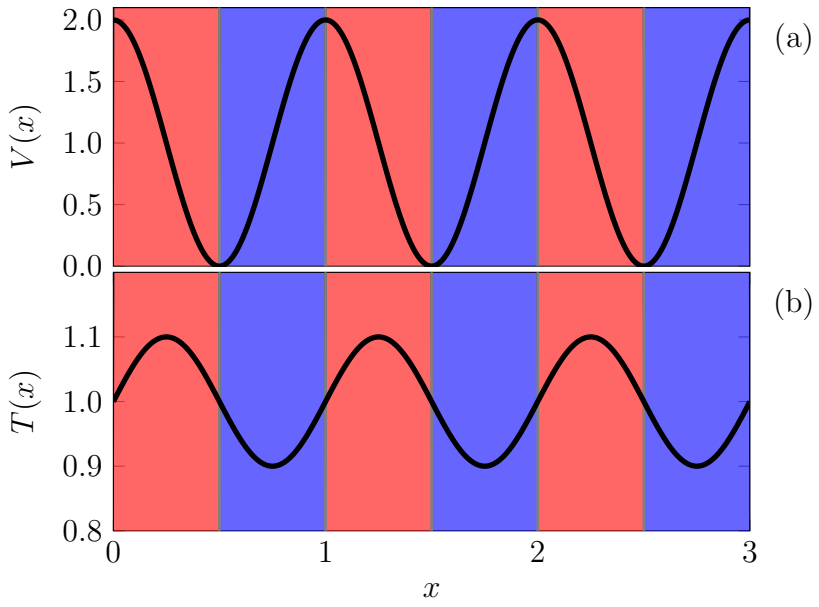

Figure 1.1: Büttiker-Landauer engine. (a) The potential ($V(x)$) that the Brownian system is placed on. (b) The temperature ($T(x)$) of the environment of the Brownian system. The regions are shaded according to whether they are hot or cold. Red indicates that the region is hot, while blue indicate that the region is cold. Particles will be agitated out of the hot regions much more frequently than they will from the cold regions, therefore, in this particular situation, we expect to see a net current to the right.

force. In this case, the system is acting as a heat engine.

Recently, heat engines and heat pumps at the microscopic scale have been considered theoretically [34, 39–44] and a Brownian Carnot engine has been realized experimentally [9] as well as a Brownian Stirling engine [10]. A recent review of colloidal heat engines, focusing on experimental realizations, is given in Ref. [7]. Furthermore, in [34], the authors consider the Büttiker-Landauer heat engine running in reverse. In doing so, they realize a refrigerator system that uses the work done on a Brownian system to make heat flow from a cold bath to a hot bath at the nanoscale. In Chap. 4, we will discuss Brownian heat engines/pumps while considering the effect that the generated heat has on the temperature of the local environment.

1.1.2 Isothermal motors

Iosthermal motors are motors that have a constant temperature. The system cannot draw heat from temperature gradients in the fashion of a Büttiker-Landauer motor, because the temperature is not changing in space or time. Therefore, isothermal motors require a net force in order to achieve directed motion. The nature of the external force varies depending on the physical nature of the system. For a Brownian particle diffusing through space, the force could be an electric or a gravitational field. An example was explored by [20] and [45] where the authors placed a Brownian particle on a corrugated surface that was then tilted. In the case of molecular motors, directed motion is achieved by converting energy from one degree of freedom to another on a tilted two dimensional landscape.

Molecular motors

The term "molecular motor" is usually reserved for biological Brownian motors [46]. In particular, molecular motors operate under isothermal conditions and convert chemical energy into work [47]. Examples include kinesins/dyneins which walk along tracks [4], or the rotary motor of a bacteria's flagellum [48]. In [49] Magnasco constructs a theoretical model for molecular motors, which was further clarified in [15]. In this theoretical description, the molecular motor is described by a diffusion process on a two dimensional potential. One degree of freedom represents the chemical state of the motor and the other degree of freedom represents the spatial displacement of the motor. Strategic positioning of the barriers on this potential surface can lead to coupling between chemical degrees of freedom and mechanical degrees of freedom. Via this mechanochemical coupling, the molecular motor can use chemical energy to do work. Throughout this thesis, we will model molecular motors on two dimensional potentials. However, there are cases where the potential in question has large valleys and forces the particle to follow a defined path [18, 19]. In these cases, we can simplify the problem by considering a single reaction coordinate that follows the path of the valleys of the potential.

In order to overcome an energy barrier, an isothermal motor must draw heat from its environment. Likewise, when an isothermal motor loses potential energy it will dump the excess energy into the environment as heat. Previous treatments have assumed that the temperature gradients from these thermal exchanges dissipate so quickly that the isothermal assumption is valid [31, 32, 40, 50, 51]. However, in Sec. 1.1.1, we saw that temperature gradients in the environment have an effect on the motion of a Brownian motor. In fact, temperature gradients can cause a Brownian motor to move against an external force. This thesis will ask whether or not the temperature gradients that a Brownian motor induces in its environment have an effect on the behavior of the Brownian motor.

1.1.3 Brownian Motors Utilizing Time Dependent Manipulations

The Brownian motors considered in Secs. 1.1.1 and 1.1.2 evolve in an environment free of time-dependent external manipulations. However, there are many classes of Brownian motors that utilize time-dependent manipulations of either the potential or the temperature. These include theoretical implementations [12, 13, 37] as well as experimental realizations [9, 10, 52]. In particular, [9] lists many experimental setups for colloidal engines that utilize time-dependent manipulations. In general, whether one is changing the potential or the temperature, one has to inject energy into the system in order to achieve a time-dependent protocol. Through time-dependent protocols, Brownian motors can achieve directed motion without the need for a net force acting on them. To illustrate how time-dependent potentials can create directed motion, we consider a two state potential. The "on" state of the potential is a sawtooth wave, while the "off" state of the potential is a flat line. When the potential is in the on state, particles will become trapped at the bottom of the sawtooth wells. When the potential is turned off, the Brownian particles will diffuse freely. If the potential is simply left in either the on state or the

off state, then no directed motion will occur. In order to get directed motion, one has to turn the potential on and off at specially chosen times. To see how we achieve directed motion by alternating between two potentials, imagine a situation where a Brownian particle is trapped in one of the wells of the sawtooth potential. If the potential is turned off for some time, then the Brownian particle may either diffuse to the right or the left. We now turn the potential back on. If the particle diffused to the left, then the most likely event will be that the particle will return to the well that it started in. On the other hand, if the particle had diffused to the right, then when the potential is turned on again, it is far more likely that the Brownian particle will move to the right. If we keep switching the potential on and off, then we will find that the Brownian particle will drift to the right. In [52], Joel et al. used precisely this idea, along with an electric field, to separate out strands of DNA.

Another slightly related time-dependent motor is a motor based on a Maxwell demon [37]. In this setup, there is a demon that knows where the particle is at all times. Using this knowledge, the demon can know precisely when to switch the potential in order to always obtain forward motion. The demon can choose between two periodic potentials with barriers. If a particle approaches a barrier from the left, then the demon will switch the potential to another potential that does not have a barrier at that point. On the other hand, if a particle approaches a barrier from the right, then the demon will do nothing and will wait for the particle to move away to the other barrier. This setup can be superior to the previous setup because the demon guarantees that the motion of the Brownian particle is always in the intended direction. However, finding an adequate demon at the nanoscale can be challenging.

In this thesis, we will not consider Brownian motors that require time-dependent protocols. In particular, all of the potentials that we will consider will not depend on time.

1.2 Modelling Brownian Motion

In principle, the trajectory of a Brownian particle could be predicted in a deterministic way through Newtownian mechanics. To do so, one would need to measure the positions and velocities of the Brownian particle and all of the molecules surrounding the Brownian particle very precisely. With this information, one would be able to simulate the system forward in time for as long as one likes. The number of molecules that one would need to consider is typically on the order of 10^{23}. Simulating the position of the Brownian particle and all of the molecules in its environment is difficult to do with present day computational constraints. Furthermore, the results obtained from such a simulation would only yield information about one particular trajectory of the Brownian particle. The principle observation behind the models of Brownian motion that we will discuss in this thesis was first made by Einstein [53]. Einstein pointed out that the motion of the Brownian particle occurs on a much slower time scale than the time scale for the environment to reach equilibrium. Therefore, the degrees of freedom needed to describe the Brownian particle can be separated from the degrees of freedom of the environment. Below, we will explain two very important descriptions of Brownian motion utilizing the separation of

time scales pointed out by Einstein.

1.2.1 Langevin Equation

The Langevin equation is a stochastic description that can be used to model the motion of a Brownian system. The Langevin equation description considers the interactions between the slow moving Brownian particle degrees of freedom and its environment to be given by a random force and a damping term. In one dimension, the Langevin equation is given by [13]:

$$m\,\ddot{x}(t) + V'[x(t)] = -\gamma\,\dot{x}(t) + \xi(t). \tag{1.1}$$

Where the $x(t)$ is the position of the particle at time t, $\dot{x}(t) \equiv \frac{\mathrm{d}x(t)}{\mathrm{d}t}$ is the velocity of the particle, $\ddot{x}(t) \equiv \frac{\mathrm{d}^2x(t)}{\mathrm{d}t^2}$ is the acceleration of the particle, m is the mass of the particle, $V'(x)$ is the derivative of the potential that the Brownian system experiences, γ is the friction coefficient of the particle and $\xi(t)$ is a Gaussian white noise. $\xi(t)$ has zero mean ($\langle\xi(t)\rangle = 0$) and $\xi(t)$ satisfies the fluctuation dissipation theorem [13]

$$\langle\xi(t)\,\xi(s)\rangle = 2\gamma k_B T\,\delta(t-s), \tag{1.2}$$

where k_B is the Boltzmann constant and T is the temperature of the environment. The Langevin equation is essentially Newton's second law with a damping term and a random noise added. In this thesis, we will be considering situations where the inertia term is negligible. In this case, we will be in the overdamped regime where the Langevin equation becomes:

$$\gamma\,\dot{x}(t) = -V'[x(t)] + \xi(t). \tag{1.3}$$

The key point of the Langevin equation is that we no longer have to simulate the entire environment in our description. This is a huge simplification and allows us to directly calculate the trajectories of single Brownian systems.

1.2.2 The Smoluchowski equation

An equivalent description of Brownian motion can be made in terms of the probability density of the Brownian system. Imagine a probability distribution $P(\boldsymbol{r},\,t)$, were $\boldsymbol{r}$ represents a coordinate in $\mathbb{R}^n$ and t represents time. When one integrates $P(\boldsymbol{r},\,t)$ over a region of space $\mathcal{V}$ at a time t, one finds the probability that the Brownian system is in $\mathcal{V}$ at time t. The Smoluchowski equation is a partial differential equation that describes how the probability distribution $P(\boldsymbol{r},\,t)$ evolves with time. Since we are using probability distributions to describe the motion of a Brownian motor, we lose information about single random trajectories of the Brownian motor in return for very precise knowledge about the ensemble behavior of the Brownian motor. The Smoluchowski

equation is given by [54],

$$\begin{aligned} \partial_t P(\boldsymbol{r}, t) &\equiv -\nabla \cdot \boldsymbol{J}(\boldsymbol{r}, t), \\ J_j(\boldsymbol{r}, t) &\equiv -\frac{1}{\gamma_j}[P(\boldsymbol{r}, t)\partial_j V(\boldsymbol{r}) + k_B T(\boldsymbol{r}, t)\partial_j P(\boldsymbol{r}, t)], \end{aligned} \tag{1.4}$$

where $\boldsymbol{J}(\boldsymbol{r}, t)$ is referred to as the probability current, γ_j is the friction coefficient of the system in the jth dimension, $V(\boldsymbol{r})$ is the potential that the system experiences, k_B is Boltzmann's constant and $T(\boldsymbol{r}, t)$ is the temperature of the environment. The temperature may be governed by a separate equation of motion, or it may be controlled externally. We will provide a specific equation of motion for the temperature in Chap. 2. To see that $\boldsymbol{J}(\boldsymbol{r}, t)$ is the probability current, one should integrate Eq. (1.4) over a volume $\mathcal{V}$. Doing so and invoking the divergence theorem, one finds:

$$\partial_t \int_{\mathcal{V}} P(\boldsymbol{r}, t)\, \mathrm{d}\boldsymbol{r} = -\oint_{\partial\mathcal{V}} \boldsymbol{J}(\boldsymbol{r}, t) \cdot \mathrm{d}\hat{\boldsymbol{n}}, \tag{1.5}$$

where $\hat{\boldsymbol{n}}$ is the unit normal vector of the surface $\partial\mathcal{V}$. Equation (1.5) tells us that the change in the probability of finding the particle in the volume $\mathcal{V}$ with respect to time is given by the integral of $\boldsymbol{J}(\boldsymbol{r}, t)$ over the surface of $\mathcal{V}$. With this in mind, it is natural to interpret $\boldsymbol{J}(\boldsymbol{r}, t)$ as a probability current.

Drift in the Smoluchowski Equation

The term $\partial_j[P(\boldsymbol{r}, t)\partial_j V(\boldsymbol{r})]$ in Eq. (1.4) is called the "drift term". This term causes the probability distribution to move down a potential gradient. To see this, consider Eq. (1.4) in one dimension, where the temperature is zero:

$$\partial_t P(x, t) = \gamma^{-1}[\partial_x P(x, t)\partial_x V(x) + P(x, t)\partial_{xx} V(x)]. \tag{1.6}$$

Now let the potential be given by $V(x) = -fx$, meaning that the potential is tilted. In this case Eq. (1.6) has the solution:

$$P(x, t) = P\left(x - \frac{ft}{\gamma}, 0\right), \tag{1.7}$$

so the probability distribution drifts in the direction of the tilt f. In general, we will be considering potentials that are tilted and which have local minima. When there are local minima in $V(\boldsymbol{r})$, the drift term will cause the probability distribution to become more concentrated around the minima of the potential.

Temperature and Temperature Gradients in the Smoluchowski Equation

The term $k_B\partial_j[T(\boldsymbol{r}, t)\partial_j P(\boldsymbol{r}, t)]$ is called the "diffusion term". The diffusion term causes the probability distribution to become broader with time. In the case of Brownian motion, the origin of the diffusion term is from collisions between the Brownian particle and particles in the

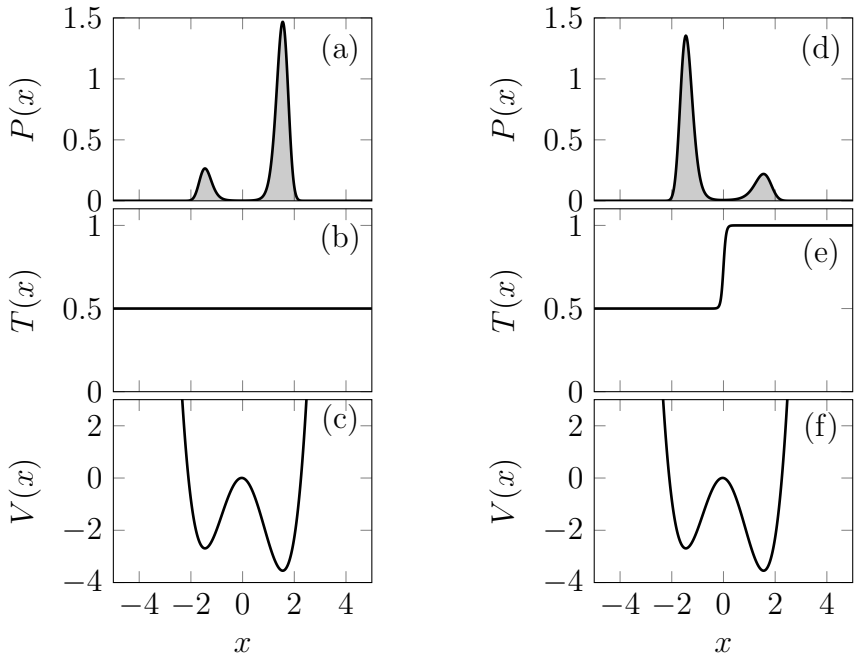

Figure 1.2: Schematic representation of the Landauer Blowtorch. We place a Brownian particle on a bistable potential and wait for it to reach equilibrium. (a-c) shows the situation where the temperature is constant and (d-f) shows a situation where the lower well is being heated externally. We see that the temperature gradient in (e) has a large effect on the steady state of the system in (d). $P(x)$ represents the probability distribution of the Brownian system, $T(x)$ represents the temperature of the environment and $V(x)$ is the potential that the Brownian system experiences. In this figure, $\gamma = 1$ and $k_B = 1$.

surrounding environment. Consider the situation where the potential is flat and the temperature is given by $T(x, t) = T_0$ (meaning that there are no temperature gradients), in this case we have:

$$\partial_t P(x, t) = \frac{k_B}{\gamma}[\partial_x T(x, t)\partial_x P(x, t) + T(x, t)\partial_{xx} P(x, t)] = \frac{k_B T_0}{\gamma}\partial_{xx} P(x, t). \tag{1.8}$$

This is in fact the diffusion equation, which causes the probability distribution to broaden with time.

Throughout this thesis, we will be dealing with a temperature that is non constant in space. Such a non constant temperature is crucial for motors like the Büttiker-Landauer engine from Sec. 1.1.1, where the temperature produces a force on the Brownian motor/particle. In [38], Landauer describes a system that helps to clarify the mechanism that allows temperature gradients to apply a force on a Brownian particle. The system is now called the Landauer blowtorch and we have recreated it in Fig. 1.2. In Fig. 1.2, we have placed a Brownian particle on a bistable potential with a temperature that does not depend on time. We then evolve the probability distribution via Eq. (1.4) until the system reaches equilibrium. At this point, the probability distribution no longer changes with time and only depends on x as shown in Fig. 1.2 (a) and (d). In Fig. 1.2 (a-c), the temperature is constant in space and we find that it is far more likely to find the Brownian particle in the lower well than it is the upper well. On the other hand, Fig. 1.2 (d-f) shows a situation where we have heated the lower well. This heating agitates the Brownian particle out of the lower well and into the upper well. Ultimately,

the temperature gradients produce a force on the Brownian particle that can enhance barrier crossing rates.

Throughout this thesis, we will discuss the effect that temperature gradients, and gradients in the potential, have on the probability distribution of a Brownian motor. Although the results shown here were derived for very simple potentials/temperature gradients in one dimension, the intuition developed here still applies to more complicated situations. In particular, we would like to stress the following points: (i) a Brownian system will be constantly forced in the direction of lower potential. This means that the Brownian system will become trapped at points where the potential has a local minima and will drift in the direction of a net force on the system. (ii) Wherever there is a temperature gradient, the Brownian motor will be agitated into the region where the temperature is lower. Landauer [38] quotes G. E. Hinton as saying the following: "Pebbles in a driveway on flat land accumulate on the side. In the driveway they are agitated (hot region). They are left undisturbed on the side (cold region), and therefore accumulate on the side. This occurs despite the fact that the traffic does not exert a directional force on the pebbles." This is exactly the physical origin of the Landauer blowtorch.

1.3 Heat and Entropy in Brownian Dynamics

The exchange of energy between a Brownian motor and its environment is fundamental to the dynamics and thermodynamics of the system. In this section, we will explore the energetics of Brownian motion in the overdamped regime described by Eq. 1.4. The results in this section have been described in Ref. [55].

Whenever a Brownian system is placed on a non-uniform potential, and its probability distribution changes, the potential energy of the Brownian system must also change. We can use Eq. (1.4) to calculate the change in energy of a Brownian motor with respect to time. In the overdamped regime, the potential energy of the system contained in a region Ω is the potential energy alone:

$$E(t) = \int_\Omega P(\boldsymbol{r}, t) V(\boldsymbol{r}) \, \mathrm{d}\boldsymbol{r}. \tag{1.9}$$

Differentiating with respect to time and using Eq. (1.4), we get:

$$\begin{aligned} \frac{\mathrm{d}E(t)}{\mathrm{d}t} &= \int_\Omega [-\nabla \cdot \boldsymbol{J}(\boldsymbol{r}, t)] V(\boldsymbol{r}) \, \mathrm{d}\boldsymbol{r} \\ &= -\int_{\partial\Omega} \boldsymbol{J}(\boldsymbol{r}, t) V(\boldsymbol{r}) \, \mathrm{d}\boldsymbol{r} + \int_\Omega \boldsymbol{J}(\boldsymbol{r}, t) \nabla V(\boldsymbol{r}) \, \mathrm{d}\boldsymbol{r}. \end{aligned} \tag{1.10}$$

Where $\partial\Omega$ is the boundary of the region Ω. The first term is equal to the work done on the system, leading us to conclude that the second term must be the heat emitted by the Brownian system into its environment. The heat density is therefore given by:

$$q(\boldsymbol{r}, t) = -\boldsymbol{J}(\boldsymbol{r}, t) \cdot \nabla V(\boldsymbol{r}, t). \tag{1.11}$$

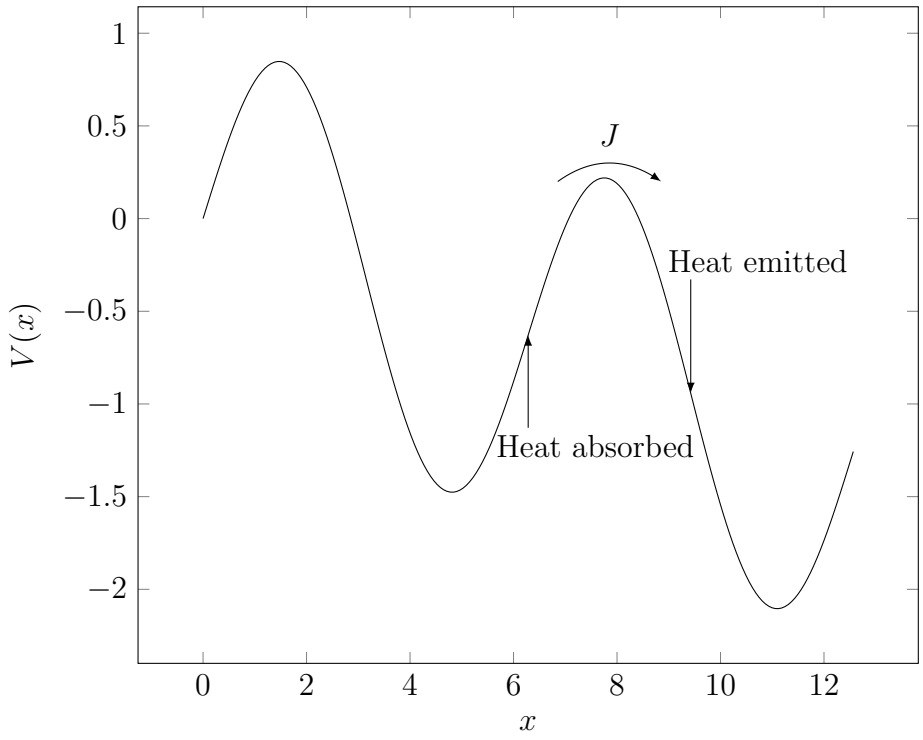

Figure 1.3: Cartoon schematic showing Brownian motors diffusing over a one dimensional landscape. We show a current J going over a barrier. In order to climb the barrier, motors have to absorb heat from the environment. The motors will emit heat into the environment as they go down the other side of the barrier.

A typical non-equilibrium barrier configuration is shown in Fig. 1.3. The position where the thermal exchanges occur on the potential is also shown. In [31] and [32], Sekimoto describes the heat that is transferred between a Brownian motor and the heat bath that it is interacting with. In doing so, he finds that the conservation of energy is upheld along a single trajectory as long as the thermal energy of the environment is considered. Here, we see that the heat produced by a Brownian system corresponds to a change in potential energy of the probability distribution.

As well as considering the energy of a Brownian system, a lot of attention has been paid to the entropy of Brownian systems interacting with their local environment, leading to the field of stochastic thermodynamics [36]. The entropy of a Brownian system is given by the Shannon entropy [55], which has the form:

$$S(t) = -k_B \int_{\Omega} P(\boldsymbol{r}, t) \log[P(\boldsymbol{r}, t)] \, \mathrm{d}\boldsymbol{r}. \tag{1.12}$$

Differentiating with respect to time and using Eq. (1.4), we find that:

$$\begin{aligned}\frac{\mathrm{d}S(t)}{\mathrm{d}t} &= -k_B \int_\Omega \partial_t P(\boldsymbol{r},\, t) \log[P(\boldsymbol{r},\, t)] + \partial_t P(\boldsymbol{r},\, t)\, \mathrm{d}\boldsymbol{r} \\ &= k_B \int_\Omega \nabla \cdot \{\boldsymbol{J}(\boldsymbol{r},\, t) + \boldsymbol{J}(\boldsymbol{r},\, t) \log[P(\boldsymbol{r},\, t)]\}\, \mathrm{d}\boldsymbol{r} - k_B \int_\Omega \boldsymbol{J}(\boldsymbol{r},\, t) \cdot \frac{\nabla P(\boldsymbol{r},\, t)}{P(\boldsymbol{r},\, t)}\, \mathrm{d}\boldsymbol{r} \\ &= \mathcal{B}(t) + k_B \int_\Omega \boldsymbol{J}(\boldsymbol{r},\, t) \cdot \left(\frac{\boldsymbol{J}(\boldsymbol{r},\, t)}{P(\boldsymbol{r},\, t) T(\boldsymbol{r},\, t)} + \frac{\nabla V(\boldsymbol{r})}{T(\boldsymbol{r},\, t)} \right) \mathrm{d}\boldsymbol{r}, \end{aligned} \tag{1.13}$$

We now split the change in entropy into separate terms:

$$\frac{\mathrm{d}S(t)}{\mathrm{d}t} = \mathcal{B}(t) + \frac{\mathrm{d}S^{\mathrm{gen}}(t)}{\mathrm{d}t} + \frac{\mathrm{d}S_e(t)}{\mathrm{d}t}, \tag{1.14}$$

where

$$\mathcal{B}(t) \equiv k_B \int_\Omega \nabla \cdot \{\boldsymbol{J}(\boldsymbol{r},\, t) + \boldsymbol{J}(\boldsymbol{r},\, t) \log[P(\boldsymbol{r},\, t)]\}\, \mathrm{d}\boldsymbol{r}, \tag{1.15}$$

$$\frac{\mathrm{d}S_e(t)}{\mathrm{d}t} \equiv k_B \int_\Omega \boldsymbol{J}(\boldsymbol{r},\, t) \cdot \frac{\nabla V(\boldsymbol{r})}{T(\boldsymbol{r},\, t)}\, \mathrm{d}\boldsymbol{r}. \tag{1.16}$$

and

$$\frac{\mathrm{d}S^{\mathrm{gen}}(t)}{\mathrm{d}t} \equiv k_B \int_\Omega \frac{\boldsymbol{J}(\boldsymbol{r},\, t) \cdot \boldsymbol{J}(\boldsymbol{r},\, t)}{P(\boldsymbol{r},\, t)\, T(\boldsymbol{r},\, t)}\, \mathrm{d}\boldsymbol{r} \geq 0, \tag{1.17}$$

$\mathcal{B}(t)$ represents the flow of entropy through the boundary of the domain $\partial\Omega$. This term can be positive or negative depending on the boundary conditions that are enforced on $P(\boldsymbol{r},\, t)$. $\frac{\mathrm{d}S_e}{\mathrm{d}t}$ represents the entropy flow into the system through heat exchanges with the environment. $\frac{\mathrm{d}S_e}{\mathrm{d}t}$ is positive when the heat exchanges cause the system's entropy to increase. However, there are cases where heat exchanges with the environment cause the system's entropy to decrease. $\frac{\mathrm{d}S^{\mathrm{gen}}}{\mathrm{d}t}$ is the entropy that is generated by the system and is always positive. Eq. (1.14) has been derived previously [44, 55] and represents the second law of thermodynamics for a Brownian system.

So far, we have covered thermal interactions between Brownian systems and their environment. Firstly we considered the time dependence of the energy of a Brownian system. In doing so, we see that Brownian systems absorb and emit heat into their environment as they undergo motion. These heat exchanges can be used to cause heat to flow from a cold reservoir to a hot reservoir in the fashion of a heat pump [34, 39–42]. Second, temperature gradients in the local environment have a strong effect on the motion of a system. These effects can be exploited to alter the steady state of a Brownian system as seen in Sec. 1.2.2, or to make the Brownian motor move against a net force as seen in Sec. 1.1.1. We also established that using Eq. (1.4) to model a Brownian motor is consistent with the second law of thermodynamics.

1.4 Thesis Aims

In this introduction, we described classes of Brownian motors and methods for modeling systems undergoing Brownian motion. We have seen that when a Brownian system diffuses over a non

uniform potential, the Brownian system exchanges heat with its environment. The heat that a Brownian system exchanges with its environment is what enables the system to overcome barriers in the potential. In previous treatments, there has been an implicit assumption that the heat exchanges do not alter the temperature of the environment. The aim of this thesis is to explore the consequence of the heat produced by a Brownian motor on the temperature of the environment. We also aim to determine whether the altered temperature of the environment has an affect on the behavior of the Brownian system itself. We will begin by formulating a mathematical model that directly quantifies how the heat produced by a Brownian system affects the temperature of its environment. The mathematical model will also describe how the altered temperature affects Brownian dynamics. The resulting mathematical description will be used to explore the physical behavior of Brownian motors with self-induced temperature gradients.

1.5 Statement of Originality

A similar model of self-induced temperature gradients has been discussed earlier by Streater [56–59] in the context of a Brownian particle. The current work goes beyond this to explore the consequences of self-induced temperature gradients for Brownian motor systems. This includes analytical and numerical calculations of the steady state solution, numerical results for barrier crossing rates relevant to Brownian motors, and a proposal for heat engines and heat pumps utilizing self-induced temperature gradients.

1.5.1 Previous Work From Honors Dissertation

My honors dissertation was on a similar topic. The theoretical results in Chap. 2 were mostly derived in my honors dissertation. The remaining chapters of the thesis were all developed as part of my Masters of Physics.

1.6 Publications

During the writing of this thesis, I was the first author on a paper published in Physical Review E, titled “Self-induced temperature gradients in Brownian dynamics” [60]. The paper mainly covers Chaps. 2 and 4 of this thesis.

Chapter 2

Theory of Self-induced Temperature Gradients

In Chap. 1, we saw that Brownian motors exchange heat with their environment. In order to explicitly model a Brownian motor exchanging heat with its environment, one must consider two equations. One for the probability distribution of the motor $P(\boldsymbol{r}, t)$ and one for the temperature of the environment $T(\boldsymbol{r}, t)$. Eq. (1.4) describes the motion of a Brownian motor on a potential given by $V(\boldsymbol{r})$ and with temperature $T(\boldsymbol{r}, t)$. Eq. (1.11) tells us that the heat density produced by the Brownian motor is given by $q(\boldsymbol{r}, t) = -\boldsymbol{J}(\boldsymbol{r}, t) \cdot \nabla V(\boldsymbol{r})$. Assuming that the temperature evolves via the heat transfer equation, with $q(\boldsymbol{r}, t)$ as a heat source, we have the following equation of motion for the temperature:

$$\partial_t T(\boldsymbol{r}, t) = -\kappa \boldsymbol{J}(\boldsymbol{r}, t) \cdot \nabla V(\boldsymbol{r}, t) + D\nabla^2 T(\boldsymbol{r}, t), \tag{2.1}$$

where κ is an as yet unknown constant with units $\mathrm{kg}^{-1}\mathrm{m}^{\mathrm{d}}\mathrm{J}^{-1}\mathrm{K}$ (d is the number of spatial dimensions) and D is the thermal diffusivity of the environment with units $\mathrm{m}^2\mathrm{s}^{-1}$. The first term in Eq. (2.1) accounts for the heat that is transferred from the Brownian motor to its environment. The second term represents thermal diffusion and by itself is usually referred to as the heat equation. In some physical situations, κ and D can depend on position, time or even the temperature itself. For simplicity in this thesis, we take κ and D to be constant. Once we enforce boundary conditions on $T(\boldsymbol{r}, t)$ and $P(\boldsymbol{r}, t)$, we arrive at the system of interest for this thesis.

The temperature gradients produced in Eq. (2.1) are neglected in isothermal models by definition (see for example Chap. 1.1.2). The assumption that temperature gradients do not affect the dynamics of Brownian motors has been discussed in [47] and rests on two key assumptions. (i) that the specific heat capacity is very large, so that any heat exchanges between the Brownian system and the local environment have a negligible effect on the environmental temperature. (ii) any temperature gradients that do occur will be dissipated very quickly into the external environment. Looking at Eq. (2.1), we see that assumption (i) is met when κ is small and that (ii) is met when D is large. In Sec. 2.4, we will explain a precise method

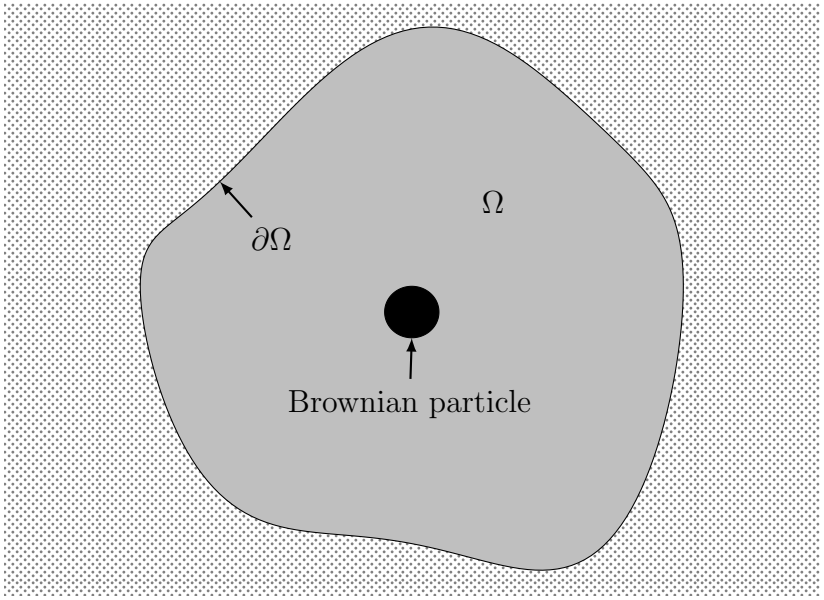

Figure 2.1: A schematic diagram of a Brownian particle contained within a region Ω, which we will refer to as the local environment. Inside Ω, Eqs. (1.4) and (2.1) hold. The motor and its local environment interact with their external environment at the boundary $\partial\Omega$ as described in Sec. 2.1. The region outside of Ω is referred to as the external environment.

for determining when assumptions (i) and (ii) hold. The physical system consisting of both Eqs. (1.4) and (2.1) will now be referred to as the "theory of Brownian motion with self-induced temperature gradients".

2.1 Boundary conditions

The boundary conditions that are considered here will be motivated from the underlying physics of the situation that we want to model. The boundary conditions that will be considered in this thesis are restricted to: periodic, Neumann and Dirichlet. Periodic boundary conditions imply a circular domain that wraps around on itself, so that a system traveling through one boundary will appear at the other boundary. There are also situations where a physical barrier, or a very high potential, will prevent the system from passing through certain boundaries. We will refer to these situations as confining. Confining boundary conditions are realized by either having $V(\boldsymbol{r})|_{\partial\Omega} \to \infty$ or simply enforcing $\boldsymbol{J}(\boldsymbol{r}, t) \cdot \hat{\boldsymbol{n}} = 0$, where $\hat{\boldsymbol{n}}$ is the unit normal vector of the boundary $\partial\Omega$. This condition implies that the current is either zero at the boundary or that the current at the boundary is perpendicular to the boundary. In either case, no current will flow through the boundary of Ω.

We also need to specify boundary conditions for the temperature. We do so as follows: whenever the probability density is periodic, we will require that the temperature is also periodic. In other cases, we will apply Dirichlet boundary conditions to the temperature, where the temperature is a known function at the boundary, or Neumann boundary conditions, where the gradient of the temperature is a known function at the boundary. Dirichlet boundary conditions correspond to physical situations where the system is in contact with a large reservoir that

can exchange arbitrarily large amounts of heat with the Brownian subsystem without changing temperature.

Neumann boundary conditions correspond to physical situations where the amount of heat that can flow through the boundary is restricted, however, the actual temperature at the boundary can change in space and time. Of particular interest, are situations where the boundaries are perfectly insulating so that no heat can pass through the boundaries ($\nabla T(\boldsymbol{r}, t) \cdot \boldsymbol{n}|_{\partial\Omega} = 0$). In these cases, the system is thermally separated from its external environment. In Sec. 2.2 we will see that the boundary conditions can affect the flow of entropy in the system as well as the energy. In Sec 2.3, we will see that the boundary conditions can affect the steady state that the system reaches as $t \to \infty$.

2.2 Thermodynamics

In this section, we will discuss the first and second laws of thermodynamics in the context of self-induced temperature gradients. Following the results from [56–59], we note that the energy of both the Brownian system and its immediate environment is given by:

$$E(t) = \int_\Omega P(\boldsymbol{r}, t)V(\boldsymbol{r}) + \rho c_p T(\boldsymbol{r}, t)\,\mathrm{d}\boldsymbol{r}, \tag{2.2}$$

where we have assumed that the environment is an incompressible fluid with density ρ and specific heat c_p. Differentiating Eq. (2.2) with respect to time and using Eqs. (1.4) and (2.1), we see that:

$$\frac{\mathrm{d}E(t)}{\mathrm{d}t} = \int_\Omega -\nabla \cdot \boldsymbol{J}(\boldsymbol{r}, t)V(\boldsymbol{r}) + \rho c_p \left[-\kappa \boldsymbol{J}(\boldsymbol{r}, t) \cdot \nabla V(\boldsymbol{r}) + D\nabla^2 T(\boldsymbol{r}, t)\right] \mathrm{d}\boldsymbol{r} \tag{2.3}$$

Using the same logic that brought us to Eq. (1.11), we find that,

$$\begin{aligned}\frac{\mathrm{d}E(t)}{\mathrm{d}t} = &-\int_{\partial\Omega} \boldsymbol{J}(\boldsymbol{r}, t)V(\boldsymbol{r}) \cdot \mathrm{d}\boldsymbol{r} + \int_\Omega \boldsymbol{J}(\boldsymbol{r}, t) \cdot V(\boldsymbol{r})\mathrm{d}\boldsymbol{r} \\ &- \kappa\rho c_p \int_\Omega \boldsymbol{J}(\boldsymbol{r}, t) \cdot V(\boldsymbol{r})\mathrm{d}\boldsymbol{r} + \rho c_p D \int_{\partial\Omega} \nabla T(\boldsymbol{r}, t) \cdot \mathrm{d}\boldsymbol{r}.\end{aligned} \tag{2.4}$$

We now define:

$$B^W(t) \equiv -\int_{\partial\Omega} \boldsymbol{J}(\boldsymbol{r}, t)V(\boldsymbol{r})\mathrm{d}\boldsymbol{r} \tag{2.5}$$

and

$$B^Q(t) \equiv \rho c_p D \int_{\partial\Omega} \nabla T(\boldsymbol{r}, t) \cdot \mathrm{d}\boldsymbol{r}. \tag{2.6}$$

The first law of thermodynamics says that $\frac{\mathrm{d}E(t)}{\mathrm{d}t} = \dot{W} + \dot{Q}$, where $\dot{W}$ is the rate of work being done on the system and $\dot{Q}$ is the rate of heat leaving the system. $B^W(t)$ represents the potential energy that is flowing through the boundary of the system and represents the work $\dot{W}$ flowing through the system. The other boundary term, $B^Q(t)$ represents the thermal energy that the system loses through the boundaries and is equal to $\dot{Q}$ from the first law of thermodynamics. If

$\kappa = \frac{1}{\rho c_p}$, then the second and third terms on the right hand side of Eq. (2.4) cancel, so Eq. (2.4) takes the required form:

$$\frac{\mathrm{d}E(t)}{\mathrm{d}t} = B^Q(t) + B^W(t). \tag{2.7}$$

Therefore, the first law of thermodynamics requires that $\kappa = \frac{1}{\rho c_p}$, with this choice, Eq. (2.1) becomes the heat transfer equation.

The second law of thermodynamics requires that the entropy of a closed system never decreases. The entropy of our system is defined as:

$$S(t) = -k_B \int_\Omega P(\boldsymbol{r},\, t) \log[P(\boldsymbol{r},\, t)]\, \mathrm{d}\boldsymbol{r} + \rho c_p \int_\Omega \log[T(\boldsymbol{r},\, t)]\, \mathrm{d}\boldsymbol{r}, \tag{2.8}$$

the first term represents the Shannon entropy of the Brownian motor [55] and the second term is the entropy of an incompressible fluid. Differentiating Eq. (2.8) with respect to time:

$$\begin{aligned}
\frac{\mathrm{d}S(t)}{\mathrm{d}t} &= -k_B \int_\Omega \partial_t P(\boldsymbol{r},\, t) \log[P(\boldsymbol{r},\, t)] + \partial_t P(\boldsymbol{r},\, t)\, \mathrm{d}\boldsymbol{r} + \rho c_p \int_\Omega \frac{1}{T(\boldsymbol{r},\, t)} \partial_t T(\boldsymbol{r},\, t)\, \mathrm{d}\boldsymbol{r} \\
&= k_B \int_\Omega \nabla \cdot \boldsymbol{J}(\boldsymbol{r},\, t) \log[P(\boldsymbol{r},\, t)] + \nabla \cdot \boldsymbol{J}(\boldsymbol{r},\, t)\, \mathrm{d}\boldsymbol{r} \\
&\quad + \rho c_p \int_\Omega \frac{1}{T(\boldsymbol{r},\, t)} \left[-\frac{1}{\rho c_p} \boldsymbol{J}(\boldsymbol{r},\, t) \cdot \nabla V(\boldsymbol{r},\, t) + D \nabla^2 T(\boldsymbol{r},\, t) \right] \mathrm{d}\boldsymbol{r} \\
&= k_B \left\{ \int_{\partial\Omega} \boldsymbol{J}(\boldsymbol{r},\, t) \log[P(\boldsymbol{r},\, t)] \cdot \mathrm{d}\boldsymbol{r} - \int_\Omega \boldsymbol{J}(\boldsymbol{r},\, t) \frac{\nabla P(\boldsymbol{r},\, t)}{P(\boldsymbol{r},\, t)}\, \mathrm{d}\boldsymbol{r} \right\} \\
&\quad - \int_\Omega \frac{\boldsymbol{J}(\boldsymbol{r},\, t) \cdot \nabla V(\boldsymbol{r},\, t)}{T(\boldsymbol{r},\, t)}\, \mathrm{d}\boldsymbol{r} + \rho c_p D \left\{ \int_\Omega \left[\frac{\nabla T(\boldsymbol{r},\, t)}{T(\boldsymbol{r},\, t)} \right]^2 \mathrm{d}\boldsymbol{r} + \int_{\partial\Omega} \frac{\nabla T(\boldsymbol{r},\, t)}{T(\boldsymbol{r},\, t)} \cdot \mathrm{d}\boldsymbol{r} \right\} \\
&= \sum_j \int_\Omega \gamma_j \frac{J_j(\boldsymbol{r},\, t)^2}{P(\boldsymbol{r},\, t) T(\boldsymbol{r},\, t)} + \rho c_p D \left[\frac{\nabla T(\boldsymbol{r},\, t)}{T(\boldsymbol{r},\, t)} \right]^2 \mathrm{d}\boldsymbol{r} \\
&\quad + \int_{\partial\Omega} \left[k_B \boldsymbol{J}(\boldsymbol{r},\, t) \log[P(\boldsymbol{r},\, t)] + \rho c_p D \frac{\nabla T(\boldsymbol{r},\, t)}{T(\boldsymbol{r},\, t)} \right] \cdot \mathrm{d}\boldsymbol{r}.
\end{aligned} \tag{2.9}$$

We have used Eqs. (1.4) and (2.1) to get to the second line. To get to the third line, we had to use integration by parts on the first term and the definition $J_j(\boldsymbol{r},\, t) = -\frac{1}{\gamma_j}[P(\boldsymbol{r},\, t)\partial_j V(\boldsymbol{r}) + k_B T(\boldsymbol{r},\, t)\partial_j P(\boldsymbol{r},\, t)]$ from Eq. 1.4 to combine the second and third terms. If we define:

$$\dot{S}^{\mathrm{gen}} \equiv \int_\Omega \sum_j \left[\gamma_j \frac{J_j(\boldsymbol{r},\, t)^2}{P(\boldsymbol{r},\, t) T(\boldsymbol{r},\, t)} \right] + \rho c_p D \left[\frac{\nabla T(\boldsymbol{r},\, t)}{T(\boldsymbol{r},\, t)} \right]^2 \mathrm{d}\boldsymbol{r} \geq 0, \tag{2.10}$$

$$\mathcal{B}^J(t) \equiv \int_{\partial\Omega} k_B\, \boldsymbol{J}(\boldsymbol{r},\, t) \log[P(\boldsymbol{r},\, t)] \cdot \mathrm{d}\boldsymbol{r} \tag{2.11}$$

and

$$\mathcal{B}^Q(t) \equiv \int_{\partial\Omega} \rho c_p D \frac{\nabla T(\boldsymbol{r},\, t)}{T(\boldsymbol{r},\, t)} \cdot \mathrm{d}\boldsymbol{r}, \tag{2.12}$$

where $\hat{\boldsymbol{n}}$ is the unit normal vector of the surface $\partial\Omega$, then

$$\frac{\mathrm{d}S(t)}{\mathrm{d}t} = \dot{S}^{\mathrm{gen}}(t) + \mathcal{B}^{J}(t) + \mathcal{B}^{Q}(t). \tag{2.13}$$

In words, Eq. (2.13) tells us that the change in entropy with respect to time is a positive term plus two boundary terms. If the system is isolated, such as when $\mathcal{B}^{J} = 0 = \mathcal{B}^{Q}$, then its entropy will always increase or stay the same, meaning that our model obeys the second law of thermodynamics. $\mathcal{B}^{J}(t)$ is the inward flow of entropy due to the probability current of the Brownian motor, while $\mathcal{B}^{Q}(t)$ is the inward flow of entropy due to the flow of heat. $\dot{S}^{\mathrm{gen}}(t)$ is the sum of two positive terms, the first one is due to the Brownian motor, which we saw in Chap. 1.3. The second term is the entropy generation due to temperature gradients in the local environment. As the temperature becomes more flat due to thermal diffusion, the entropy of the environment increases.

The boundary conditions affect the physics of a Brownian motor. In particular, the boundary conditions affect the way in which entropy evolves with time. For example, let us consider a confining case where $V(\boldsymbol{r})|_{\partial\Omega} \to \infty$. In this case, the current passing through the boundary is zero, meaning that $\mathcal{B}^{J}(t)$ is zero. Interestingly, we do not have to be so strict to find situations where $\mathcal{B}^{J}(t)$ is zero. Consider the case where we impose boundary conditions on the probability distribution and the current that are periodic in one direction and confining in another. As with the case where $V(\boldsymbol{r})|_{\partial\Omega} \to \infty$, the confining parts will lead to a vanishing entropy generation. As for the periodic sections, there will be two sections of $\partial\Omega$, say $\partial\Omega_1$ and $\partial\Omega_2$ that are periodic to one another. Along these sections, the probability distributions will match, and the escaping currents will have opposite signs. Therefore, their contributions to the integral in Eq. (2.11) cancel. By inspecting Eq. (2.12), we can see that if the heat passing through the boundary is zero, then $\mathcal{B}^{Q}(t) = 0$.

2.3 Steady State

The steady state is the state that the system reaches as $t \to \infty$, the steady state is defined by $\partial_t P(\boldsymbol{r}, t) = 0 = \partial_t T(\boldsymbol{r}, t)$. In the steady state, the following equations hold:

$$\nabla \cdot \boldsymbol{J}_{\mathrm{ss}}(\boldsymbol{r}) = 0 \tag{2.14}$$

and

$$-\frac{1}{\rho c_p}\boldsymbol{J}_{\mathrm{ss}}(\boldsymbol{r}) \cdot \nabla V(\boldsymbol{r}) + D\nabla^2 T_{\mathrm{ss}}(\boldsymbol{r}) = 0. \tag{2.15}$$

The first equation states that $\boldsymbol{J}_{\mathrm{ss}}(\boldsymbol{r})$ is a divergence free field in the steady state and the second equation expresses the local conservation of energy [c.f. (Eq. 2.3)]. The steady state first and second laws of thermodynamics read as:

$$B^{W}_{\mathrm{ss}} + B^{Q}_{\mathrm{ss}} = 0 \tag{2.16}$$

and

$$\dot{S}^{\text{gen}}_{\text{ss}} + \mathcal{B}^{J}_{\text{ss}} + \mathcal{B}^{Q}_{\text{ss}} = 0. \tag{2.17}$$

Eq. (2.16) is redundant as it is a special case of Eq. (2.15) that holds at the boundaries. Eq. (2.17) tells us that in the steady state, entropy generated in the interior is balanced by entropy flowing through the boundaries.

2.3.1 Equilibrium Steady States

In this section, we will consider situations where the steady state is in equilibrium. In this case, $\boldsymbol{J}_{\text{ss}}(\boldsymbol{r}) = 0$ everywhere and there is no entropy generated in the steady state. Since the steady state current is zero, the steady state temperature is found by solving the Laplace equation subject to the boundary conditions. An interesting case is when the net heat flowing through the boundaries is held at zero. One example which we will refer to in Chap. 4 is the case where $\nabla T(\boldsymbol{r},\, t)\cdot\boldsymbol{n}|_{\partial\Omega} = 0$. Mathematically, all that Eqs. (2.14) and (2.15) tell us about $T_{\text{ss}}(\boldsymbol{r})$ is that it is constant, T_{ss}. However, if we were to say that the system started in some initial state with energy E_{i}, then the conservation of energy reads:

$$E_{\text{i}} = \int_{\Omega} P_{\text{ss}}(\boldsymbol{r})V(\boldsymbol{r}) + \rho c_p T_{\text{ss}}\,\mathrm{d}\boldsymbol{r} \tag{2.18}$$

Where

$$P_{\text{ss}}(\boldsymbol{r}) = \mathcal{N}\exp\left[-\frac{V(\boldsymbol{r})}{k_B T_{\text{ss}}}\right], \tag{2.19}$$

where $\mathcal{N}$ is a normalization constant. Equation (2.19) is a Boltzmann distribution with temperature T_{ss}. Here we see that although self-induced temperature gradients are no longer present in the steady state, the heat that was dumped into the environment during the transient phase of the system has a lasting affect on the final temperature. In Chap. 4 we will return to this situation and explore it numerically. It is also worth noting that because the isothermal models of Brownian motion from Chap. 1.1.2 do not explicitly conserve the energy of the system, the steady state that they reach does not depend on the choice of initial conditions.

We also note that when $\boldsymbol{J}_{\text{ss}}(\boldsymbol{r}) = 0$ everywhere, $\nabla^2 T_{\text{ss}}(\boldsymbol{r}) = 0$, so the shape of $T_{\text{ss}}(\boldsymbol{r})$ only depends on the boundary conditions. In this case,

$$P_{\text{ss}}(\boldsymbol{r}) \propto \exp\left\{-\int^{r} \mathrm{d}\boldsymbol{r'}\frac{\nabla V(\boldsymbol{r'})}{k_B T_{\text{ss}}(\boldsymbol{r'})}\right\}. \tag{2.20}$$

Since the current is zero, $\mathcal{B}^{J}_{\text{ss}} = 0$ and $\dot{S}^{\text{gen}}_{\text{ss}} = -\mathcal{B}^{Q}_{\text{ss}}$, so the entropy generated is entirely due to temperature gradients. If there is no heat flowing through the boundaries ($\nabla T(\boldsymbol{r})|_{\partial\Omega} = 0$), then $\dot{S}^{\text{gen}}_{\text{ss}} = 0$, $T_{\text{ss}}(\boldsymbol{r}) = T_0$ is constant and $P_{\text{ss}}(\boldsymbol{r}) \propto \exp\{-V(\boldsymbol{r})/T_0\}$ has the familiar Boltzmann form.

2.3.2 Non Equilibrium Steady States

Although $\partial_t P(\boldsymbol{r}, t) = 0$ in the steady state, there can still be a non zero probability current. To understand this, consider a one dimensional periodic domain $x \in [a, b]$, where $V(x) = -fx$ for some non zero f. Since the domain is periodic, a motor passing through the point $x = b$ will emerge at $x = a$. If there are no self-induced temperature gradients and if the temperature is constant in space and time (say $T(x) = T_0$), then $P_{\text{ss}}(x) = \frac{1}{b-a}$. Using Eq. (1.4), we see that:

$$J_{\text{ss}} = -\gamma^{-1} \frac{1}{b-a} f. \tag{2.21}$$

A physical example of this situation would be a Brownian particle on a circular domain that is subject to a constant torque.

We now turn our attention to systems where $\boldsymbol{J}_{\text{ss}}(\boldsymbol{r}) \neq 0$, we will begin with the one dimensional case. Suppose that we have a potential of the form:

$$V(x) = V_0(x) - fx, \tag{2.22}$$

where $V_0(x)$ is periodic with period L and where f is some tilting force. In one dimension, Eq. (2.14) tells us that $J_{\text{ss}}(x)$ is independent of x. Now, we can integrate Eq. (2.15) twice to find:

$$T_{\text{ss}}(x) = \frac{J_{\text{ss}}}{\rho c_p D} \int_0^x V(x')\, \mathrm{d}x' + c_1 x + c_2, \tag{2.23}$$

where c_1 and c_2 are constants that can be determined once the boundary conditions are known. Suppose that we allow our domain to extend out in either direction. Eq. (2.23) tells us that for a finite tilt f, the temperature grows as x^2. The origin of this phenomenon is that as the Brownian motor descends the potential, it dumps heat into the environment. Since heat can only dissipate in the x coordinate, the temperature will grow unbounded.

In higher dimensions, there are more degrees of freedom for heat to dissipate into. Therefore, we can avoid the pathological case in one dimension by diffusing the excess heat into an extra degree of freedom. Consider a two dimensional domain $(x, y) \in [0, L] \times [-l, l]$ where the potential is confining in the y direction and tilted periodic in the x direction: $V(x, y) = V_0(x, y) - fx$, where $V_0(x, y) = V_0(x + L, y)$ and $V_0(x, y) \to \infty$ as $y \to \pm l$. Now suppose that the temperature and the probability distribution are both periodic in the x direction and that the temperature is held fixed at the boundary in the y direction, i.e. $P(0, y) = P(L, y)$, $T(0, y) = T(L, y)$ and $T(x, \pm l) = b(x)$ for some given function $b(x)$. This case is explored in more detail in Figs. 5.2 and 5.3 of Chap. 5. Because the potential is confining in the y direction, we know that $\boldsymbol{J}_{\text{ss}}(x, \pm l) \cdot \hat{\boldsymbol{y}} = 0$, we now integrate Eq. (2.15) over the two dimensional domain:

$$D \int_{-l}^{l} \mathrm{d}y \int_0^L \mathrm{d}x\, \nabla \cdot [\nabla T_{\text{ss}}(x, y)] = \frac{1}{\rho c_p} \int_{-l}^{l} \mathrm{d}y \int_0^L \mathrm{d}x\, \boldsymbol{J}_{\text{ss}}(x, y) \cdot \nabla V(x, y). \tag{2.24}$$

We can use the divergence theorem on the left hand side to give:

$$\text{LHS} = D\left\{\int_0^L \mathrm{d}x\,\partial_y T_{\text{ss}}(x,\,l) + \int_l^{-l} \mathrm{d}y\,\partial_x T_{\text{ss}}(L,\,y) + \int_L^0 \mathrm{d}x\,\partial_y T_{\text{ss}}(x,\,-l) + \int_{-l}^{l} \mathrm{d}y\,\partial_x T_{\text{ss}}(0,\,y)\right\}. \tag{2.25}$$

As for the right hand side, we compute the x integral via integration by parts:

$$\text{RHS} = \frac{1}{\rho c_p}\int_{-l}^{l}\mathrm{d}y\left\{\Big[[\boldsymbol{J}_{\text{ss}}(x,\,y)V(x,\,y)]\cdot\boldsymbol{n}\Big]_{x=0}^{L} - \int_0^L \mathrm{d}x\,[\nabla\cdot\boldsymbol{J}_{\text{ss}}(x,\,y)]V(x)\right\}. \tag{2.26}$$

Noting that $\nabla\cdot\boldsymbol{J}_{\text{ss}}(x,\,y) = 0$, we can rearrange the LHS and RHS to give:

$$D\left\{\int_0^L \mathrm{d}x\,[\partial_y T_{\text{ss}}(x,\,l) - \partial_y T_{\text{ss}}(x,\,-l)] + \int_{-l}^{l}\mathrm{d}y\,[\partial_x T_{\text{ss}}(L,\,y) - \partial_x T_{\text{ss}}(0,\,y)]\right\} = \frac{1}{\rho c_p} fL\int_{-l}^{l}\mathrm{d}y\,\boldsymbol{J}_{\text{ss}}(L,\,y)\cdot\hat{\boldsymbol{x}}. \tag{2.27}$$

The LHS of Eq. (2.27) represents the heat flowing out of the system in the y direction, while the RHS represents the heat that is being produced by self-induced temperature gradients. Eq. (2.27) tells us that a steady state can be achieved on a two dimensional domain as long as the heat escaping the system (LHS of Eq. (2.27)) is equal to the work done on the system (RHS of Eq. (2.27)). These equations describe a system on a circular domain in x such that there is no physical way for heat to escape from the boundaries at $x = 0$ or $x = L$. This means that as well as $T_{\text{ss}}(0,\,y) = T_{\text{ss}}(L,\,y)$, we also have that $\partial_x T_{\text{ss}}(0,\,y) = \partial_x T_{\text{ss}}(L,\,y)$. Therefore, the second term on the LHS of Eq. (2.27) should be zero and we require that all of the heat escapes through the boundaries at $y = \pm l$. In Chap. 5 we will focus on numerical results on tilted two dimensional potentials that allow heat to dissipate in the y direction. We will show examples of how the heat flows when extra degrees of freedom are considered.

2.4 Dimensionless Parameters

Eqs. (1.4) and (2.1) contain many physical parameters relating to the properties of the environment and the Brownian system. In order to determine the regimes of our system and to make our numerical work easier, it is illustrative to reduce the equations of motion to their dimensionless form. For simplicity we will assume that $\gamma_j = \gamma$ in all dimensions. We now define L to be a characteristic length scale such that, on average only one Brownian motor is contained in the volume L^d, where d is the number of dimensions. We also define E_0 to be the energy scale of the potential barriers experienced by the motor. Alternatively, if there is a well defined temperature T_0 at the boundary, then we will set $E_0 = k_B T_0$. When possible, the latter technique is preferable because in this case, the potential will be scaled by $k_B T_0$. This is useful because Brownian motion on a potential with barrier heights b is often divided into two regimes [25, 46]: The deep well regime ($b > 5k_B T_0$) or the shallow well regime ($b < 5k_B T_0$).

If the potential is scaled by $k_B T_0$, then we can tell which regime we are in by looking at the barrier heights of our potential.

We now let $\hat{\boldsymbol{r}} \equiv \frac{\boldsymbol{r}}{L}$, $\hat{V}(\boldsymbol{r}) \equiv \frac{V(\boldsymbol{r})}{E_0}$ and $\hat{T}(\hat{\boldsymbol{r}}, t) \equiv k_B T(\boldsymbol{r}, t)/E_0$, with these definitions, we can write:

$$\partial_{\hat{t}} \hat{P}(\hat{\boldsymbol{r}}, \hat{t}) = -\hat{\nabla} \cdot \hat{\boldsymbol{J}}(\hat{\boldsymbol{r}}, \hat{t}), \tag{2.28}$$

$$\hat{\boldsymbol{J}}(\hat{\boldsymbol{r}}, \hat{t}) = -[\hat{P}(\hat{\boldsymbol{r}}, \hat{t})\hat{V}(\hat{\boldsymbol{r}}, \hat{t}) + \hat{T}(\hat{\boldsymbol{r}}, \hat{t})\hat{\nabla}\hat{P}(\hat{\boldsymbol{r}}, \hat{t})] \tag{2.29}$$

and

$$\partial_{\hat{t}} \hat{T}(\hat{\boldsymbol{r}}, \hat{t}) = -A\hat{\boldsymbol{J}}(\hat{\boldsymbol{r}}, \hat{t}) \cdot \hat{\nabla}\hat{V}(\hat{\boldsymbol{r}}) + B\hat{\nabla}^2 \hat{T}(\hat{\boldsymbol{r}}, t). \tag{2.30}$$

Where we have also defined $\hat{P}(\hat{\boldsymbol{r}}, \hat{t}) \equiv L^d P(\hat{\boldsymbol{r}}, \hat{t})$ and $\hat{t} \equiv \frac{E_0}{\gamma L^2} t$. In Eq. (2.30), we have defined the dimensionless parameters

$$A \equiv \frac{k_B}{\rho c_p} \frac{1}{L^d} \tag{2.31}$$

and

$$B \equiv \frac{\gamma D}{E_0}. \tag{2.32}$$

If we think of L^d as the volume occupied by one Brownian motor, then $\frac{1}{L^d}$ can be interpreted as the concentration of Brownian motors in phase space. With this in mind, we interpret A^{-1} to be the dimensionless heat capacity of the environment. As for B, note that temperature gradients will diffuse more rapidly with larger D and that Brownian motors will diffuse more rapidly for a larger value of $\frac{\gamma}{E_0}$. Therefore, B indicates how quickly temperature gradients diffuse relative to the rate of evolution of the Brownian motor. If A is made large, then any heat released or absorbed by the Brownian motor will have a large effect on the temperature of the environment. On the other hand, if B is made large, then any temperature gradients that are present will diffuse away rapidly. Suppose that we impose boundary conditions so that $\hat{T}(\hat{\boldsymbol{r}}, \hat{t})|_{\partial\Omega} = T_0$ and we have $A \ll 1 \ll B$. Any temperature gradients that form will quickly disappear and we will be left with $\hat{T}(\hat{\boldsymbol{r}}, \hat{t}) = T_0$ everywhere. In this regime, it is justifiable to ignore Eq. (2.30) and just deal with Eq. (2.29) by itself. Alternatively, if we do not have $A \ll 1$, then we will find that Eq. (2.30) will rapidly reach its steady state, however this steady state will not be free of self-induced temperature gradients. In this regime, we may adiabatically eliminate Eq. (2.30) in favor of its steady state solution. When we are in the regime $A \sim B$, both Eqs. (2.29) and (2.30) are required to describe both the dynamic and the steady state of the system.

In the steady state, we have:

$$\boldsymbol{J}(\boldsymbol{r}) \cdot \nabla V(\boldsymbol{r}) = \frac{B}{A} \nabla^2 T. \tag{2.33}$$

So, the steady state is determined by a single dimensionless parameter given by:

$$\frac{B}{A} = \frac{\gamma D \rho c_p L^d}{E_0 k_B} = \frac{k \gamma L^d}{E_0 k_B}, \tag{2.34}$$

where for the second equality we used that the thermal diffusivity D is given by $D = \frac{k}{\rho c_p}$, where k is the thermal conductivity of the environment with units $\mathrm{W}/(\mathrm{m} \cdot \mathrm{K})$. This means that although we need to know both B and A to know how long a system takes to reach the steady state, we only need to know the ratio $\frac{B}{A}$ to find the steady state. If $\frac{B}{A}$ is large, then self-induced temperature gradients will have a small effect on the Brownian system. Alternatively, if $\frac{B}{A}$ is small, then self-induced temperature gradients will have a large effect on the Brownian system.

For the remainder of this thesis, we will use the dimensionless equations [Eq. (2.29) and (2.30)] to model self-induced temperature gradients in Brownian motor dynamics. However, we will drop the hats for notational convenience.

Chapter 3

Numerical Methods

The key dimensionless equations describing Brownian motion with self-induced temperature gradients are:

$$\begin{aligned} \partial_t P(\boldsymbol{r}, t) &= -\nabla \cdot \boldsymbol{J}(\boldsymbol{r}, t), \\ \boldsymbol{J}(\boldsymbol{r}, t) &= -[P(\boldsymbol{r}, t) V(\boldsymbol{r}, t) + T(\boldsymbol{r}, t) \nabla P(\boldsymbol{r}, t)] \end{aligned} \tag{3.1}$$

and

$$\partial_t T(\boldsymbol{r}, t) = -A \boldsymbol{J}(\boldsymbol{r}, t) \cdot \nabla V(\boldsymbol{r}) + B \nabla^2 T(\boldsymbol{r}, t). \tag{3.2}$$

These equations can only be solved analytically in some special cases. For every other case, we will have to resort to numerical techniques to solve the system of equations. In this chapter, we will describe numerical techniques that we have developed to solve the coupled set of equations. We will show that our numerical techniques converge on the expected analytical results when available. In Section 3.3 we will also show that the numerical techniques are self-consistent when applied on a fine enough grid.

3.1 Finite Volume methods

The finite volume method is a numerical scheme for solving partial differential equations [61]. To illustrate the idea behind the finite volume method, consider Eq. (3.1). This equation tells us how the probability distribution evolves with time. The essential idea of the finite volume method is to divide the computational domain into cells. If the probability distribution is given at $t = 0$, then one can calculate the probability of being in each cell at $t = 0$. In order to find the probability of a particular cell at a later time, one must use Eq. (3.1) to calculate the flux of probability leaving and entering the cell. Upon doing so, one finds that the problem goes from being a partial differential equation for $P(\boldsymbol{r}, t)$, to a system of ordinary equations for the probabilities of each cell. The strength of the finite volume method is that the flux of probability leaving one cell must be equal to minus the flux from the adjacent cell. Therefore, if probability is conserved in the original equation, then the finite volume method will numerically conserve probability in the discretized equation. In this chapter, we will explain how we calculate the

fluxes in our equations and how we solve the resulting ordinary differential equations.

We have chosen to use the finite volume method, because it is well suited to conservation equations. However, Eq. (3.2) is not in the form of a conservation equation, since the first term is a source term that cannot be written as the divergence of a vector field. However, as discussed in Chap. 2, energy is a conserved property. This means that the energy density

$$u(\boldsymbol{r},\, t) = P(\boldsymbol{r},\, t)V(\boldsymbol{r}) + \frac{1}{A}T(\boldsymbol{r},\, t), \tag{3.3}$$

evolves via

$$\partial_t u(\boldsymbol{r},\, t) = -\nabla \cdot \left[V(\boldsymbol{r})\boldsymbol{J}(\boldsymbol{r},\, t) - \frac{B}{A}\nabla T(\boldsymbol{r},\, t)\right], \tag{3.4}$$

which is in the form of a conservation equation. Using the set of two conservation Eqs. (3.1) and (3.4) we can solve our system numerically to find $P(\boldsymbol{r},\, t)$ and $T(\boldsymbol{r},\, t)$ [via Eq. (3.3)] as a function of time.

The numerical approach we use consists of discretizing Eqs. (3.1) and (3.4) in space via finite volumes and propagating the system forward in time using the method of lines [62]. We will first explain this process in one spatial dimension and in Sec. 3.1.2, we will extend the technique to two dimensions. We discretize using a uniformly spaced grid, with grid spacing Δx and each grid point denoted with an index $i : i \in 1,\, 2,\, ...,\, N$, where N is the number of grid points. The grid points are, $x_i = x_0 + i\Delta x$ where x_0 is the left boundary of the system. We also define $f_i = f(x_i)$ for any function of x. We will sometimes refer to points such as $x_{i+\frac{1}{2}}$, these points correspond to the points $x = x_0 + \left(i + \frac{1}{2}\right)\Delta x$. In order to find the value $f(x_{i+\frac{1}{2}})$, we use linear interpolation. If we define

$$\bar{p}_i = \frac{1}{\Delta x}\int_{x_{i-1}}^{x_i} P(x)\,\mathrm{d}x, \tag{3.5}$$

$$\bar{u}_i = \frac{1}{\Delta x}\int_{x_{i-1}}^{x_i} u(x)\,\mathrm{d}x, \tag{3.6}$$

and

$$J_i = -\left[P_i(\partial_x V)_i + T_i(\partial_x P)_i\right], \tag{3.7}$$

$$K_i = J_i V_i - \frac{B}{A}(\partial_x T)_i, \tag{3.8}$$

then the discretized equations of motion become

$$\frac{\mathrm{d}\bar{p}_i}{\mathrm{d}t} = \frac{1}{\Delta x}[J_{i-\frac{1}{2}} - J_{i+\frac{1}{2}}], \tag{3.9}$$

$$\frac{\mathrm{d}\bar{u}_i}{\mathrm{d}t} = \frac{1}{\Delta x}[K_{i-\frac{1}{2}} - K_{i+\frac{1}{2}}]. \tag{3.10}$$

Evaluating the spatial derivatives $(\partial_x P)_i$ and $(\partial_x T)_i$ via finite differences, we get:

$$\begin{aligned}\frac{\mathrm{d}\bar{p}_i}{\mathrm{d}t} = \frac{1}{\Delta x}\Bigg[&\bar{p}_{i-1}\left(-\frac{(\partial_x V)_{i-\frac{1}{2}}}{2} + \frac{T_{i-1}+T_i}{2\Delta x}\right)\\ &+\bar{p}_i\left(-\frac{(\partial_x V)_{i-\frac{1}{2}} - (\partial_x V)_{i+\frac{1}{2}}}{2}\right.\\ &\qquad\left.-\frac{T_{i-1}+2T_i+T_{i+1}}{2\Delta x}\right)\\ &+\bar{p}_{i+1}\left(\frac{(\partial_x V)_{i+\frac{1}{2}}}{2} + \frac{T_{i+1}+T_i}{2\Delta x}\right)\Bigg],\end{aligned} \tag{3.11}$$

$$\begin{aligned}\frac{\mathrm{d}\bar{u}_i}{\mathrm{d}t} = \frac{1}{\Delta x}\Bigg[&-\left(\bar{p}_{i-\frac{1}{2}}(\partial_x V)_{i-\frac{1}{2}} + T_{i-\frac{1}{2}}\frac{\bar{p}_i - \bar{p}_{i-1}}{\Delta x}\right)V_{i-\frac{1}{2}}\\ &+\left(\bar{p}_{i+\frac{1}{2}}(\partial_x V)_{i+\frac{1}{2}} + T_{i+\frac{1}{2}}\frac{\bar{p}_{i+1} - \bar{p}_{i-1}}{\Delta x}\right)V_{i+\frac{1}{2}}\\ &+\frac{B}{A\Delta x}\left(T_{i-1} - 2T_i + T_{i+1}\right)\Bigg],\end{aligned} \tag{3.12}$$

where from Eq. (3.3) we have

$$T_i = A\left(\bar{u}_i - \bar{p}_i V_i\right). \tag{3.13}$$

To simulate the system, at each time step we use Eqs. (3.11), (3.12) and (3.13) to update $\bar{p}_i$, $\bar{u}_i$ and T_i, respectively. Given initial and boundary conditions, this set of equations can be solved numerically as a system of ordinary differential equations (ODEs) coupled to an algebraic equation. These differential equations are solved using Julia [63], where we use the DifferentialEquations.jl package [64].

3.1.1 Numerically calculating the steady state

Setting the left hand side of Eqs. (3.9) and (3.10) to zero gives us a very natural way of finding the steady state of the system. We can also apply the boundary conditions to P and T directly, depending on the physical situation that we are modeling. One particular case of interest is the case where the probability density is periodic (and normalized), while the temperature is held fixed at both ends, so that $T_1 = T_l$ and $T_N = T_r$. An example of such a case is explored

in Chap. 4.4. In order to solve this problem, we have to solve $2N$ equations given by:

$$J_{i-\frac{1}{2}} = J_{i+\frac{1}{2}} \quad \forall\, i \in 2, ..., N-2, \tag{3.14a}$$

$$K_{i-\frac{1}{2}} = K_{i+\frac{1}{2}} \quad \forall\, i \in 2, ..., N-2, \tag{3.14b}$$

$$\sum_{i=1}^{N} \bar{p}_i = \frac{1}{\Delta x}, \tag{3.14c}$$

$$\bar{p}_1 = \bar{p}_N \tag{3.14d}$$

$$T_1 = T_l, \tag{3.14e}$$

$$T_N = T_r. \tag{3.14f}$$

Eqns. (3.14) are non-linear in both P and T, so they cannot be written as a matrix equation. Instead, we must use iterative numerical techniques suited to non-linear equations. In order to do this, Eq. (3.14) is input into JuMP.jl [65], as a root finding problem and solved using the Ipopt solver [66].

3.1.2 Two Dimensions

The idea of the finite volume method is the same in two dimensions as it is in one dimension. However, here a two dimensional domain $(x,\, y) \in [x_1,\, x_{N_x}] \times [y_1,\, y_{N_y}]$ is discretized onto a grid with orthogonal gridlines and constant grid spacing. On this grid, we have N_x points in the x direction and N_y points in the y direction. In two dimensions, we integrate our variable over the i, jth control volume, so that:

$$\begin{aligned} \bar{p}_{i,\,j} &\equiv \int_{x_{i-1}}^{x_i} \mathrm{d}x \int_{y_{i-1}}^{y_i} \mathrm{d}y\, P(x,\, y), \\ \bar{u}_{i,\,j} &\equiv \int_{x_{i-1}}^{x_i} \mathrm{d}x \int_{y_{i-1}}^{y_i} \mathrm{d}y\, u(x,\, y). \end{aligned} \tag{3.15}$$

Like the one dimensional case, we use the divergence theorem to find how $p_{i,\,j}$ and $u_{i,\,j}$ change with time. Without evaluating the current, we find:

$$\begin{aligned} \frac{\mathrm{d}\bar{p}_{i,\,j}}{\mathrm{d}t} &= -\oint_{\partial \mathcal{V}_{i,\,j}} \boldsymbol{J} \cdot \hat{\boldsymbol{n}}, \\ \frac{\mathrm{d}\bar{u}_{i,\,j}}{\mathrm{d}t} &= -\oint_{\partial \mathcal{V}_{i,\,j}} \boldsymbol{K} \cdot \hat{\boldsymbol{n}} \end{aligned} \tag{3.16}$$

where $\oint_{\partial \mathcal{V}_{i,\,j}}$ represents a surface integral over the boundary of the $(i,\, j)$th control volume and where $\hat{\boldsymbol{n}}$ represents the unit normal vector of the control volume. Here we see the added difficulty of two dimensions, not only do we have to compute the current at every control volume, but we also need to integrate the current over the surface of the control volume. We use the finite difference method from Eqs. (3.11) and (3.12) to calculate the current in both directions separately. Meanwhile, we use the second order midpoint rule to calculate the surface

integrals. Putting this together, we get the following definitions:

$$\begin{aligned}
\boldsymbol{J}(x_{i-\frac{1}{2}},\, y_j)\cdot\hat{\boldsymbol{x}} &= -\left[\frac{1}{2}(P_{i-1,\,j}+P_{i,\,j})\nabla_x V\left(x_i-\frac{\Delta x}{2},\, y_j\right)+\frac{1}{2}(T_{i-1,\,j}+T_{i,\,j})\frac{P_{i,\,j}-P_{i-1,j}}{\Delta x}\right],\\
\boldsymbol{J}(x_i,\, y_{j-\frac{\Delta x}{2}})\cdot\hat{\boldsymbol{y}} &= -\left[\frac{1}{2}(P_{i,\,j-1}+P_{i,\,j})\nabla_y V\left(x_i,\, y_j-\frac{\Delta y}{2}\right)+\frac{1}{2}(T_{i,\,j-1}+T_{i,\,j})\frac{P_{i,\,j}-P_{i,j-1}}{\Delta y}\right],\\
\frac{\mathrm{d}\bar{p}_{i,\,j}}{\mathrm{d}t} &= \{[\boldsymbol{J}(x_{i-\frac{1}{2}},\, y_j)\cdot\hat{\boldsymbol{x}}-\boldsymbol{J}(x_{i+\frac{1}{2}},\, y_j)\cdot\hat{\boldsymbol{x}}]\Delta y\\
&\quad+[\boldsymbol{J}(x_i,\, y_{j-\frac{\Delta x}{2}})\cdot\hat{\boldsymbol{y}}-\boldsymbol{J}(x_i,\, y_{j+\frac{\Delta x}{2}})\cdot\hat{\boldsymbol{y}}]\}\Delta x,\\
\frac{\mathrm{d}\bar{u}_{i,\,j}}{\mathrm{d}t} &= \{[\boldsymbol{K}(x_{i-\frac{1}{2}},\, y_j)\cdot\hat{\boldsymbol{x}}-\boldsymbol{K}(x_{i+\frac{1}{2}},\, y_j)\cdot\hat{\boldsymbol{x}}]\Delta y\\
&\quad+[\boldsymbol{K}(x_i,\, y_{j-\frac{\Delta x}{2}})\cdot\hat{\boldsymbol{y}}-\boldsymbol{K}(x_i,\, y_{j+\frac{\Delta x}{2}})\cdot\hat{\boldsymbol{y}}]\}\Delta x
\end{aligned}\tag{3.17}$$

This strategy is referred to as the centered difference method (CDM) [61] and has $\mathcal{O}(\Delta x^2)$ spatial convergence.

3.1.3 Boundary Conditions

In both one and two dimensions, we will need to enforce boundary conditions for our equations to make sense. To see why, consider Eq. (3.11) and let $i = 1$. In this case we get the equation:

$$\begin{aligned}
\frac{\mathrm{d}\bar{p}_1}{\mathrm{d}t} = \frac{1}{\Delta x}\Bigg[&\bar{p}_0\left(-\frac{(\partial_x V)_{-\frac{1}{2}}}{2}+\frac{T_0+T_1}{2\Delta x}\right)\\
&+\bar{p}_0\left(-\frac{(\partial_x V)_{-\frac{1}{2}}-(\partial_x V)_{\frac{1}{2}}}{2}\right.\\
&\qquad\left.-\frac{T_0+2T_1+T_2}{2\Delta x}\right)\\
&+\bar{p}_2\left(\frac{(\partial_x V)_{\frac{3}{2}}}{2}+\frac{T_2+T_1}{2\Delta x}\right)\Bigg].
\end{aligned}\tag{3.18}$$

Among other things, this equation requires the quantity $\bar{p}_0$, which we do not know. In order to solve this problem, we use the idea of ghost cells [67]. In this strategy, the value of $\bar{p}_0$ is determined by the boundary conditions. For example, imagine that we apply Dirichlet boundary conditions to the probability distribution, so that $P(x,\, t) = P_L$ for $x < x_1$ and $P(x,\, t) = P_R$ for $x > x_N$. In this case, we would let $\bar{p}_0 = P_L$ and $\bar{p}_{N+1} = P_R$. If we make similar definitions for the temperature and the potential just outside of the domain, then Eq. (3.11) will be well defined for all values of i.

When employing the ghost cell technique, Dirichlet boundary conditions are the easiest type of boundary condition to implement. We will also consider Neumann boundary conditions, confining boundary conditions and periodic boundary conditions. In this thesis, we only consider the special case of Neumann boundary conditions where the gradient is set to zero at the boundaries. When this is the case, we add two equations to the ODEs that we solve. These are $\bar{p}_0 = \bar{p}_1$ for the left side and $\bar{p}_{N+1} = \bar{p}_N$ for the right side. Note that, unlike Dirichlet

boundary conditions, Neumann boundary conditions do not give us a fixed value for the ghost cells. Instead, when we are working with Neumann boundary conditions, we have to add some algebraic equations to our set of ODEs.

The remaining types of boundary conditions that we apply are periodic and confining boundary conditions. For both of these types of boundary condition, we will apply the boundary conditions to the currents rather than to the variables. For example, confining boundary conditions can be realized by setting the currents leaving the system to zero. An easier way to obtain confining boundary conditions is to simply let the potential become very large near the boundary. As for periodic boundary conditions, we make sure that the current leaving one side is the same as the current entering the other side. For example, the heat flowing from cell i to cell $i+1$ is given by $Q_{i\to i+1} = \frac{B}{A}\frac{T_{i+1}-T_i}{\Delta x}$. So if the flow of heat is to be periodic, then we require that $Q_{N\to 1} = \frac{B}{A}\frac{T_2-T_N}{\Delta x}$ and $Q_{1\to N} = \frac{B}{A}\frac{T_2-T_{N-1}}{\Delta x}$.

In two dimensions, every cell on the boundary requires its own ghost cell. The cells at the corners of our domain will require two ghost cells. We use the same rules as in one dimension to decide the value of the ghost cell for Dirichlet boundary conditions. For every other type of boundary condition, we add boundary equations in the same way as we did for one dimensional boundary conditions.

3.2 Spectral methods

When our system is on a periodic domain, we can discretize our equations by transforming them into Fourier space. In particular, the technique that we will employ is called the Fourier-Galerkin method [68]. We will first describe this method in one dimension, on the interval $x \in [0,\, 1]$, where we have the inner product $\langle f(x),\, g(x)\rangle \equiv \int_0^1 \mathrm{d}x\, f(x)\overline{g(x)}$. We choose the basis functions:

$$v_k(x) = \exp(-i2\pi kx) : k \in -\frac{N}{2},\, -\frac{N}{2}+1,\, ...,\, \frac{N}{2}, \tag{3.19}$$

for some $N \in \mathbb{N}$, which represents our cutoff frequency. With these basis functions, we have $\langle v_k(x),\, v_{k'}(x)\rangle = \delta_{k-k'}$, so our basis is orthonormal. We can now use these basis functions to find the weak form of Eq. (2.29):

$$\langle \partial_t P(x,\, t),\, v_{k'}(x)\rangle = \langle \partial_x[P(x,\, t)(\partial_x V(x) - f) + T(x,\, t)\partial_x P(x,\, t)],\, v_{k'}(x)\rangle. \tag{3.20}$$

Likewise, the weak form of Eq. (2.30) is given by:

$$\begin{aligned}\langle \partial_t T(x,\, t),\, v_{k'}(x)\rangle =& -A\langle [P(x,\, t)(\partial_x V(x) - f) + T(x,\, t)\partial_x P(x,\, t)]\partial_x V(x),\, v_{k'}(x)\rangle \\ &+ B\langle \partial_x^2 T(x,\, t),\, v_{k'}\rangle.\end{aligned} \tag{3.21}$$

We now make the following definitions:

$$\begin{aligned} P(x,\,t) &= \sum_k a_k(t) v_k(x), \\ T(x,\,t) &= \sum_l b_l(t) v_l(x), \\ V(x) &= \sum_m c_m v_m(x), \end{aligned} \tag{3.22}$$

which we can substitute into Eqs. (3.20) and (3.21). After some algebra, we find:

$$\frac{\mathrm{d}a_{k'}}{\mathrm{d}t} = -4\pi^2 \left(\sum_{m+k=k'} k a_k m c_m + a_k m^2 c_m \right) - i2\pi f k' a_{k'} - 4\pi^2 \left(\sum_{l+k=k'} l b_l k a_k + b_l k^2 a_k \right), \tag{3.23}$$

for the weak form of Eq. (2.29) and:

$$\begin{aligned} \frac{\mathrm{d}b_{k'}}{\mathrm{d}t} = A \Bigg[& i4\pi f m' c_{m'} + f^2 + i2\pi \left(\sum_{k+m+m'=k'} a_k m c_m m' c_{m'} \right) \\ & + 4\pi^2 \left(\sum_{k+l+m'=k'} b_l k a_k m' c_{m'} \right) \\ & - i2\pi f \sum_{k+l=k'} b_l k a_k \Bigg] - 4\pi^2 B k'^2 b_{k'}, \end{aligned} \tag{3.24}$$

for the weak form of Eq. (2.30). We notice that there are terms of the form:

$$S_{k'} = \sum_{i+j=k'} u_i v_j. \tag{3.25}$$

If k' runs over N values, then these terms require $\mathcal{O}(N^2)$ operations to compute. However, since Eq. (3.25) can be thought of as the convolution of the vectors u and v, one can use the fast Fourier transform to compute the products in only $\mathcal{O}(\frac{3}{2}N \log N)$ operations. Defining

$$\boldsymbol{k} = \begin{pmatrix} -\frac{N}{2} \\ -\frac{N}{2}+1 \\ \vdots \\ \frac{N}{2}-2 \\ \frac{N}{2}-1 \end{pmatrix}, \quad \boldsymbol{a} = \begin{pmatrix} a_{-\frac{N}{2}} \\ a_{-\frac{N}{2}+1} \\ \vdots \\ a_{\frac{N}{2}-2} \\ a_{\frac{N}{2}-1} \end{pmatrix}, \quad \boldsymbol{b} = \begin{pmatrix} b_{-\frac{N}{2}} \\ b_{-\frac{N}{2}+1} \\ \vdots \\ b_{\frac{N}{2}-2} \\ b_{\frac{N}{2}-1} \end{pmatrix}, \quad \boldsymbol{c} = \begin{pmatrix} c_{-\frac{N}{2}} \\ c_{-\frac{N}{2}+1} \\ \vdots \\ c_{\frac{N}{2}-2} \\ c_{\frac{N}{2}-1} \end{pmatrix} \tag{3.26}$$

and explicitly writing the products as convolutions yields:

$$\begin{aligned}\frac{\mathrm{d}\boldsymbol{a}}{\mathrm{d}t} &= -4\pi^2[(\boldsymbol{k}\circ\boldsymbol{a})*(\boldsymbol{k}\circ\boldsymbol{c})+\boldsymbol{a}*(\boldsymbol{k}^2\circ\boldsymbol{c})-(\boldsymbol{k}\circ\boldsymbol{b})*(\boldsymbol{k}\circ\boldsymbol{a})-\boldsymbol{b}*(\boldsymbol{k}^2\circ\boldsymbol{a})]-i2\pi f\boldsymbol{k}\circ\boldsymbol{a},\\ \frac{\mathrm{d}\boldsymbol{b}}{\mathrm{d}t} &= A[i4\pi f(\boldsymbol{m}\circ\boldsymbol{c})+f^2+i2\pi\{\boldsymbol{a}*[(\boldsymbol{k}\circ\boldsymbol{c})*(\boldsymbol{k}\circ\boldsymbol{c})]\}\\ &\quad+4\pi^2\{\boldsymbol{b}*[(\boldsymbol{k}\circ\boldsymbol{a})*(\boldsymbol{k}\circ\boldsymbol{c})]\}-i2\pi f\boldsymbol{b}*(\boldsymbol{k}\circ\boldsymbol{a})]\end{aligned} \tag{3.27}$$

where $\circ$ represents the Hadamard product (elementwise multiplication).

This spectral discretization has reduced two partial differential equations into $2N$ ordinary differential equations specifying the coefficients a_k and b_l. As with the finite volume method, we can directly solve the ordinary differential equations to get the dynamic state of the system and we can set the left hand side of the equation to zero to find the steady state. In order for the steady state to be normalized, we must have $\int_0^1 \mathrm{d}x\, P(x,\, t) = \int_0^1 \mathrm{d}x\, \sum_k a_k v_k(x) = a_0 = 1$. Therefore, once we find the Jacobian for the right hand side, we must add this condition in order to find the steady state. Similar to the finite volume method, we must choose our grid size carefully so that the trade off between computation time and accuracy is met.

3.3 Convergence analysis

In general, a numerical technique will not exactly agree with the true solution of the partial differential equation that it is trying to solve. As well as this, our system of equations can only be solved analytically in a very small number of cases. In this section, we will test out our numerical techniques in two ways. (i) We will solve the equation analytically and check that the numerical solution converges on the analytical solution for a fine enough grid (proving that the numerics are consistent with the true solution in some cases). (ii) When there is no analytical solution, we will check that our numerical solution converges to some solution as the grid is refined (proving that the numerics are self-consistent in some cases). We will perform convergence analyses for both the finite volume method and the spectral method separately.

3.3.1 Boltzmann distribution

If the steady state of the system is in equilibrium with the environment (no energy is exchanged with the environment in the steady state), then the steady state of the system will be a Boltzmann distribution. This will be true regardless of whether or not self-induced temperature gradients are considered. Therefore, one way to test our numerical methods is to simulate the system forward in time on an equilibrium potential with a constant temperature and see whether or not the system reaches the Boltzmann distribution after some time. Another slightly related technique is to insert the discretized Boltzmann distribution into the right hand side of the ODEs described earlier. If the ODEs have correctly discretized the system, then their right hand sides should return zero when the Boltzmann distribution inserted. Figure 3.1 shows the results with the finite volume method and 3.2 shows the results with the spectral method.

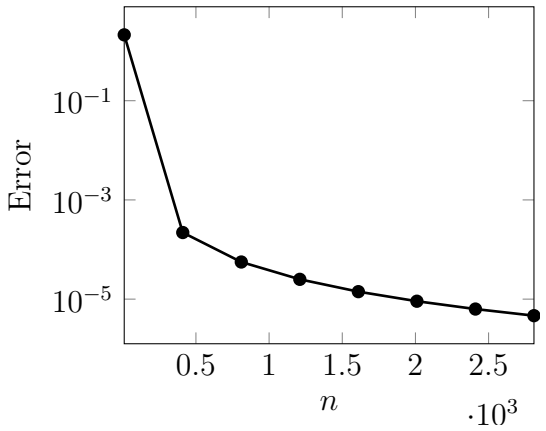

Figure 3.1: Finite volume convergence to the Boltzmann distribution. For each n, we calculated the Boltzmann distribution on an $n \times n$ grid and we then calculated the net flux in and out of each cell using Eq. 3.17. We then subtracted the minimum flux from the maximum flux. We used the two dimensional potential $V(x, y) = \cos(2\pi x) + 8y^2$ on the domain $(x, y) \in [0, 1] \times [-1, 1]$. The temperature was fixed at $T(x, y) = 1$.

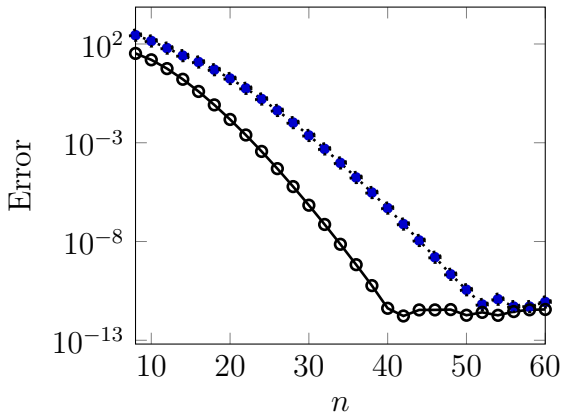

Figure 3.2: Spectral convergence to the Boltzmann distribution, n represents the cutoff frequency for both the x and y direction. The circular markers represent the potential $V(x, y) = \sin(2\pi x)$ and the squares represent the potential $V(x, y) = 6[\sin(2\pi x) + \sin(2\pi y)]$. In both cases, the temperature was set to $T(x, y) = 1$

Figure 3.1 shows the finite volume method converging to the Boltzmann distribution. In Fig. 3.1, we see that at first the error decreases quite rapidly and then when n gets larger, the decrease becomes less steep. In Sec. 3.1.2, we pointed out that the central difference method converges with $\mathcal{O}(\Delta x^2)$. As we increase the number of grid points, n, the grid spacing Δx goes down like $\frac{1}{n}$. Therefore, we expect the error of the finite volume method to decrease as $\mathcal{O}(\frac{1}{n^2})$.

In Fig. 3.2, we calculate the error for the spectral method. In Fig. 3.2, we calculate the spectral error on an equilibrium potential. In order to calculate the error, we inserted the Boltzmann distribution (and a constant temperature) into Eq. (3.27). If our technique correctly discretizes the system then we should get back a vector of zeros. Therefore, we define the spectral error to be the norm of the returned vector. In Fig. 3.2, we see that the error for the spectral method decreases exponentially (a straight line on the log scale). For different potentials, the convergence is slightly different, however, the exponential property remains. We also see that once the method reaches a certain accuracy, increasing the number of frequencies no longer increases the accuracy of the method. The initial exponential convergence is common with spectral discretizations and is sometimes referred to as spectral convergence [68, 69]. The reason that this exponential convergence does not continue indefinitely is due to floating point error in our computational implementation. In all of our numerical computations, we use 64 bit floating point values to store numbers. Arbitrary real numbers cannot be perfectly represented by floating point numbers, so every computation has an associated floating point error. When the discretisation error becomes less than the accumulated floating point error, increasing the number of frequencies will not improve our numerical approximation. Instead, we would have to increase our floating point precision. This would slow down our computations and would only benefit us if we wanted very high precision. In this thesis, we will not require higher precision than the precision shown in Fig. 3.2, so we will only use 64 bit floating point numbers.

3.3.2 Convergence to a Non-Equilibrium Steady State

Here we consider cases where even the steady state cannot be found analytically. In Fig. 3.3, we find the steady state for multiple grid sizes. For each grid size, the result is linearly interpolated onto the finest grid (which has N grid points in each direction). We then compare the interpolated result to the result calculated using the fine grid. To compare the interpolated result $\phi^{\text{Itp}}_{i,j}$ to the result on the fine grid $\phi^{\text{Fine}}_{i,j}$, we first calculate a new array $E_{i,j} \equiv \phi^{\text{Itp}}_{i,j} - \phi^{\text{Fine}}_{i,j}$. $E_{i,j}$ tells us how poorly the interpolated result approximates the result on the fine grid. In order to reduce this difference to a single number, we calculate $\text{Error} = \max(E_{i,j}) - \min(E_{i,j})$.

In Figs. 3.3 and 3.4, we show the convergence to the steady state for the finite volume method and the spectral method respectively. Once again, we see that the finite volume methods converge with $\mathcal{O}(\Delta x^2)$, while the spectral methods converge exponentially.

Iterative Convergence

For each of the points in Figs. 3.3 and 3.4 we had to iterate from a certain initial condition to the steady state. In the case of the finite volume methods, we needed to solve the following

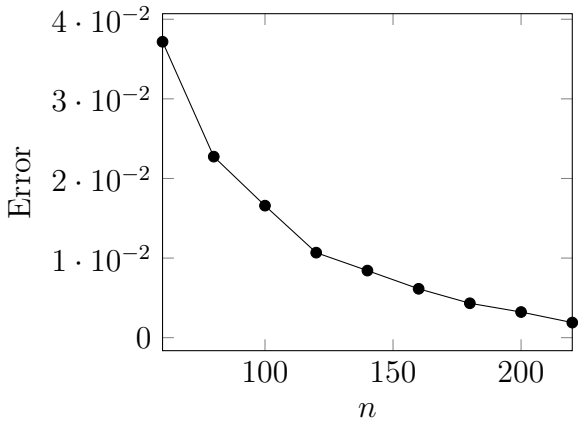

Figure 3.3: Finite volumes convergence to the steady state. For each n, we use n points in the x and y directions. We then interpolate the result onto the finest grid size and compared the difference between the fine grid and the coarse one. We used the two dimensional potential $V(x,\, y) = \cos(2\pi x) + 10y^2 - x$ on the domain $(x,\, y) \in [0,\, 1] \times [-1,\, 1]$. The temperature was fixed at the boundaries so that $T(x,\, y = \pm 1) = 1$, we also set $\frac{B}{A} = 1$.

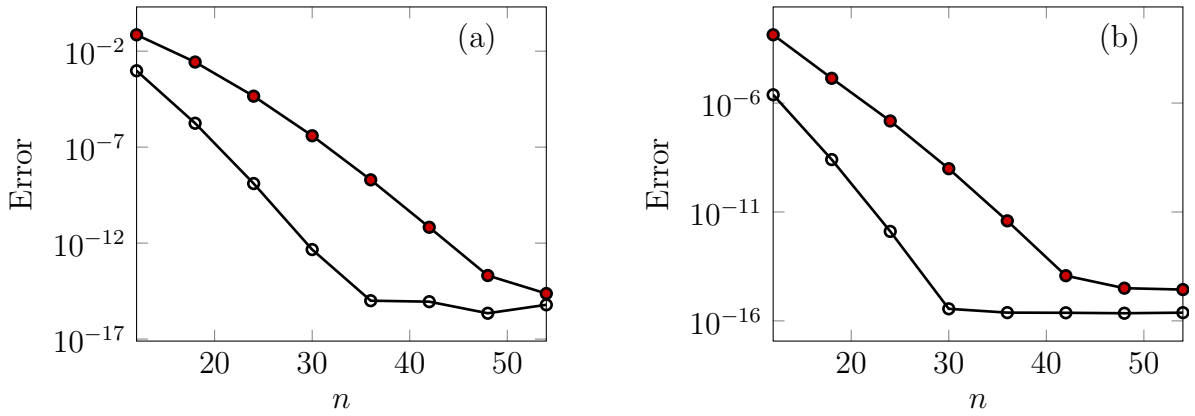

Figure 3.4: Spectral convergence to the steady state. The unfilled circled represent the potential $V(x,\, y) = \cos(2\pi x) + 2\cos(2\pi y)$, while the filled circles represent the potential $V(x,\, y) = \cos(2\pi x) + 6\cos(2\pi y)$. In both figures, we imposed a force given by $f = \hat{\boldsymbol{x}} + 0.5\hat{\boldsymbol{y}}$ and we set $\frac{B}{A} = 1$ and $T_0 = 1$.

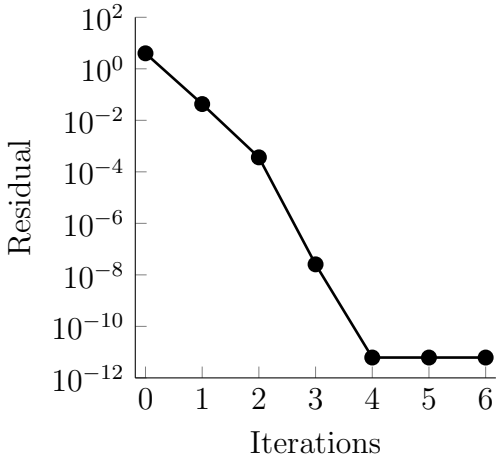

Figure 3.5: Iterative convergence for the finite volume methods on a 100×100 grid. At each iteration we calculate the residual to be Residual $= \frac{1}{N_x N_y} \sum_{i,\,j} (\frac{\mathrm{d}\bar{p}_{i,\,j}}{\mathrm{d}t})^2 + (\frac{\mathrm{d}\bar{u}_{i,\,j}}{\mathrm{d}t})^2$. We consider the potential $V(x) = -3x + 4\cos(2\pi x) + 20y^2$ on the domain $(x,\, y) \in [0,\, 1] \times [-1,\, 1]$. Both the temperature and the probability distribution are periodic in the x direction and we set $T(x,\, y = \pm 1) = 1$. In this figure, we have set $\frac{B}{A} = 1$.

equations:

$$\begin{aligned} \frac{\mathrm{d}\bar{p}_{i,\,j}}{\mathrm{d}t} &= 0 \quad \text{for all } i,\, j \\ \frac{\mathrm{d}\bar{u}_{i,\,j}}{\mathrm{d}t} &= 0 \quad \text{for all } i,\, j. \end{aligned} \tag{3.28}$$

For the spectral methods, we had to solve the equations:

$$\begin{aligned} \frac{\mathrm{d}\boldsymbol{a}}{\mathrm{d}t} &= \mathbf{0}, \\ \frac{\mathrm{d}\boldsymbol{b}}{\mathrm{d}t} &= \mathbf{0}. \end{aligned} \tag{3.29}$$

In both cases, these are a set of non linear equations which can be solved using Newton's method. In Figs. 3.5 and 3.6, we show the iterative convergence for the spectral and the finite volume methods respectively. In both cases, we see that Newton's method very rapidly finds a solution to the non linear equations.

3.4 Chapter Summary

We have developed two numerical schemes for solving Eqs. (3.1) and (3.2) both in one dimension and in two dimensions. The first scheme that we describe is an adaptation of the finite volume method, which exploits the underlying physics of our system. In particular, we exploited the fact that our system conserves energy and probability. We can apply our finite volume methods to systems with a number of boundary conditions. In particular, we can consider systems that have Dirichlet or Neumann boundary conditions or systems where the probability distribution is confined. We can also consider systems that are periodic in one direction while having arbitrary

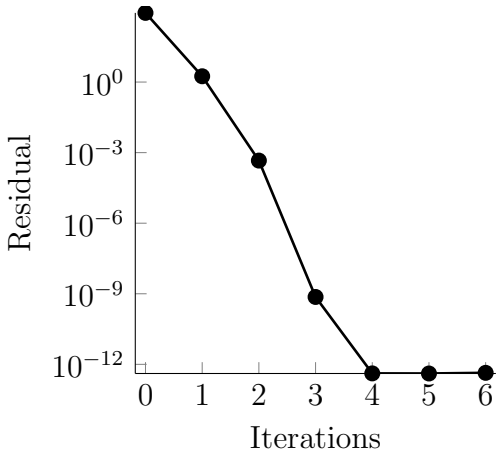

Figure 3.6: Iterative convergence for the spectral methods with a cuttoff frequency of $n_c = 128$. We use an iterative method to find the steady state of a two dimensional system. The system is placed on the potential $V(x) = -0.4x + 4[\cos(2\pi x) + \sin(4\pi x)]$ over the domain $x \in [0, 1]$. We define the residual as being given by Residual $= \frac{1}{n_c}\sum_i (\frac{\mathrm{d}\boldsymbol{a}_i}{\mathrm{d}t})^2 + (\frac{\mathrm{d}\boldsymbol{b}_i}{\mathrm{d}t})^2$. $\frac{B}{A} = 1 \times 10^{-2}$.

boundary conditions in the other direction.

Another interesting case is where the system is fully periodic. Assuming that the system is fully periodic limits the number of physical situations that one can model. In particular, when the system is fully periodic, no heat can escape through the bundary of the system. However, when modeling a fully periodic domain, one can use Fourier spectral methods. The Fourier spectral method involves discretizing the equations of motion by writing the temperature and the probability as a Fourier series. The non linear terms in Eqs. (3.1) and (3.2) correspond to convolutions of the coefficients in the Fourier series. We use established Fourier transform methods to compute these convolutions, therefore significantly increasing our computational efficiency.

In Sec. 3.3, we provided results describing how our methods converged as we increased the grid size in our approximations. Our spectral methods converged exponentially while our finite volume methods converged as $\mathcal{O}(\Delta x^2)$. We found that, even on a two dimensional domain, we are able to make our spectral discretisation error smaller than floating point error brought about by 64 bit floating point numbers. The rapid convergence of spectral methods is well known in the literature [68, 69]. We cannot reach such high precision with the finite volume methods. However, the finite volume methods allow us to explore a richer set of boundary conditions than the spectral methods.

Chapter 4

One Dimensional Potentials

In this chapter, we will consider Brownian motors diffusing over one dimensional potentials. Throughout this chapter, we will use the dimensionless Eqs. (3.1) and (3.2) introduced in Chap. 2.4. Before we consider specific one dimensional potentials, we will note that there are certain general results on one dimensional potentials that can help guide us. As discussed in Chap. 2.3, in one dimension the steady state current ($J_{\rm ss}$) is constant and the steady state temperature is given by Eq. (2.23), which has the dimensionless form:

$$T_{\rm ss}(x) = J_{\rm ss}\frac{B}{A}\int_0^x V(x')\,{\rm d}x' + c_1 x + c_2. \tag{4.1}$$

If $J_{\rm ss} = 0$, then the temperature is a straight line, which is what we would expect from the heat equation alone. If $J_{\rm ss} \neq 0$, then the temperature develops oscillations that remain in the steady state. As discussed in Chap. 2.3, if the potential is confining and if $T_{\rm ss}$ does not depend on x, then $J_{\rm ss} = 0$. When $J_{\rm ss} = 0$, the steady state probability distribution becomes the Boltzmann distribution,

$$P_{\rm ss}(x) = \mathcal{N}\exp\left[-\frac{V(x)}{T_{\rm ss}}\right], \tag{4.2}$$

meaning that the system is in equilibrium with its environment. The steady state temperature depends on the boundary conditions and on the initial energy of the system. The steady state form of our system in a confining potential is the only situation that we can completely solve analytically. For all other cases, we will employ the numerical techniques discussed in Chap. 3.

In this chapter, we will consider some potentials that have equilibrium steady states. Strictly speaking, these types of potentials are not related to Brownian motors, however, we will see that they help clarify some of the physics behind self-induced temperature gradients. Sec. 4.1 will consider Brownian dynamics on a bistable potential. We will use the bistable potential to directly demonstrate the effect of self-induced temperature gradients on the steady state of an equilibrium system. Also, since the bistable potential can be thought of as two stable states separated by a barrier, we will use the bistable potential to demonstrate the effect that self-induced temperature gradients have on barrier crossing rates, which are important for Brownian motors [14,35]. In Sec. 4.2, we discuss Brownian dynamics on a metastable potential. This will give us an opportunity to focus on barrier crossing in a case where the Brownian parti-

cles are only crossing the barrier in one direction. We will use this to show how the parameters A and B create different scenarios for barrier crossing.

A tightly coupled Brownian motor can be approximated by a one dimensional potential [13, 18, 19]. Brownian motors are out of equilibrium systems, because they continually exchange energy with their environment. We are interested in the steady state of these out of equilibrium systems. For one dimensional time-independent potentials (the subject of this chapter), there are two types of potentials that admit out of equilibrium steady states. The first possibility is a tilted potential on an infinite domain. However, in Chap. 2, we saw that this type of one dimensional system does not have a meaningful steady state when self-induced temperature gradients are being considered. The second possibility is a tilted periodic potential on a finite domain where a particle passing through one side will appear on the other side. This type of potential will be the subject of Secs. 4.3 and 4.4, where we will see that the non-zero steady state current strongly influences the steady state of the system. Sec. 4.3 will be the first scenario that we will consider that will be relevant to Brownian motors [18, 19, 44]. We will see that self-induced temperature gradients reduce the rate at which a Brownian motor descends a tilted periodic potential. Finally, Sec. 4.4 will present a heat engine and a heat pump that utilizes self-induced temperature gradients.

4.1 Bistable Potential

In this section, we will consider a bistable potential of the form:

$$V(x) = -a\left\{\sinh(x) + b\log[\cosh(x)] - c\,x^4\right\} \text{ for } x \in [x_0,\, x_1], \tag{4.3}$$

as shown in Fig. 4.1 (a). The exact form of Eq. 4.3 is arbitrary. It is only important that the potential is confining and has two stable states. For the potential in Fig. 4.1, the bistable potential has local minima at $x_a \approx -2$ and $x_c \approx 2$ with an intermediate maximum at $x_b \approx 0$. A Brownian particle moving from x_a to x_c will have to overcome a barrier of height $V_+ \equiv V(x_b) - V(x_a)$ and a Brownian particle moving from x_c to x_a will have to overcome a barrier of height $V_- \equiv V(x_b) - V(x_c)$.

Many investigations in statistical mechanics begin with the bistable potential [22, 25, 26, 38]. Here, we will use the bistable potential to introduce aspects of self-induced temperature gradients without adding the complexity that comes with other potentials. In [38], Landauer used the bistable potential to understand how an imposed temperature gradient affects the relative occupation of states of a Brownian particle. Here, we will see that self-induced temperature gradients can have a similar effect. In this section, we will consider the steady state of a system on a bistable potential as well as numerical results for transient states. We will see that self-induced temperature gradients alter barrier crossing rates and can affect the long term steady state.

To introduce the notation and language that we use to describe the motion of a Brownian particle, we will first consider a regime where self-induced temperature gradients are negligible

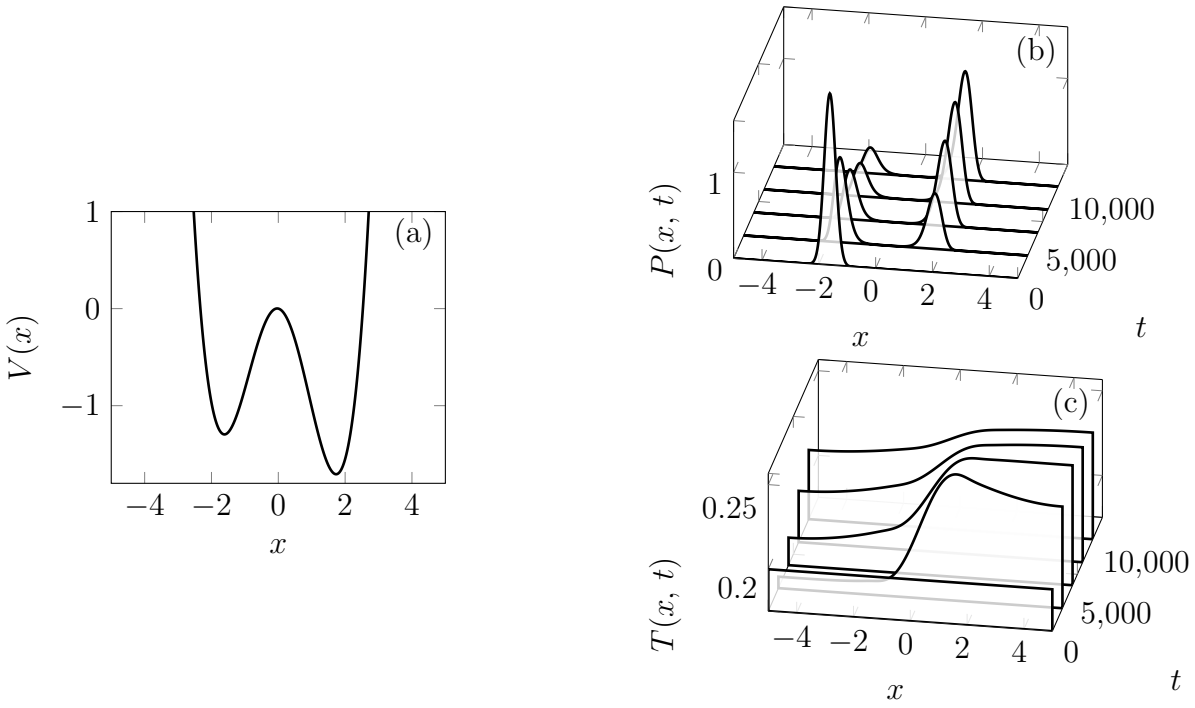

Figure 4.1: (a) Bistable potential given by Eq. (4.3) where we have $x \in [-5, 5]$, $a = 30$, $b = 0.08$ and $c = 1.5$. (b) Probability distribution as a function of time. (c) Temperature as a function of time. Simulation parameters are $B = 0.005$ and $A = 1$.

and where $\Delta V_+ \approx 1$ and the temperature of the environment is a constant $0 < T_0 \leq \frac{1}{5}$. As $\frac{\Delta V_+}{T_0} \ll 1$, this is often referred to as the *deep-well* regime. In [25], Kramers reduces this deep-well situation to one where the particle can be trapped in the upper well with probability $p_+(t) = \int_{x_0}^{x_b} P(x, t)\,\mathrm{d}x$ or in the lower well with probability $p_-(t) = \int_{x_b}^{x_1} P(x, t)\,\mathrm{d}x = 1 - p_+(t)$. The particle occasionally jumps from the upper well to the lower well with a rate r_+ and from the lower well to the upper well with rate r_-. Kramers found that r_+ and r_- are given by:

$$r_+ = \frac{[V''(x_a)|V''(x_b)|]^{\frac{1}{2}}}{2\pi} \exp\left[-\frac{V(x_b) - V(x_a)}{T_0}\right]$$

and

$$r_- = \frac{[V''(x_c)|V''(x_b)|]^{\frac{1}{2}}}{2\pi} \exp\left[-\frac{V(x_b) - V(x_c)}{T_0}\right]. \tag{4.4}$$

With these definitions, $p_+(t)$ is then given by the equation:

$$\frac{\mathrm{d}p_+(t)}{\mathrm{d}t} = -r_+ p_+(t) + r_-[1 - p_+(t)]. \tag{4.5}$$

Equations (4.4) and (4.5) help to clarify the physics and terminology related to a Brownian particle in a bistable well. The prefactors in Eq. (4.4) show us that if the bottom of a well has a large curvature, then the particle will escape more quickly. Likewise, if the barrier at x_b is very sharp, then both escape rates are increased. However, noting the fact that the prefactors are raised to the power of $\frac{1}{2}$, we see that the rates are not very sensitive to the curvature of

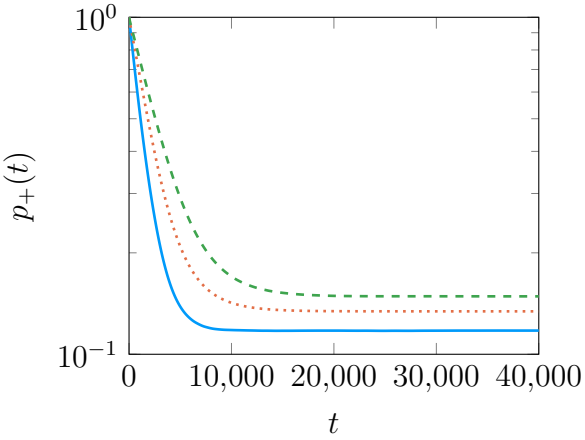

Figure 4.2: Evolution of $p_+(t)$ as a function of time: $p_+(t)$ is obtained by integrating the probability distribution over the interval $[-\infty, x_b]$. The potential is given by Eq. (4.3) where we have $x \in [-5, 5]$, $a = 30$, $b = 0.08$ and $c = 1.5$. We begin with the probability distribution in the upper well (meaning that $p_+(0) = 1$). The (blue) solid line represents $A = 0$, (where the Kramers' regime is expected to hold), the (orange) dotted line represents $A = 0.5$, and the (green) dashed line represents $A = 1$. B is held fixed at 0.005. Note that the y axis is a logarithmic scale.

the potential. The dominant determining factors are the temperature of the environment T_0 and the potential differences V_+ and V_-. In particular, raising the barrier heights reduces the barrier crossing rates because a Brownian particle requires more energy to cross the barrier. On the other hand, increasing the temperature will increase the barrier crossing rate. This is because when the temperature is higher, the Brownian particle is subjected to larger thermal fluctuations. Therefore, events where the particle can draw enough energy from the environment to overcome the barrier become more frequent.

Equation (4.5) shows us how the two wells exchange Brownian particles. We can find the steady state by setting the left hand side of Eq. (4.5) to zero, yielding:

$$\frac{p_+}{p_-} = \frac{r_-}{r_+} = \sqrt{\frac{V''(x_c)}{V''(x_a)}} \exp\left(-\frac{V(x_a) - V(x_c)}{T_0}\right). \tag{4.6}$$

Equation (4.6) tells us that the lower well can be made favorable in the steady state by increasing $V(x_a) - V(x_c)$. Also, as discussed earlier, when the temperature is decreased, the Brownian particle will overcome the barrier less frequently, therefore making the lower well more favorable.

When self-induced temperature gradients cannot be neglected, the above intuitions need to be modified. In order to account for self-induced temperature gradients, we use the numerical techniques from Chap. 3. Fig. 4.1 (b) and (c) shows the results from a situation where the probability distribution begins in the upper well and the temperature is initially flat. For boundary conditions, we apply confining boundary conditions to the probability distribution ($J(x, t) = 0$ at the boundaries) and we set the gradient of the temperature at the boundaries to zero (the system exchanges no thermal energy with its environment). Figure 4.1 (b) shows the probability distribution evolving with time. Here, we can see that the probability distribution

relaxes into a local steady state in each of the wells while gradually moving towards the lower well. This behavior is expected from Kramers' regime. Figure 4.1 (b) shows that although the temperature is initially flat, it develops gradients as time goes on. We see that at first, the temperature becomes lower in the upper well and higher in the lower well. As the system reaches its steady state, we see that the temperature becomes flat and is slightly higher than it was initially. We interpret this as follows: In order to overcome the barrier at x_b, the particle draws heat from the environment, therefore cooling the upper well. The particle then dumps heat into the environment as it descends the slope on the other side of the barrier. Due to these heat exchanges, the upper well cools down while the lower well heats up (see $t = 5000$ in Fig. 4.1 (c)). Due to this temperature gradient, the flow of particles from the upper well to the lower well is reduced. Meanwhile, the flow from the lower well to the upper well is increased. Therefore, the net flow of particles from the upper well to the lower well is reduced. For longer times ($t > 5000$ in Fig. 4.1 (c)), the temperature gradients flatten out due to heat diffusion. Since the particle adds more heat than it removes, the temperature at long times is larger than the initial temperature. The larger the value of A, the larger the steady state temperature. An increased value of the steady state temperature leads to an increase of the steady state value of p_+, as can be seen in Fig. 4.2.

Since energy is conserved in this particular system, self-induced temperature gradients have an effect on the steady state. Because the potential is confining, the steady state current is zero, so the steady state temperature is constant (T_{ss}) and the steady state probability distribution takes on the Boltzmann form $P_{\mathrm{ss}}(x) = \mathcal{N} \exp[-V(x)/T_{\mathrm{ss}}]$, where $\mathcal{N}$ is a normalization constant. As discussed in Chap. 2, the steady state temperature can be found by invoking the conservation of energy. The one-dimensional form of the conservation of energy in this case reads:

$$E_i = \mathcal{N} \int_{x_0}^{x_1} \exp\left[-\frac{V(x)}{T_{\mathrm{ss}}}\right] V(x)\,\mathrm{d}x + \frac{1}{A}(x_1 - x_0)T_{\mathrm{ss}}, \tag{4.7}$$

where E_i is the initial energy of the system. Note that the steady state temperature (T_{ss}) does not depend on B. The reason that B does not affect the steady state here is that $J_{\mathrm{ss}} = 0$, meaning that the Brownian particle does not exchange heat with its environment in the steady state. Therefore, although B controls how quickly the temperature reaches equilibrium, it does not control the actual value of T_{ss}. Fig. 4.2 shows $p_+(t)$ for multiple values of A while holding B fixed. Since larger values of A lead to larger steady state temperatures, we see that more particles are found in the upper well at long times when A is larger. Figure 4.2 also shows us that A has an effect on the barrier crossing rates. When A is larger, the opposing temperature gradient created by self-induced temperature gradients is also larger, therefore reducing the net flow from the upper well to the lower well.

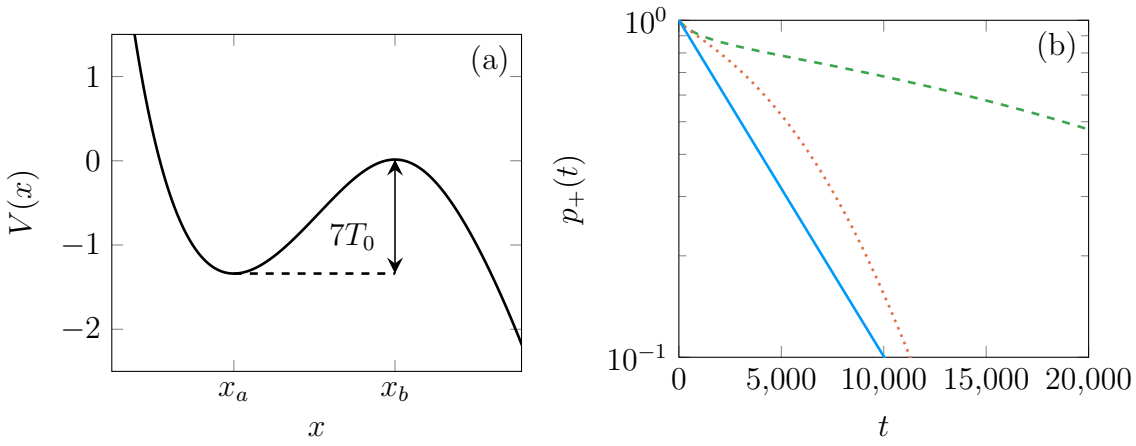

Figure 4.3: Metastable potential given by Eq. (4.8); T_0 is the initial temperature $T_0 = 0.2$. (b) Logarithmic plot of $p_+(t)$ as a function of time. $p_+(t)$ is obtained by integrating the probability distribution over the interval $[-\infty, x_b]$. In all plots, $A = 0.5$, while the (blue) solid line represents $B = 10$ (where Kramers' regime is expected to hold), (orange) dotted line $B = 1 \times 10^{-3}$, and (green) dashed line $B = 1 \times 10^{-4}$.

4.2 Metastable Potential

In this section, we will consider a metastable potential of the form:

$$V(x) = -b\{\sinh(x) + a\log[\cosh(x)]\}, \tag{4.8}$$

where $a = 7$ and $b = 2$. The potential is plotted in Fig. 4.3 (a). If a Brownian particle located at x_a, overcomes the barrier at x_b, the potential rapidly decreases to $-\infty$ and the particle will never return to x_a. Using Kramers' description we say that $r_- = 0$, substituting into Eq. (4.5), we find that:

$$p_+(t) = p_+(0)\exp(-r_+t). \tag{4.9}$$

Fig. 4.3 (b) shows $p_+(t)$ for multiple values of A while B is held fixed. In this case, we have chosen to impose Dirichlet boundary conditions so that $T(x, t) = T_0$ at the boundaries. When $A = 0$ (solid blue line), Kramers' regime holds and $p_+(t)$ decays exponentially via Eq. (4.9). However, when $A \neq 0$, the Brownian particle creates temperature gradients in its environment and we find that the decay is no longer exponential and can no longer be described by Eq. (4.9). The reason for this is that as the Brownian particle overcomes the barrier at x_b, it will cool down the well at x_a while heating up the slope to the right of x_b in a similar way to that discussed in Sec. 4.1. These temperature gradients oppose the current of the particles over the barrier. If B is small, then the gradients will not diffuse away quickly. On the other hand, if B is large, then the temperature gradients will quickly diffuse away and the system can be approximated by Kramers' rate.

Because the decay in Fig. 4.3 (b) is not exponential when B is small, we cannot even define effective barrier crossing rates to replace Eq. (4.5). The decay is not exponential because the

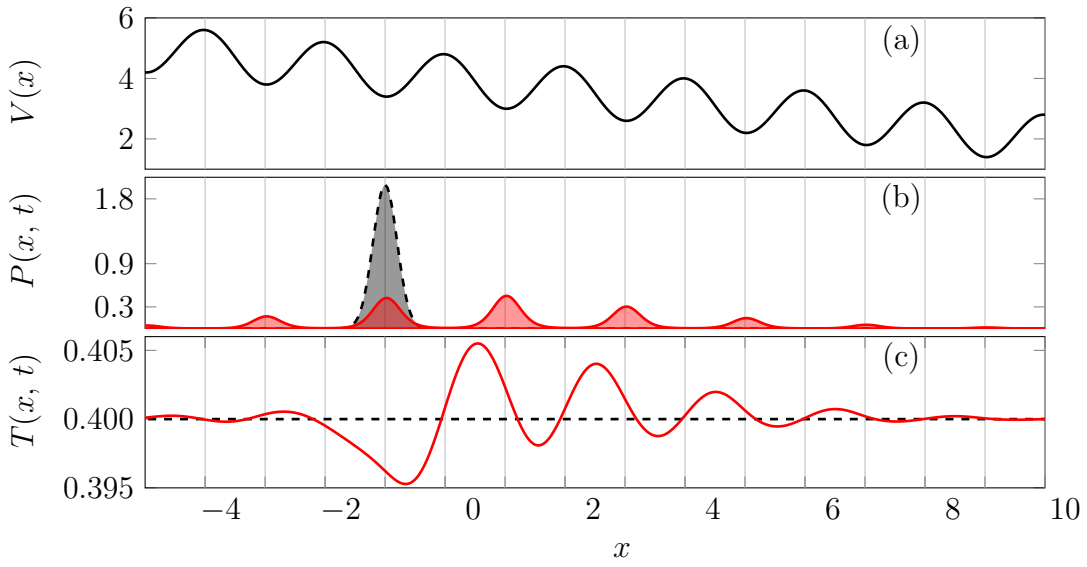

Figure 4.4: Time evolution on a tilted periodic potential. (a) The tilted periodic potential given by Eq. (4.10), here we have $f = 0.2$ and $v_0(x) = 0.8\sin(2\pi x) + 4$. (b) Probability distribution as a function of time and space. (c) Temperature of the environment as a function of time and space. In (b) and (c) the (black) dashed line represents $t = 0$, while the (red) solid line represents $t = 50$. The simulation parameters are $A = 0.01$ and $B = 0.005$.

opposing force from the self-induced temperature gradients is not constant with time. At first, when the population in the upper well is large, the current over the barrier is also large. This means that the particle will be exchanging a lot of heat with the environment. As $p_+(t)$ gets smaller, the current passing over the barrier must also get smaller, meaning that the Brownian particle exchanges less heat with its environment. At the same time, the temperature gradients will be flattening out due to heat diffusion. All of this means that the opposing force will start off at zero (when the temperature is flat), reach a maximum (when the temperature gradient is maximum), then the opposing force will go away as the temperature becomes flat again.

4.3 Tilted Periodic Potential

A tilted periodic potential, with period L is given by:

$$V(x) = -fx + v_0(x), \quad \text{where} \quad v_0(x) = v_0(x + L) \tag{4.10}$$

as shown in Fig. 4.4. In this section, we will imagine a scenario where $x \in [x_0, x_1 = x_0 + L]$, $P(x_0, t) = P(x_1, t)$ and $T(x_0, t) = T(x_1, t)$. Physically, these boundary conditions correspond to a circular domain where x_0 and x_1 are the same point. If $f \neq 0$, then $V(x)$ is not periodic, so a particle that travels once around the loop will lose $-f(x_1 - x_0)$ in potential energy. Because there is nowhere for heat to dissipate in this system, the steady state does not exist when $f \neq 0$ (as discussed in Chap. 2).

Figure 4.4 (b) and (c) shows a system where at $t = 0$, the Brownian motor is contained in a well at $x = -1$ and the temperature is flat. At $t = 50$, Fig. 4.4 (b) shows that the

Brownian motor has diffused down the potential while becoming trapped in the local minima of the potential. Similar to Sec. 4.1, the Brownian motor draws heat from the environment in order to overcome a barrier while emitting heat into the environment as it descends the slope on the other side. These exchanges of heat cause the temperature to oscillate in space. The oscillations in the temperature are out of phase with the oscillations in the potential and oppose the downwards motion of the Brownian motor. In [28], Büttiker shows that when the temperature oscillates out of phase with the potential, it can produce a force on the Brownian particle. Here we see that the self-induced temperature oscillations are out of phase with the potential and therefore maximize the force resisting the flow downhill. If $B \gg A$, then the temperature gradients will flatten out and the temperature will rise uniformly. In this case, self-induced temperature gradients will enhance the motion of the Brownian motor. This observation could have an impact on Brownian motors. If the Brownian motor moves at a time scale that is much faster than the time scale of heat diffusion, then self-induced temperature gradients will reduce the motion of the Brownian motor. Alternatively, if the Brownian motor moves at a slower time scale than the time scale for heat diffusion, then self-induced temperature gradients will enhance the motion of the motor.

4.4 Transferring Heat and Work

Here we will show a Brownian heat engine and heat pump on a tilted periodic potential that utilizes self-induced temperature gradients.

The setup is described in Fig. 4.5, the system is contained in $x \in [x_C, x_H]$, the boundary conditions for the temperature are $T(x_C, t) = T_C$ and $T(x_H, t) = T_H$. The potential has the tilted periodic form shown in Fig. 4.5. Finally, we impose periodic boundary conditions on the probability distribution $[P(x_C, t) = P(x_H, t)]$. Physically, this boundary condition means that a particle reaching one side will pass through the other side. Every time that a particle goes around the loop, its potential energy will change by $\Delta V = -f(x_H - x_C)$. Therefore energy has to be put into the system in order to keep the system going. As discussed in Chap. 1, the energy for a Brownian motor can come from a variety of sources, including an out of equilibrium chemical concentration. In this chapter, we will be interested in the transfer of energy in the steady state.

The tilted periodic form of the potential means that the steady state temperature will not be uniform. We show some examples of the steady state temperature in Fig. 4.6. In Fig. 4.6 (b), ΔT is small and we see that the temperature has the form of a parabola with periodic oscillations imposed on top of it. In Fig. 4.6 (c), ΔT is much larger, so the predominant heat flow is due to diffusion. As $\Delta T \to \infty$, the temperature tends towards a straight line. We can explain these observations more precisely by substituting the tilted periodic potential into Eq. (4.1), setting $x_C = 0$ and applying the boundary conditions, upon which we find:

$$T_{\rm ss}(x) = -\frac{B}{A} J_{\rm ss} \left[\frac{f}{2} x^2 + \frac{1}{2\pi} \sin(2\pi x) \right] + c_1 x + c_2, \tag{4.11}$$

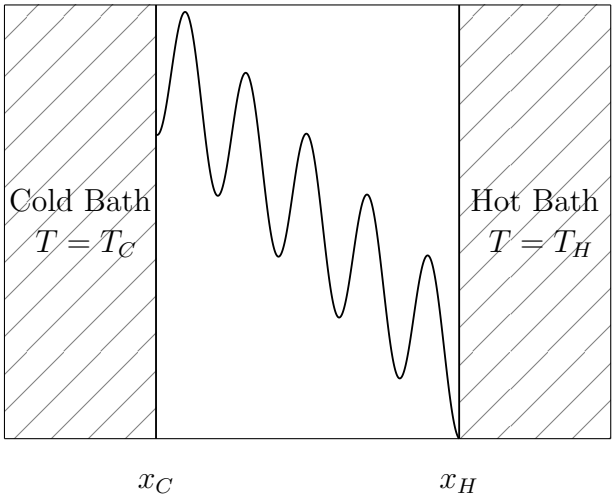

Figure 4.5: Schematic of the setup for the heat engine or heat pump system with $V(x) = -fx - \cos(2\pi x)$. The temperature is held fixed at the boundaries ($T(x_C, t) = T_C$ and $T(x_H, t) = T_H$).

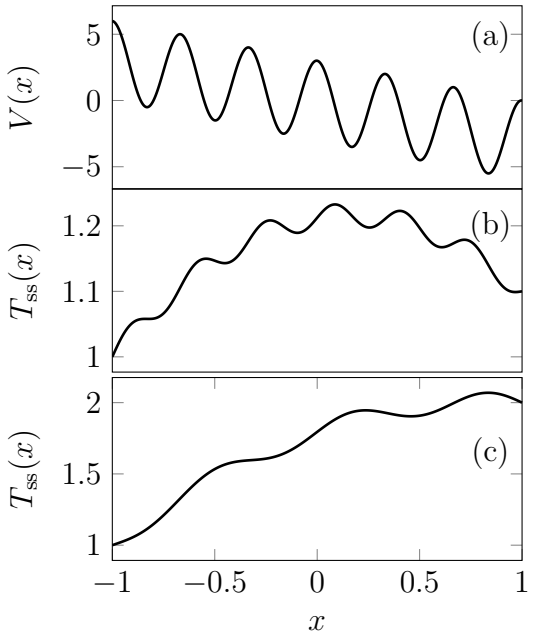

Figure 4.6: A realization of the setup described in Fig. 4.5. The potential in (a) is given by $V(x) = \frac{3}{2}\sin(6\pi x) - 3x$. In (b) $\Delta T = 0.1$ and in (c) $\Delta T = 1$. We have set $x_C = -1$ and $x_H = 1$.

where

$$\begin{aligned} c_1 &= \frac{1}{x_H}\left\{\Delta T + \frac{B}{A}J_{\rm ss}\left[\frac{f}{2}x_H^2 + \frac{1}{2\pi}\sin(2\pi x)\right]\right\}, \\ c_2 &= T_C, \\ \Delta T &\equiv T_H - T_C. \end{aligned} \tag{4.12}$$

If $f > 0$, then $J_{\rm ss} > 0$ (steady state current to the right) and if $f < 0$ then $J_{\rm ss} < 0$ (steady state current to the left). Therefore the parabolic part of the steady state temperature is always concave down and leads to heat dissipating into the hot bath and the cold bath. The dimensionless form of the heat due to temperature gradients is $Q(x,\,t) = -\frac{B}{A}\partial_x T(x,\,t)$. This means that if the slope of the temperature is non zero at the boundary, then the system will exchange heat with its greater environment. The heat being exchanged with the hot bath is $\dot{Q}_H = -\frac{B}{A}\partial_x T(x)|_{x=x_H}$ and the heat being exchanged with the cold bath is given by $\dot{Q}_C = \frac{B}{A}\partial_x T(x)|_{x=x_C}$. Using Eq. (4.11), we find that:

$$\begin{aligned} \dot{Q}_C &= \frac{B}{Ax_H}\left\{\Delta T + \frac{B}{A}J_{\rm ss}\left[-x_H - \frac{f}{2} + \frac{1}{2\pi}\sin(2\pi x_H)\right]\right\} \\ \dot{Q}_H &= -\frac{B}{Ax_H}\left\{\Delta T + \frac{B}{A}J_{\rm ss}\left[-\frac{f}{2}x_H^2 + \frac{1}{2\pi}\sin(2\pi x_H) - \cos(2\pi x_H)x_H\right]\right\}. \end{aligned} \tag{4.13}$$

If we let x_H be an integer, then when ΔT is small, $\dot{Q}_C < 0$ and $\dot{Q}_H > 0$, which means that the system is behaving as a heat pump. As ΔT gets larger, we will find that $\dot{Q}_C$ and $\dot{Q}_H$ will change sign. At the same time, $T_{\rm ss}(x)$ becomes a straight line going from T_C at x_C to T_H at x_H. In this case, the gradient of the temperature creates a force on the Brownian motor that opposes the force from the potential. If ΔT is great enough, then the thermal force will overcome the potential force and the Brownian motor will move against the potential ($J_{\rm ss} < 0$). Physically, this means that the Brownian motor is drawing heat from the environment in order to do work on the potential in the fashion of a heat engine.

We can understand the above results in terms of the first and second laws of thermodynamics as discussed in Chap. 2.2. In the steady state, the energy of the system is not changing, meaning that the work done on the Brownian particle is equal to minus the net heat exchanged with the environment. In other words, the first law becomes $\dot{W} - \dot{Q}_C - \dot{Q}_H = 0$ where $\dot{W} = J_{\rm ss}\Delta V$ is the rate of work done on the system and $\dot{Q}_H = -\frac{B}{A}\partial_x T(x)|_{x=x_H}$ and $\dot{Q}_C = \frac{B}{A}\partial_x T(x)|_{x=x_C}$ are the rate of heat flowing from the hot and cold bath respectively. When $\dot{W} > 0$ and $\dot{Q}_H > 0$, the system is behaving as a heat engine as discussed above. The first law efficiency of a heat engine is given by $\eta_I^{\rm HE} = \dot{W}/\dot{Q}_H$. In words, the first law efficiency is the ratio of the work done by the system to the energy that the system draws from the hot bath. The first law of thermodynamics prohibits the heat engine efficiency from exceeding one. However, the second law of thermodynamics puts a much stronger constraint on the efficiency which was first recognized by Carnot. To see this bound, we note that in the steady state, Eq. 2.13 becomes $\dot{S}_{\rm ss}^{\rm gen} \geq 0 = -\mathcal{B}_{\rm ss}^J - \mathcal{B}_{\rm ss}^Q$. Since $P_{\rm ss}(x)$ is periodic, $\mathcal{B}_{\rm ss}^J$ vanishes and we are left

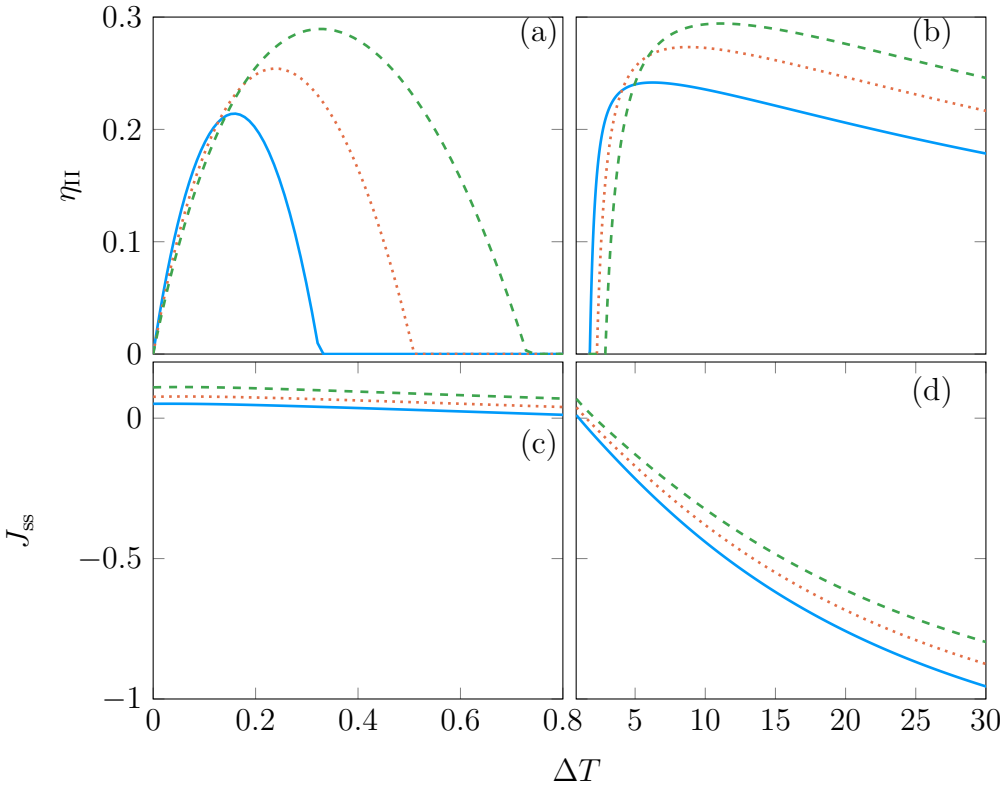

Figure 4.7: Second law efficiency as a function of $\Delta T = T_H - T_C$ with the system shown in Fig. 4.5. (a) The efficiency of the system for small ΔT where the system behaves as a heat pump. (b) Efficiency of the system for large ΔT where the system behaves as a heat engine. (c) and (d) show the steady state current J_{ss} as a function of ΔT. The (blue) solid line represents a tilt of $f = 0.6$, the (orange) dotted line represents $f = 1$ and the (green) dashed line represents $f = 3$.

with:

$$\dot{S}_{\rm ss}^{\rm gen} \geq 0 = -\frac{\dot{Q}_C}{T_C} - \frac{\dot{Q}_H}{T_H},$$
$$\implies \frac{Q_C}{Q_H} \leq -\frac{T_C}{T_H},$$

so,

$$\eta_I^{\rm HE} \leq 1 - \frac{T_C}{T_H}. \tag{4.14}$$

So the heat engine efficiency is less than one and approaches one in the limit $T_C/T_H \to 0$. As discussed earlier, the system can also behave as a heat pump, where $\dot{Q}_H < 0$, $\dot{Q}_C > 0$ and $\dot{W} < 0$. For a heat pump, the first law efficiency (or coefficient of performance) is $\eta_I^{\rm HP} = \dot{Q}_H/\dot{W}$. In this case, the first law of thermodynamics does not prohibit the efficiency from becoming larger than one. Applying the second law of thermodynamics like we did above, we find that:

$$\eta_I^{\rm HP} \leq \frac{1}{1 - \frac{T_C}{T_H}}. \tag{4.15}$$

By noting these upper bounds on the efficiencies, we define the second law efficiencies as:

$$\eta_{II}^{\rm HE} = \eta_I^{\rm HE} \left(1 - \frac{T_C}{T_H}\right)^{-1},$$
$$\eta_{II}^{\rm HP} = \eta_I^{\rm HP} \left(1 - \frac{T_C}{T_H}\right), \tag{4.16}$$

where both efficiencies are bounded by one.

In order to find the steady state, we use the one dimensional steady state techniques discussed in Chap. 3.1.1. We define a system with known values of x_C, x_H, T_C, T_H and f, we then use numerical techniques to find the steady state current $J_{\rm ss}$. Then, using Eq. 4.12, we have $\dot{W} = J_{\rm ss} f(x_H - x_C)$, $\dot{Q}_C = -\frac{B}{A}c_1$ and $\dot{Q}_H = J_{\rm ss}\Delta V + \frac{B}{A}c_1$. From these equations $\eta_{II}^{\rm HE}$ and $\eta_{II}^{\rm HE}$ can be found by substitution, we show the results of such calculations in Fig. 4.7. In Fig. 4.7 (a) and (b), we show how the efficiency varies with ΔT for various values of f, a close inspection shows that Fig. 4.7 agrees with the intuitions that we introduced earlier. When $\Delta T < 1$ [Fig. 4.7 (a)], the system acts as a heat pump. In this case, the current flows down the slope of the potential [$J_{\rm ss} > 0$; see Fig. 4.7 (c)]. This non zero current creates oscillations in the temperature that cause the system to draw heat from the cold bath and deposit heat into the hot bath. However, as ΔT becomes larger [Fig. 4.7 (b)], the dominant heat flow is from heat diffusion, so heat flows from the hot bath to the cold bath. As discussed earlier, once ΔT becomes large enough, this leads to $J_{\rm ss} < 0$ [see Fig. 4.7 (d)] meaning that the system does work and is acting as a heat engine. As ΔT increases further, $\dot{Q}_C$ increases and the heat engine efficiency goes to zero.

4.5 A Two Dimensional System Embedded in One Dimension

In general, we do not require that the heat diffuses out of the system at only one point. We can also consider a situation where a Brownian motor is tightly confined in one direction, while heat is able to dissipate radially. Such a situation results in a quasi two dimensional situation that can be modeled by solving a one dimensional equation. In this case, the equation of motion reads as:

$$\begin{aligned} \partial_t T(x,\,t) &= -AJ(x,\,t)\partial_x V(x) + B_1\partial_x^2 T(x,\,t) + B_2(T(x,\,t) - T_0), \\ \partial_t P(x,\,t) &= \partial_x\Big[[\partial_x V_0(x) - f]P(x,\,t) + T(x,\,t)\partial_x P(x,\,t)\Big] \end{aligned} \tag{4.17}$$

where the $B_2(T(x,\,t) - T_0)$ term represents the systems thermal interactions with a heat bath at constant temperature T_0 in the radial direction. A physical motivation for this equation of motion is given in App. A. The true system being modeled is two dimensional, however, the potential is given by an infinite square well in the y direction, we are also restricted by the assumptions explained in App. A. If we let $V(x) = V_0(x) - fx$, where $V_0(x)$ is periodic with period L, then the steady state will have a non zero current. In the steady state, we find that the temperature has oscillations that are out of phase with the potential as in previous sections. However, in this case, the temperature does not develop a parabolic component. This is because heat flows out of the side of the system through the third term of Eq. (4.17). We now set $V(x) = a\cos(2\pi x) - fx$ for $x \in [0,\,1]$ and explore the system as a function of the barrier size a and the force f. In Secs. 4.1 and 4.2, we noted that describing the system with barrier crossing rates was questionable, because when self-induced temperature gradients are involved, the rates are altered and can become time-dependent. Here we will explore this problem a little further by seeing how the current on a tilted periodic potential depends on time when one uses Eq. (4.17) as the equation of motion for the temperature. In Fig. 4.8, we start the system off with constant probability ($P(x,\,t=0) = 1$) and with constant temperature ($T(x,\,t=0) = 1$). We then calculate the current at the point $x = 1$ as a function of time. We see that the current oscillates around before reaching a stable steady state current. We also see that, when the force is small, the steady state current is smaller when A is larger. On the other hand, when the force is larger, the steady state current increases with A. When the force is small the steady state current is also small, so the average temperature is not increased very much. Alternatively, when the force is large the average steady state temperature is larger, the current becomes enhanced by self-induced temperature gradients.

In Fig. 4.9, we calculate the steady state current for multiple values of f and $\frac{B}{A}$. We see that when f is small, J_{ss} is also small. We also see that when $\frac{B}{A} \neq 0$, self-induced temperature gradients reduce the steady state current. However, when the force is large enough, we see that self-induced temperature gradients increase the steady state current. Similar to previous sections, whenever the steady state current is non zero, the temperature will develop oscillations

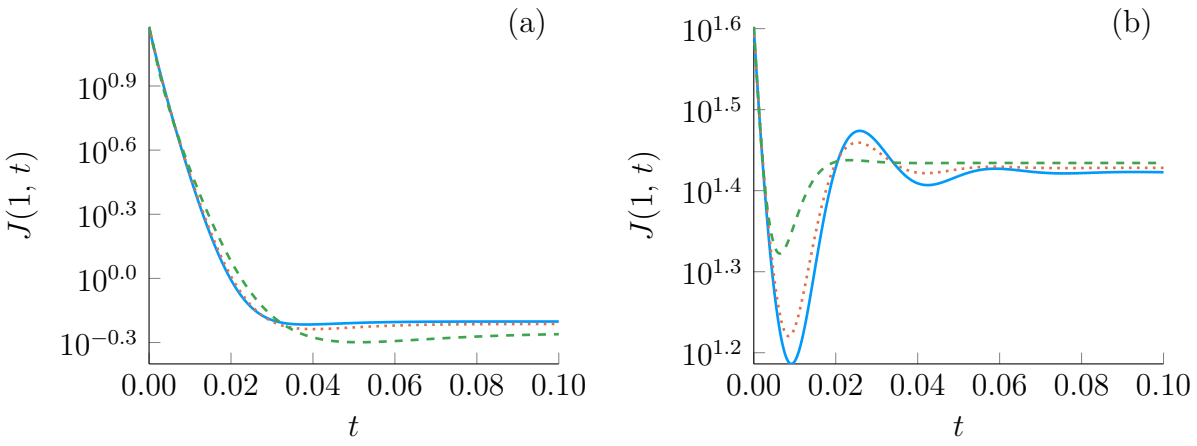

Figure 4.8: Current at the point $x = 1$ as a function of time. The potential is given by $V(x) = a\cos(2\pi x) - fx$ and $x \in [0, 1]$. (a) $f = 15$ and $a = 10$ (b) $f = 40$ and $a = 10$. In both plots, $B_1 = 1$, $B_2 = 1000$. The solid (blue) line represents $A = 0$, which is the case where self-induced temperature gradients can be ignored, the dotted (orange) line represents $A = 1$ and the dashed (green) line $A = 5$. In all of these plots, $T_0 = 1$.

that resist the downhill motion of the Brownian motor. However, when the force gets larger, the excess heat produced by the Brownian motor cannot be diffused away as easily, so the average temperature will rise. When this happens self-induced temperature gradients will enhance the motion of the Brownian motor.

4.6 Chapter Summary

This chapter demonstrated the behavior of Brownian systems with self-induced temperature gradients diffusing over one dimensional potentials. We saw that self-induced temperature gradients can affect the dynamical and steady state properties of the system. When $B \ll A$, the temperature gradients that form tend to reduce the motion of the Brownian particle. Alternatively, if $B \sim A$ and if heat is not allowed to escape the system, then self-induced temperature gradients will enhance the motion of a Brownian particle.

In our model for self-induced temperature gradients, we need to be very explicit about the flow of heat into and out of the system. In this chapter, we saw that imposing different boundary conditions on the temperature had a significant impact on the behavior of the system. For example, in Sec. 4.1 we set the gradient of the temperature $\partial_x T(x, t)$ to be zero at the boundaries. We find that the system only had a steady state if the potential allows equilibrium steady states for the Brownian motor. Moreover, when the steady state exists, we find that the steady state is dependent on the initial energy of the system. The reason for this behavior is that by setting the gradient of the temperature to be zero at the boundaries, we create a system that does not exchange heat with its greater environment. Such a system is rather problematic on a non equilibrium potential because when a Brownian motor is out of equilibrium, it will add heat into the local environment. If the excess heat is not allowed to flow out of the system through the boundaries, then the thermal energy of the system will rise indefinitely. On the

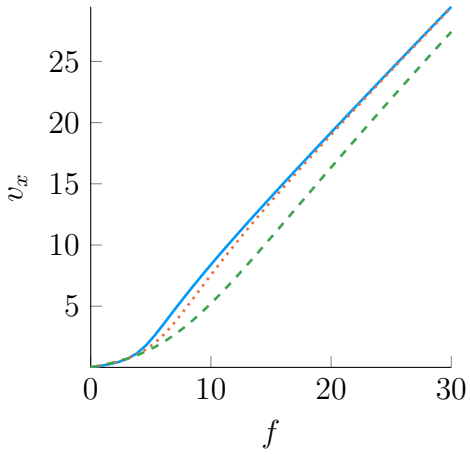

Figure 4.9: Steady state current as a function of f. In this figure, the the potential is given by $V(x) = -fx + 2\cos(2\pi x)$ and the line colors represent different values of $\frac{B_1}{A}$. The (blue) solid line represents the case where self-induced temperature gradients can be ignored, the (orange) dotted line represents $\frac{B_1}{A} = 0.25$ and the (green) dashed line represents $\frac{B_1}{A} = 1$. In this figure, $T_0 = 1$ and $B_2 = 10$.

other hand, if the potential confines the Brownian motor to a certain region, then the steady state current will be zero. So, on an equilibrium potential, the Brownian motor will only exchange heat with its environment during its transient, non equilibrium phase. However, as $t \to \infty$, the Brownian motor will reach equilibrium and it will no longer exchange heat with its environment. When this occurs any temperature gradients will disappear due to heat diffusion, therefore causing the temperature to become constant in the steady state. Because energy is conserved, the value of the temperature in the steady state depends on the initial energy of the system. Although the equilibrium potentials considered in this chapter shed some light on the physics of self-induced temperature gradients, we are not able to use an equilibrium system as a useful model of a Brownian motor. The reason is that a Brownian motor must be out of equilibrium (non zero current) in order to perform its function [13].

The other way that self-induced temperature gradients affect on the steady state is if $J_{\text{ss}} \neq 0$. In this case, we reach a non-equilibrium steady state where thermal energy is being constantly added into the environment and where work is being done on the Brownian system. In this chapter, we demonstrated a non equilibrium steady state on a tilted periodic potential. We then exploited the temperature gradients created by self-induced temperature gradients to implement a heat engine and a heat pump. We were able to calculate the heat produced by the heat engine/pump as well as calculating the efficiency. In contrast to the heat engines and heat pumps considered in [34, 39–44], we directly accounted for the effect that heat exchanges had on the temperature of the environment.

Unfortunately, one dimensional potentials offer very limited ways for heat to diffuse into the greater environment. This can lead to situations where a steady state does not exist. In the next chapter, we will explore two dimensional potentials where we can apply Dirichlet boundary conditions that allow heat to flow out of the system. We will see that this offers a much richer set of possible steady states that better describe the reality of Brownian motors.

Chapter 5

Two Dimensional Potentials

In this chapter, we will explore self-induced temperature gradients for a Brownian motor diffusing over a two dimensional potential. In Chap. 4, we found that one dimensional descriptions of out of equilibrium Brownian motors were problematic due to the limited degrees of freedom available to the system. In this chapter, we consider self-induced temperature gradients on a range of two dimensional potentials.

The physical problem that occurred in the setup of Sec. 4.4 was that the probability distribution and all of its derivatives are periodic, while the same does not hold for the temperature. The other case that we explored in Chap. 4, involved embedding the Brownian motor in a two dimensional domain that allows heat to escape through the sides of the domain. This setup gave us valuable insight into the behavior of a Brownian motor exchanging heat with its environment on a two dimensional domain. At the same time, the setup avoided some of the complications that we will find inherent in two dimensional systems. In spite of this success, the setup forces us to follow the assumptions explained in App. A.

In this chapter, we no longer have to deal with these limiting assumptions and we remove many of the restrictions that were present in Chap. 4. We will find that some of the behaviors present in one dimensional systems will carry over to two dimensional systems. However, in general, the two dimensional systems will behave in a more complex manner. In particular, the results in this chapter are more difficult to obtain numerically as well as being more difficult to visualize. We will therefore introduce each situation very carefully along with example solutions. We will explore our two dimensional potentials in a systematic way that directly demonstrates the effect that self-induced temperature gradients have on the current of a Brownian motor. The chapter is organized as follows: Secs. 5.1 and 5.2 consider a Brownian motor on a potential that is tilted and periodic in the x direction, while confining in the y direction. We explore the consequences of the Brownian motor drifting down the potential in the x direction while heat escapes the system in the y direction. We explicitly quantify the drift in Sec. 5.2.1 and we explore the impact that self-induced temperature gradients have on the drift. In Sec. 5.3, we use the accumulated knowledge from the previous sections in order to implement two dimensional heat engines and heat pumps. We explore the effect of self-induced temperature gradients on the efficiency of our heat engine and heat pump systems.

5.1 Tilted Channel

In this section, we will consider a potential on the region $[0,\, 1] \times [-1,\, 1]$ of the form:

$$V(x) = V_0(x,\, y) - fx, \tag{5.1}$$

where

$$V_0(x = 1,\, y) = V_0(x = 0,\, y). \tag{5.2}$$

An example is shown in Fig. 5.1. For boundary conditions, we require that that the probability distribution is confined in the y direction while the temperature is fixed at $y = \pm 1$. Since the probability distribution and the temperature are periodic,

$$\boldsymbol{J}(0,\, y) \cdot \hat{\boldsymbol{x}} = \boldsymbol{J}(1,\, y) \cdot \hat{\boldsymbol{x}}, \tag{5.3}$$

and

$$\nabla T(0,\, y) \cdot \hat{\boldsymbol{x}} = \nabla T(1,\, y) \cdot \hat{\boldsymbol{x}}. \tag{5.4}$$

Since the Brownian system is confined to $y \in [-1,\, 1]$,

$$\boldsymbol{J}(x,\, -1) \cdot \hat{\boldsymbol{y}} = 0 = \boldsymbol{J}(x,\, 1) \cdot \hat{\boldsymbol{y}} \tag{5.5}$$

and since the temperature is held fixed at the sides of the domain,

$$T(x,\, -1) = T_0 = T(x,\, 1). \tag{5.6}$$

First, we consider the simplest case, where $V_0(x,\, y)$ has no variation in the x direction. We set $f = 1$ and $V_0(x,\, y) = 10y^2$. The fact that the potential is harmonic in the y direction is particularly interesting because a harmonic potential can be considered to be a second order expansion of an arbitrary well around its stationary point. The steady state probability distribution and the steady state temperature are found by solving Eqs. (3.1) and (3.2) using the steady state finite volumes method described in Sec. 3.1.2. The steady state is shown for $\frac{B}{A} = 1$ in Fig. 5.2. In Fig. 5.2 (a), we see that the probability distribution is constant in the x direction and that it decays to zero as $y \to \pm 1$. From Fig. 5.1 (b), we can see that the temperature is also constant in the x direction, it reaches its maximum at $y = 0$ and as $y \to \pm 1$, $T(x,\, y) \to T_0$. Figure 5.1 (c) shows the steady state entropy generation, which we calculated using the formula

$$\dot{S}^{\text{gen}}(x,\, y) \equiv \sum_j \left[\frac{J_j(x,\, y)^2}{P(x,\, y)T(x,\, y)}\right] + \frac{B}{A}\left[\frac{\nabla T(x,\, y)}{T(x,\, y)}\right]^2 \geq 0, \tag{5.7}$$

which is the dimensionless form of Eq. 2.10. The temperature, the probability distribution and the entropy generation are all constant in the x direction due to symmetry. Therefore, Eq. 5.7 tells us that the entropy generation is constant in the x direction.

Due to the non zero force in the x direction, there is in fact a non-zero steady state current in

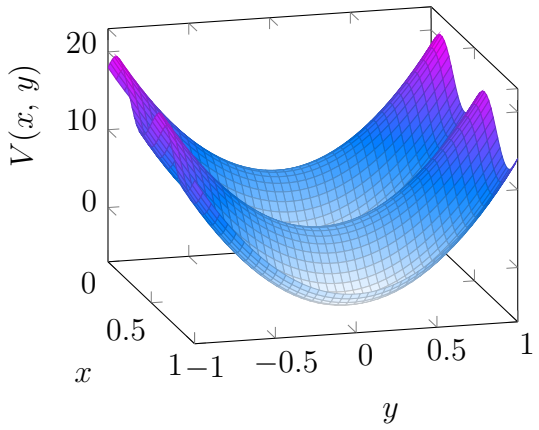

Figure 5.1: Two dimensional potential that is harmonic in the y direction. The potential has periodic barriers and wells and is described by the equation $V(x, y) = 3\sin(4\pi x) + 20y^2 - 4x$. The potential confines the Brownian motor in the y direction. In the steady state, we expect that there will be a net flow downhill in the x direction.

the x direction. Because of the non zero steady state current, the Brownian motor is exchanging heat with its environment and because the temperature is held fixed at $y = \pm l$, the heat will flow out in the y direction. In terms of energetics, this case is a loss process where all of the work being done on the system is lost as heat through the boundaries.

5.2 Tilted Periodic Channel

In Chap. 4.3, we explored Brownian motion with self-induced temperature gradients on a tilted periodic potential. We found that self-induced temperature gradients reduced the steady state current of the Brownian motor flowing down the potential. The steady state of the two dimensional version of the tilted periodic potential is shown in Fig. 5.3. In the figure, we have set $V_0(x, y) = 4\cos(2\pi x) + 10y^2$ and $f = 5$. The potential has a well (local minimum) located at $x = 0.5$. In order to pass through the point $x = 1$, the system has to overcome a barrier, which has height 8 in our dimensionless units. Since the temperature at the boundaries is given by $T_0 = 1$, we conclude that when the force is zero, the barrier height is $8k_BT_0$ (see discussion in Chap. 2.4). Because the barrier height is greater than $5k_BT_0$, we can establish that the system in Fig. 5.3 is in the deep well regime.

In Fig. 5.3 (a), we see that the steady state probability distribution is trapped inside the wells of the potential. Figure 5.3 (b) shows the corresponding steady state temperature, we have superimposed the heat on top of the temperature as a velocity plot. The shape of the temperature in Fig. 5.2 (b) is due to the fact that the Brownian motor draws heat from its environment in order to overcome the barriers, while dumping the heat on the other side of the barrier. We have shown these steady state currents in Fig. 5.3 (c). In Fig. 5.3 (c), we see that the Brownian motor flows in the direction of increasing x and that it develops vortices at the bottom of the well at $x = 0.5$. As with the case in Sec 5.1, the net heat flows out the sides of the domain and the system can be classified as a loss process. The behavior is more apparent if we consider a slice through the system. In Fig. 5.4, we see that at $y = 0$ (the center

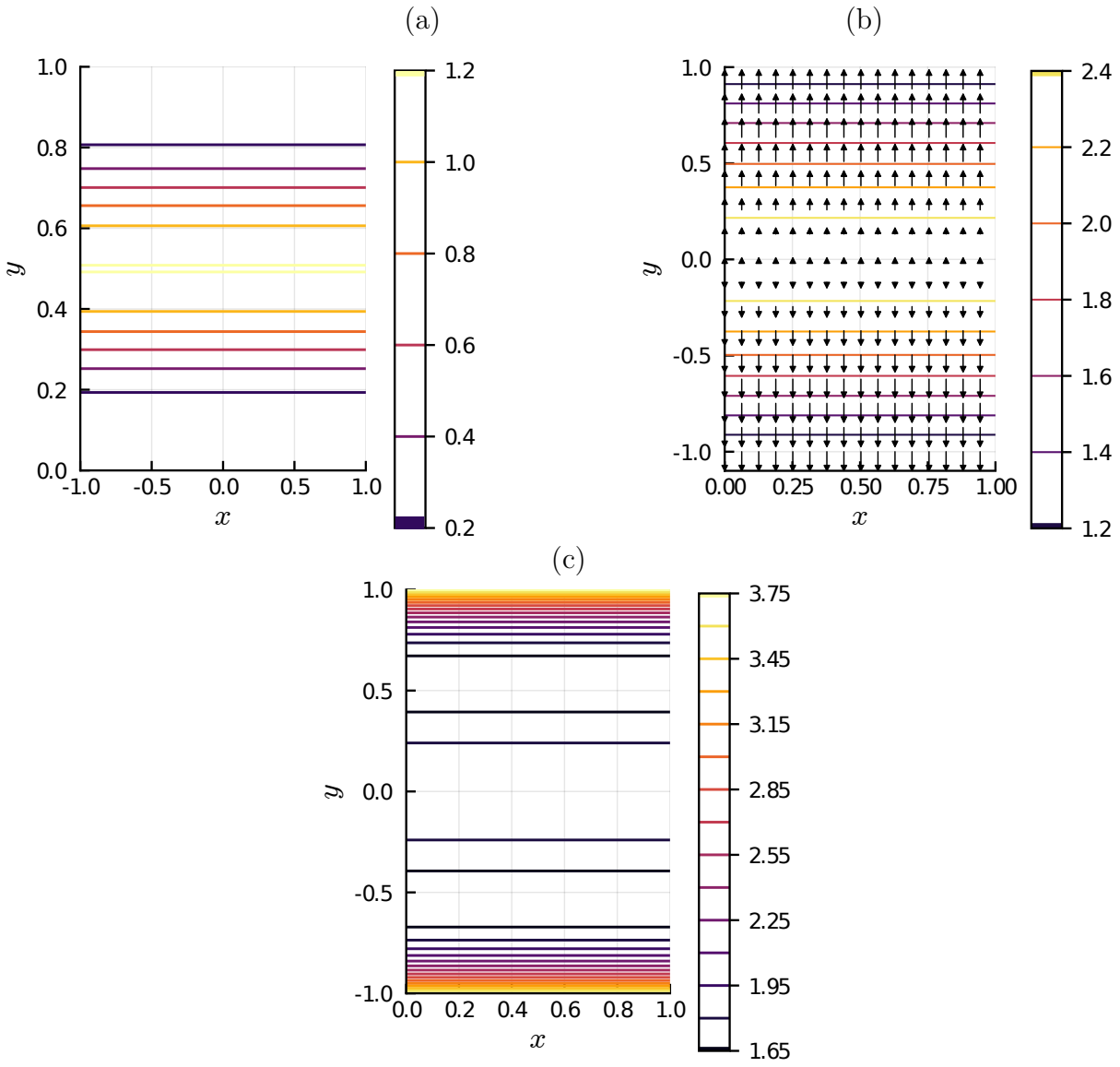

Figure 5.2: Steady state for a potential that is constant in the x direction. All quantities are continuously varying and are visualized with a contour plot. (a) Steady state probability distribution (b) steady state temperature with a velocity plot of the gradient of the temperature (c) steady state entropy generation. The potential is given by Eq. 5.1 with $V_0(x, y) = 10y^2$ and $f = 2$. In this figure, we set $\frac{B}{A} = 1$

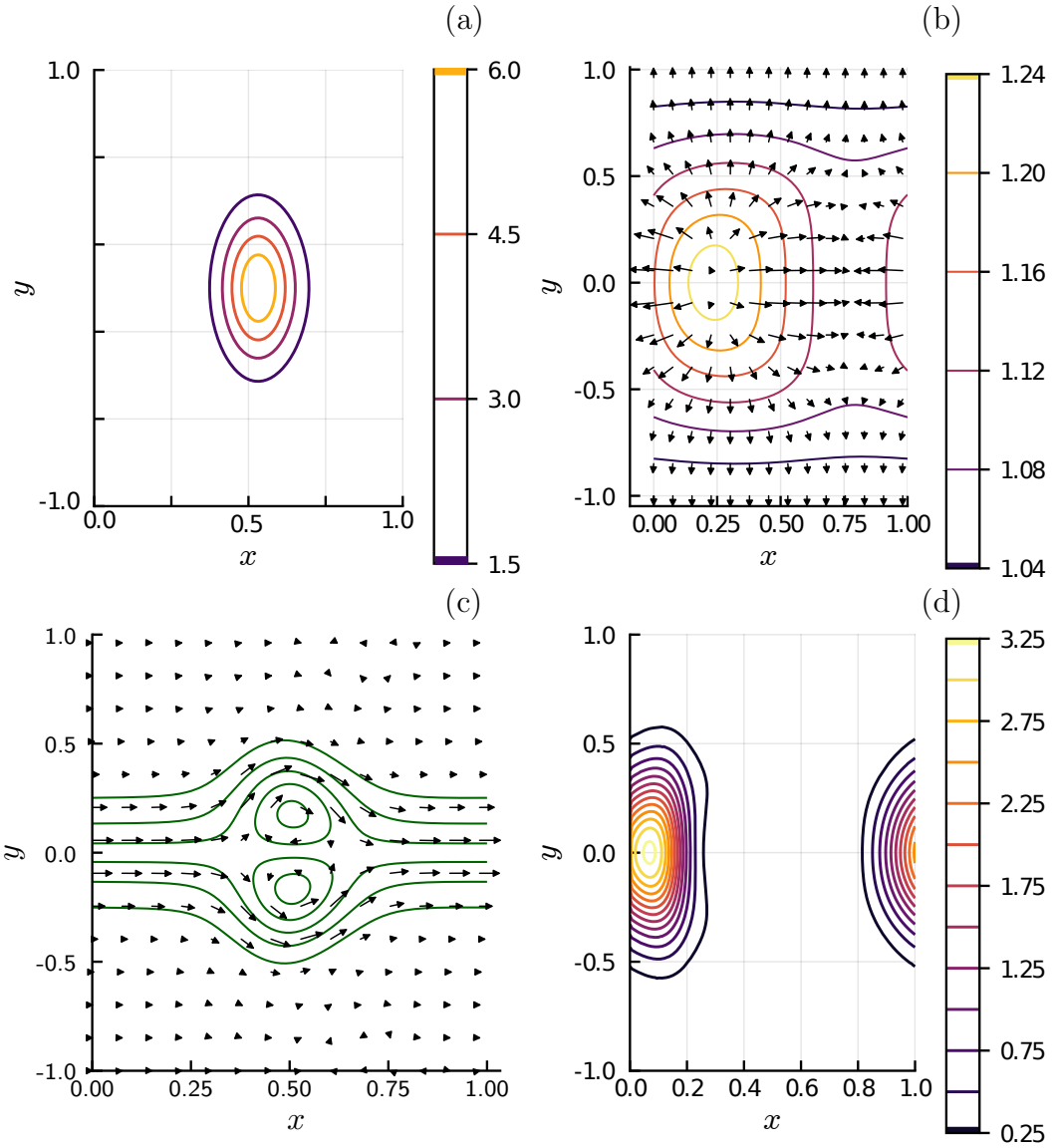

Figure 5.3: Single channel with periodic barriers and wells, the potential is given by Eq. 5.1 with $V_0(x, y) = 4\cos(2\pi x) + 10y^2$, $f = 5$. The potential has a well (local minimum) at the point $x = 0.5$, the Brownian motor has to overcome a barrier located at $x = 1$. (a) Steady state probability distribution (b) steady state temperature (c) steady state probability current ($J_{ss}(x, y)$). We have plotted the current as a velocity plot (black arrows) as well as plotting contours of the stream function to aid visualization. The stream function was calculated by numerically integrating the probability current. (d) steady state entropy generation. In this figure, $\frac{B}{A} = 1$. (a), (b) and (d) are continuously varying and are visualized with a contour plot.

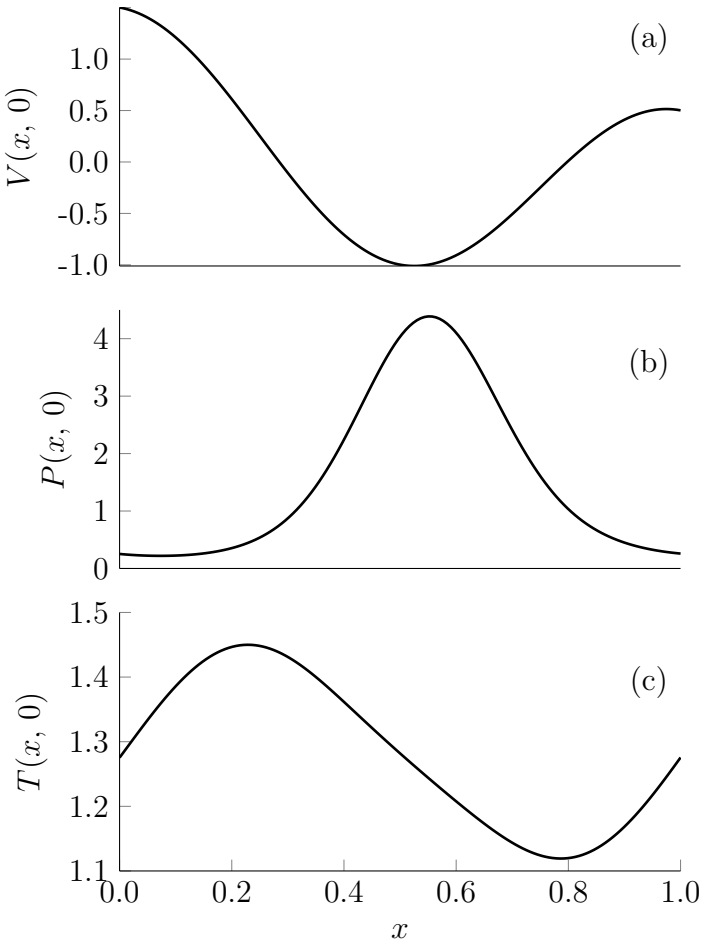

Figure 5.4: One dimensional slice of the two dimensional steady state. The potential is given by $V(x,\, y = 0) = \cos(2\pi x) - 0.5x$. The slice was taken through the line where $y = 0$, which is the lowest point in the potential. Since this is the lowest point, the center is where the probability distribution is maximum. The temperature distribution from which this figure was taken from has $T(x,\, y = \pm l) = 1$. (a) is the potential, (b) is the probability distribution and (c) is the temperature.

of the domain), the temperature is slightly higher than its value $T_0 = 1$ at the boundaries. The temperature gradients in Fig. 5.4 have the same form as the temperature gradients in Fig. 4.4. As was the case in one dimension, the temperature gradients resist the motion of the Brownian motor downhill in the fashion of a Büttiker-Landauer heat engine.

Due to the temperature gradients and due to the non zero steady state current, the steady state is out of equilibrium and entropy is being generated. We have shown the entropy generation in Fig. 5.3 (d), where we see that most of the entropy is generated at the points where the Brownian motor is either overcoming or descending a barrier. In the center of the well, the Brownian motor reaches equilibrium with its environment, so no entropy is generated at the bottom of the well. However, when the Brownian motor overcomes the barrier in the potential, it exchanges heat with the environment. Due to these heat exchanges, the barrier is the point where the system is furthest from equilibrium and where most of the entropy is generated.

5.2.1 The Steady State Drift on a Tilted Periodic Potential

In Figs. 5.2 and 5.3, we see that the current mostly flows in the direction of the force f. In Fig. 5.3, we see that near the bottom of the well, there is some current flowing in the y direction. Let us now define the quantity:

$$v_x = \int_0^L \mathrm{d}x \int_{-l}^{l} \mathrm{d}y \, \boldsymbol{J}(x, y) \cdot \hat{\boldsymbol{x}}, \tag{5.8}$$

which we will refer to as the drift. The drift tells us how much current there is flowing downhill in the direction of the force. The drift does not give us much information about the current in the y direction, however, it can help to inform us on the energetics of the Brownian motor. First, consider the case where $V_0(x, y)$ is constant in the x direction and confining in the y direction (for example Fig. 5.2, where $V_0(x, y) = 10y^2$). In this case, the steady state probability distribution and the steady state temperature is constant in the x direction. Since the potential in the y direction is confining, the steady state current in the y direction is zero. Using this information, we find that, $\boldsymbol{J} \cdot \hat{\boldsymbol{x}} = -[P(x, y, t)(\partial_x V(x, y) - f) + T(x, y, t)\partial_x P(x, y, t)] = -P(\boldsymbol{r}, t)f$. In this case, the steady state current (and the steady state drift) is independent of the temperature. Since the steady state drift is independent of the temperature, self-induced temperature gradients do not have an effect on the steady state drift. This does not mean that there are no temperature gradients in the steady state. In Fig. 5.2 (b), we have shown that the temperature varies in the y direction. However, since the temperature is not varying in the x direction, the flow of heat does not have an effect on the drift.

On the other hand, Fig. 5.3 shows a case where $V_0(x, y)$ depends on x and y. In these cases, self-induced temperature gradients can have an effect on the steady state drift. Figure 5.5 shows the drift for the potential $V(x, y) = -fx + 40y^2 + p_2 \sin(2\pi x)$. The figure shows the drift as a function of the force f and the barrier size p_2. In Fig. 5.5, we see that, on a given potential with a given force, the steady state drift can change with the value of $\frac{B}{A}$. When the force is small ($f < 2$), the drift is reduced by self-induced temperature gradients. When the force gets a little bit larger, we see a crossover point where self-induced temperature gradients enhance the drift flowing downhill.

The second way that we can alter the steady state drift is by changing the size of the barriers in the potential while leaving the force constant, as shown in Fig. 5.5 (b). We notice that at first, the drift is enhanced by self-induced temperature gradients. However, for larger barrier sizes the drift is reduced by self-induced temperature gradients.

One can understand this behavior in a similar way to the results in Chap. 4. The key thing to note is that there are two competing phenomena at play. First, when the Brownian motor diffuses down an oscillating potential, it creates oscillations in the temperature that resist the drift of the motor going down the potential. The second effect comes into play as the force gets larger, when this happens the drift also gets larger, so the total amount of heat being dumped into the environment increases with the force. However, the amount of heat that can escape through the sides of the domain is given by $\frac{B}{A}\int_0^1 \mathrm{d}x \, \nabla T(x, y) \cdot \hat{\boldsymbol{y}}$. So, the only way that the

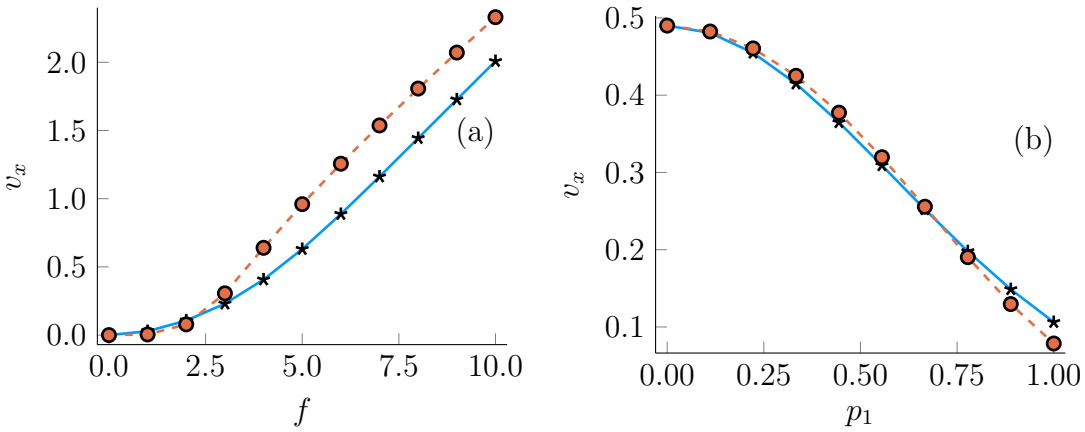

Figure 5.5: Steady state drift (Eq. 5.8) on the potential $V(x, y) = -fx + p_1 \cos(2\pi x) + 10y^2$. The temperature was held fixed at the y boundaries ($T(x, y = \pm l) = 1$). (a) Drift as a function of the force f, while the barrier size is held fixed at $p_1 = 0.75$. (b) Steady state drift as a function of the barrier size p_1 while the force is held fixed at $f = 5$. The (blue) solid line represents $\frac{B}{A} = 1$ and the (orange) dashed line represents $\frac{B}{A} = 60$. The lines joining the markers are a linear interpolation.

excess heat can diffuse out of the system is if the gradient of the temperature is raised. As the force increases, the average temperature will get larger. This increased temperature enhances the motion of the Brownian motor.

With this information in mind, we can understand Fig. 5.5 as being the result of the two competing effects described above. Effect one is that the drift going downhill creates oscillations in the temperature that resist the downhill motion. And effect two is that when the drift is very large, the excess heat being produced causes the average temperature to become larger and this increased temperature enhances the downhill drift. Now we can see that in Fig. 5.5, when $f < 2.5$, effect one dominates and the drift is reduced by self-induced temperature gradients. At about $f = 2.5$, we see that effect one and effect two cancel each other and the drift is the same as when self-induced temperature gradients are not present. For $f > 2.5$, effect two is dominant and self-induced temperature gradients enhance the steady state drift. Figure 5.5 (b) can be understood in a very similar way: when p_2 is small, effect two is dominant, so self-induced temperature gradients enhance the steady state drift. However, as the barrier size increases, the steady state drift decreases, so effect one becomes more relevant. For $p_2 > 0.7$, we see that effect one dominates and self-induced temperature gradients reduce the drift flowing downhill.

In hindsight, the results from Fig. 5.5 could have been anticipated from Chap. 4.5. However, by solving the system on a two dimensional domain, we allow ourselves to consider potentials that take on arbitrary shapes in the y direction. Furthermore, we are no longer restricted by the assumptions explained in App. A.

5.3 Two Dimensional Heat Engine and Heat Pump

In Chap. 4.4, we were able to implement a heat engine and a heat pump on a one dimensional potential that utilized self-induced temperature gradients. We required that the probability

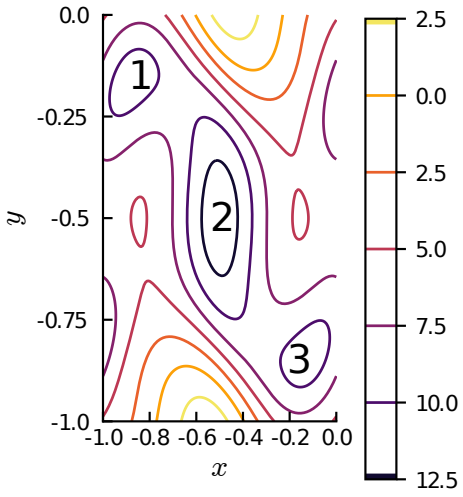

Figure 5.6: Contour plot of the potential used to realize a two dimensional heat engine and heat pump, the potential is given by Eq. 5.9, with $a = 10$, $b = 4$ and $c = 10$. The boundary conditions on the temperature are imposed at $y = -1$ and $y = 0$. The hot bath (temperature T_H) is located at $y = 0$ and the cold bath (temperature T_C) is located at $y = -1$. The figure shows that the potential forms a snake like channel which has three strategically placed wells. We have labeled these wells in the figure, so that they can be referred to in the text.

distribution was periodic and that the temperature was held fixed at both ends. This meant that there was a discontinuity in the temperature and that there was a point in our system that exchanged thermal energy with the environment while not allowing probability current to flow in or out of the system. Keeping with the main theme of the current chapter, we implement a two dimensional heat engine and heat pump with temperature baths that are separated in space. Because our heat baths are separated in space, the two dimensional heat engines that we will consider in this section do not have the interpretation issues present in our one dimensional system from Chap. 4.4. The idea behind the heat engine is shown in Fig. 5.6, where we see that the potential forms a snake-like channel for the Brownian system to pass through. The potential is given by $V(x,\, y) = V_0(x,\, y) - fx$, where:

$$V_0(x,\, y) = -a \exp\left\{-\frac{1}{2}[\sin(2\pi x) + \sin(2\pi y) + 2\cos(\pi y)]^2\right\} + c(y + 0.5)^4 - b\cos(2\pi x)\cos(2\pi y), \tag{5.9}$$

for a given channel depth a, confining parameter c and barrier height b. For the remainder of this section, we will consider the domain $(x,\, y) \in [-1,\, 0] \times [-1,\, 0]$. Now, we set the temperature to be equal to T_H at $y = 0$ and T_C at $y = -1$, where we have $T_H > T_C$. The difference in temperature between the hot bath and the cold bath is $\Delta T \equiv T_H - T_C$. The channel itself contains strategically placed wells and barriers that allow us to couple the heat flow in the y direction to a probability current in the x direction.

In the steady state, we expect the following to happen: The Brownian motor will be mostly confined to the channel and the probability distribution will have maxima at the wells in the potential. The temperature in well 1 will be quite close to T_H, while the temperature in well 3 will be closer to T_C, the temperature at well 2 will be roughly the average of T_C and T_H.

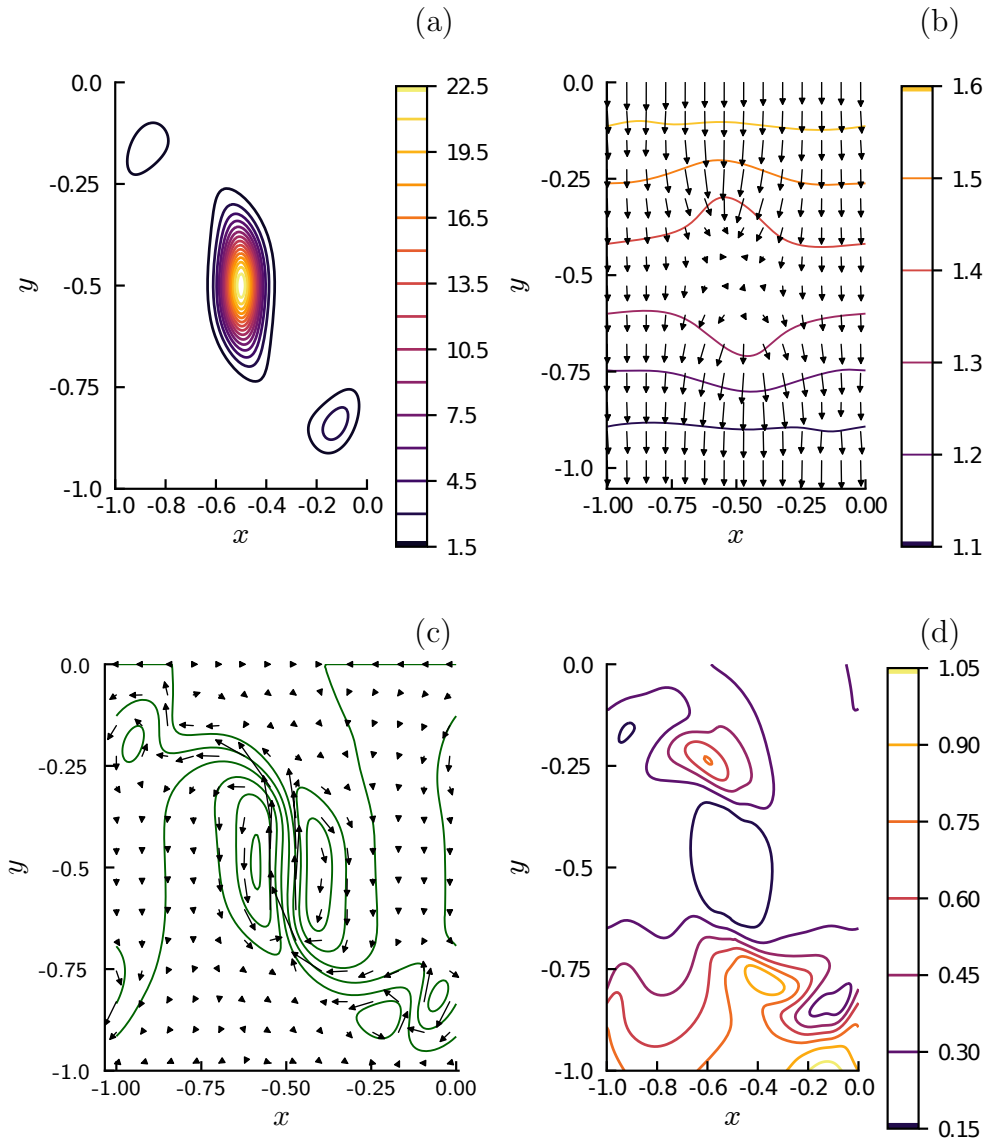

Figure 5.7: Two dimensional heat engine. This figure uses the potential given by Eq. (5.9), with $a = 10$, $b = 4$, $c = 10$ and $f = 0.4$. (a) Steady state probability distribution (b) steady state temperature, the temperature was held fixed at the edges with $T_H = 1.7$ and $T_C = 1$. The contours represent the temperature and the arrows represent the gradient of the temperature (flow of heat). (c) steady state probability current. The arrows represent the probability current and the contours represent the streamfunction of the probability current. (d) Steady state entropy generation. In this figure, $\frac{B}{A} = 1$. (a), (b) and (d) are continuously varying and are visualized with a contour plot.

Since well 1 has a higher temperature than well 2, there will be a current flowing from well 1 to well 2 as described in Chap. 1.1.1. Likewise, we will find that there is a current flowing from well 2 to well 3. In the steady state, we expect that there will be a current that flows from $1 \to 2 \to 3$. Meaning that the drift is negative, the negative drift will remain, even if there is some positive force in the x direction. This means that the Brownian motor is absorbing heat from the temperature baths at $y = 0$ and $y = -1$ in order to do work. The work being done is given by $W = v_x f L$, where v_x is the drift from Eq. (5.8), which is now going against the force f. We show an example of the system acting as a heat engine in Fig. 5.7. Fig. 5.7 (c) shows the system drifting in the direction of decreasing x (against the external force). In addition to an uphill drift, the system also shows vortices in the center well (well 2). Figure 5.7 (d) shows the entropy generation in the steady state. Similar to the case in Sec. 5.2, most of the entropy is generated at places where the system has to overcome barriers.

The heat engine scenario described above can be understood in the absence of self-induced temperature gradients. However, when we introduce self-induced temperature gradients, the uphill drift creates temperature gradients that resist the flow of the Brownian motor. The uphill drift observed in our system is reduced by self-induced temperature gradients. Figure 5.7 (b) shows the oscillations in the temperature that occur. The temperature gradients shown in Fig. 5.7 (b) inhibit the system from acting as a heat engine. However, temperature gradients are crucial for the system to work as a heat pump. The heat pump works by running the heat engine in reverse, this occurs when the force f is large (or when ΔT is small).

When the force is large compared to ΔT, the drift will be downhill. A downhill drift means that work is being done on the Brownian system, so the engine is running in reverse. In Fig. 5.8, we consider a situation where ΔT is small and the drift is downhill. Figures 5.8 (a) and (c) show the probability distribution and the steady state current of the Brownian motor respectively. In Figs. 5.8 (a) and (c), we see that the Brownian system flows is the same direction as the force and that in the well 2, vortices begin to develop in the probability current. Fig. 5.8 (b) shows how the current from Fig. 5.8 (a) affects the temperature. In Fig. 5.9, we have integrated the temperature in the x direction, therefore showing the average temperature as a function of y to aid visualization. In Fig. 5.9, we see that heat is flowing from the hot bath to the cold bath in the fashion of a heat pump. This reversal of the flow of heat only occurs when the downhill drift of the Brownian system is large enough to overcome the flow of heat in the y direction due to thermal diffusion.

The heat being drawn from the hot bath is given by $Q_H = -\frac{B}{A}\int_{-1}^{0} \mathrm{d}x\, \nabla T(x, y = -l) \cdot \hat{\boldsymbol{y}}$. We define the efficiency of the heat engine to be $\eta_{\mathrm{II}}^{\mathrm{HE}}$ as given by Eq. (4.16). Figure 5.10 (a) shows the efficiency of the system for small values of ΔT, where the system acts as a heat pump. Figure 5.10 (b) shows the efficiency of the system for larger values of ΔT, where the system acts as a heat engine. Figures. 5.10 (c), (d) show the respective drifts flowing in the system. Figure 5.10 demonstrates the effect that self-induced temperature gradients have on a heat engine and a heat pump. In Figs. 5.10 (c) and (d), we see that the drift is closer to zero for larger values of $\frac{B}{A}$. This is because self-induced temperature gradients resist the motion of

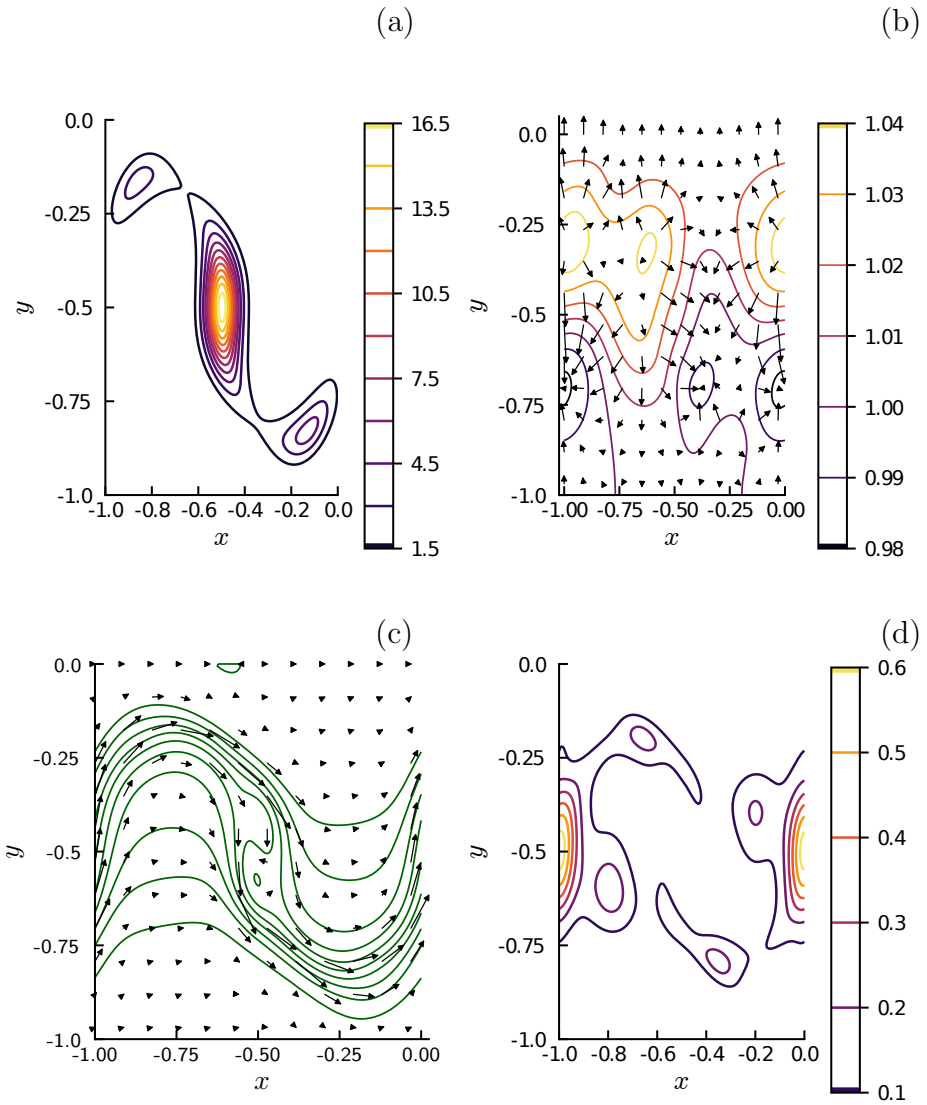

Figure 5.8: Two dimensional heat pump steady state. The Brownian motor is placed on the potential given by Eq. (5.9), with $a = 10$, $b = 2$, $c = 10$ and $f = 0.8$. (a) Steady state probability distribution. (b) Steady state temperature, the temperature was held fixed at $y = -1$ and $y = 0$, with $T_C = 1$ and $T_H = 1.01$. (c) steady state probability current (d) steady state entropy generation. In this figure, $\frac{B}{A} = 1$. (a), (b) and (d) are continuously varying and are visualized with a contour plot.

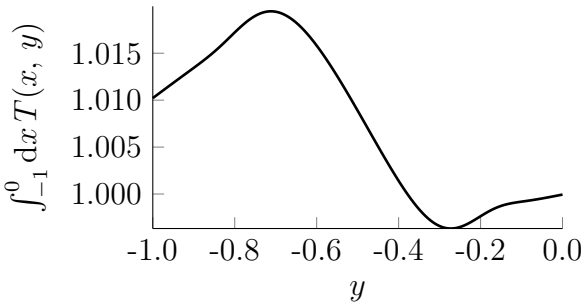

Figure 5.9: Average temperature in the y direction for the heat pump shown in Fig. 5.8. By integrating in the x direction, we can now visualize how the temperature varies in the y direction. In particular, we see that the heat flows from the cold bath to the hot bath, so the system is now acting as a heat engine.

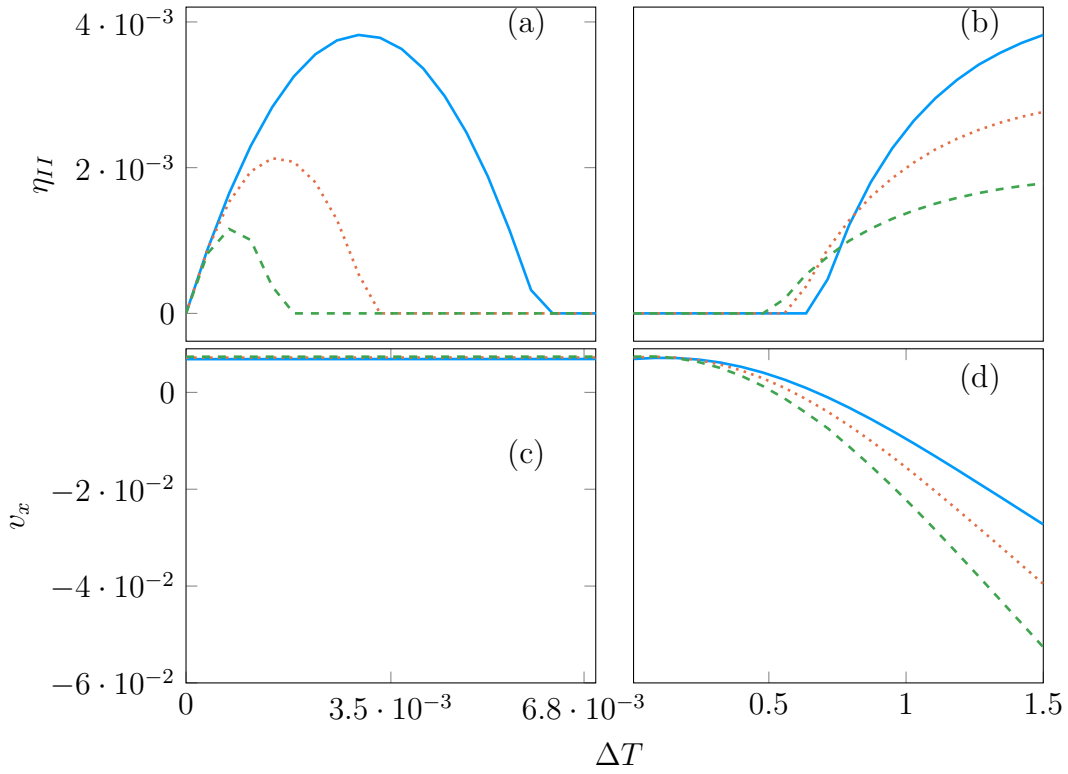

Figure 5.10: Efficiency of the two dimensional heat engine and heat pump. (a) shows the heat pump efficiency for small values of ΔT. (b) shows the heat engine efficiency for large values of ΔT. (c) and (d) show the corresponding drifts (v_x). For this figure, we used the potential given by Eq. (5.9), with $a = 10$, $b = 4$, $c = 10$ and $f = 0.4$. The (blue) solid line represents $\frac{B}{A} = 1$, the (orange) dotted line represents $\frac{B}{A} = 2.25$ and the (green) dashed line represents $\frac{B}{A} = 5$.

the Brownian motor. When $\frac{B}{A}$ is made larger, we see that the heat pump efficiency is reduced. At the same time, when $\frac{B}{A}$ is made larger, we find that a larger value of ΔT is required for the system to act as a heat engine. We also notice that once ΔT is large enough, self-induced temperature gradients actually enhance the efficiency of the system acting as a heat engine. When $\frac{B}{A}$ is small, self-induced temperature gradients will be large. Self-induced temperature gradients enhance the heat pump efficiency because they enhance the temperature gradients seen in Fig. 5.9, therefore increasing $\dot{Q}_H$. Understanding the efficiency of the heat engine is a little more difficult. In Fig. 5.10 (d), we see that self-induced temperature gradients reduce the uphill drift v_x of the heat engine. Since $W = v_x f L$, self-induced temperature gradients should also reduce the efficiency of the heat engine. In Fig 5.10 (d), we see that this is true for small enough ΔT. However, when ΔT gets larger, self-induced temperature gradients will reduce $\dot{Q}_H$. Since $\eta_{II}^{HE} = \frac{\dot{W}}{\dot{Q}_H}(1 - \frac{T_C}{T_H})^{-1}$, the reduction of $\dot{Q}_H$ caused by self-induced temperature gradients increases the efficiency of the heat engine. The increase in efficiency comes with a reduced power output of the heat engine.

5.4 Chapter Summary

Including two dimensions into our analysis helped to clarify some of the one dimensional results in Chap. 4. Considering two dimensional systems also introduces new physical phenomena that are not present in one dimension. In one dimension, heat has to flow out through a particular point in the domain, meaning that the gradient of the temperature is discontinuous at the point where heat flows out of the system. In two dimensions, we were able to fix the temperature along a section of the boundary. Along this section, the system is in contact with a thermal reservoir. Because the heat could flow out of the system along these designated portions of the boundary, we could realize a system where the temperature was periodically continuous and smooth along one degree of freedom. The fact that heat could be dissipated through additional degrees of freedom was anticipated in Chap. 2.3.2. Later, in Chap. 4.5, we described a reduced two dimensional system that allowed heat to dissipate radially in a one dimensional system embedded in a higher dimensional system. In Secs. 5.1, we were explicitly able to visualize the way in which heat can escape the system by providing an extra degree of freedom. The results obtained in Sec. 5.1 agree with the findings in Chaps. 2.3.2 and 4.5 as well as providing new insight. We found that the steady state current caused the average temperature of the domain to rise and that excess heat flowed through the boundaries (where the temperature was fixed at $T_0 = 1$). Section 5.2 built on the ideas of Sec. 5.1 by considering a potential that was tilted and contained periodic barriers and wells. In Sec. 5.2, we showed the entropy that a Brownian motor produces in the steady state. We found that the Brownian motor was in equilibrium at the bottom of the wells of the potential and that all of the entropy was generated as the Brownian motor crossed the barriers of the potential. In Sec. 5.1, we showed that when a Brownian motor crosses barriers in two dimensions, it produces temperature gradients that reduce the motion of the motor. These temperature gradients resist the motor in the fashion of a Büttiker-Landauer heat engine. The slow down present in two dimensions agrees with our results in one dimension from Secs. 4.3 and 4.5.

In order to quantify the slow down effect that self-induced temperature gradients have on a Brownian motor, we defined the drift v_x [Eq. (5.8)], in Sec. 5.2.1. We calculated the drift for multiple barrier heights and forces on a two dimensional tilted periodic potential. By observing the drift for multiple barrier heights and forces, we were able to see how self-induced temperature gradients affect the drift of a Brownian motor. We pointed out that there are two competing effects that are brought about by self-induced temperature gradients. The first effect was that barrier crossing induces temperature gradients that resist the motion of the Brownian motor. The second effect was that the excess heat produced by the Brownian motor causes the average temperature to rise. The rise in temperature then enhances barrier crossing rates. In Secs. 4.1, 4.2 and 4.3, we pointed out the time dependent effects of self-induced temperature gradients on one dimensional systems. Section 5.2.1 adds another phenomena that one must account for when considering barrier crossing in relation to Brownian motors. Even in the absence of self-induced temperature gradients, barrier crossing rates in the overdamped regime is a highly complex and exciting field of study [25, 35, 46]. Section 5.1 shows us that there is

still much to learn.

Throughout this chapter, we have obtained two dimensional results analogous to the one dimensional results from Chap. 4. In Sec. 5.3, we realize a two dimensional heat engine and heat pump analogous to the results of Chap. 4.4. The principle for the heat engine that we have implemented can be realized without self-induced temperature gradients, while the heat pump relies on self-induced temperature gradients. We found that self-induced temperature gradients tend to dampen the motion of the Brownian motor. This means that when self-induced temperature gradients are are present, a larger temperature difference is required in order for the system to operate as a heat engine. At the same time, self-induced temperature gradients are able to use work done on a Brownian system to make heat flow from a cold bath to a hot bath in the fashion of a heat pump. Similar to the heat pump in Sec. 4.4, both the heat pump and the heat engine could be realized on the same potential simply changing either the force f or the temperature difference ΔT.

Chapter 6

Conclusion

6.1 Summary of Thesis Achievements

In this thesis, we have formulated a theory of Brownian motors with self-induced temperature gradients. Previous works acknowledge that Brownian motors exchange heat with their environment [31, 32, 40, 50, 51]. In this thesis, we have gone further by considering the impact that these heat exchanges have on the temperature of the environment and how this in turn affects the Brownian motor. In Chap. 2, we developed a simple theory of Brownian motion with self-induced temperature gradients. We found that the theory was consistent with the first and second laws of thermodynamics. We were also able to quantify the entropy generated by a Brownian system with self-induced temperature gradients. Furthermore, we explored the properties of the steady state of a Brownian system that involves self-induced temperature gradients. We explored the steady state both in the equilibrium case as well as the non equilibrium case, which is more relevant to Brownian motors. We also explored the nature of the steady state with different boundary conditions applied to the temperature. We showed that a non equilibrium Brownian system could only have a steady state if heat could flow out of the system through the boundaries. In particular, we showed that a Brownian system on a domain that is periodic in one degree of freedom only has a steady state if the heat produced by the Brownian system can flow out through an additional degree of freedom. To aid further exploration, we found a dimensionless form for our equation of motion. This dimensionless form gave us two parameters, A and B to describe the behavior of the system. This allowed us to discuss the different regimes of self-induced temperature gradients and their validity. We also found that in the steady state, the system could be described by just one parameter $\left(\frac{B}{A}\right)$ which informed us on the magnitude of the impact of self-induced temperature gradients on Brownian motion.

In order to explore Brownian motors with self-induced temperature gradients further, we developed two numerical schemes for solving the system in Chap. 3. Both numerical schemes could be applied to the dynamical state and in the steady state. The first scheme adapted the finite volume method to solve a modified version of our equations of motion. The modified equations of motion exploited the underlying physical properties of our system. We utilized the fact that our system conserves energy to reformulate our system into two conservation equations.

One equation describes how the probability distribution of the Brownian system evolves with time and the other describes how the the energy density evolves with time. The energy density includes the energy density of the Brownian system as well as the thermal energy density of the environment. The second numerical scheme that we employed was a spectral approach, which we can use to solve our equations on a periodic domain. We wrote our equations of motion as a Fourier series and we solved the equations for the coefficients of the expansions. For both numerical schemes, we checked the results against theoretical results where possible. We showed that the numerical methods are consistent with the analytical solution where the analytical solution existed. We also checked that both schemes would converge as we refined our grid size, proving that the numerical schemes are self-consistent.

With these numerical schemes in place, we were able to further explore the influence of self-induced temperature gradients on Brownian motors. In particular, we found that self-induced temperature gradients reduce barrier crossing rates in one dimension and two dimensions. We considered the case of a single barrier separating an upper well and a lower well. We found that as a Brownian system flows from the upper well to the lower well, it cools down the upper well and heats up the lower well. This creates a force that pushes the Brownian system into the higher well in the fashion of the Landauer blowtorch [38]. We then considered Brownian motion on a tilted periodic potential with multiple wells separated by barriers. In the absence of self-induced temperature gradients, the tilted periodic potential is used to model tightly coupled Brownian motors [13, 18, 19]. When self-induced temperature gradients are considered, the downhill drift of the Brownian motor forms temperature gradients that heat up the ascending edges of each barrier and cool down the descending edges. These temperature gradients resist the downhill drift of the Brownian system in the fashion described by Büttiker [28] and van Kampen [29]. Since self-induced temperature gradients alter barrier crossing rates, the Kramers' rates used to describe Brownian motors in the deep-well regime [25, 35] cannot be used to describe Brownian motors with self-induced temperature gradients. In both cases, self-induced temperature gradients have a damping effect on the motion of the Brownian system. We also found that when the steady state was out of equilibrium, self-induced temperature gradients caused a net rise in the thermal energy of the environment. In one dimension, we allowed the excess heat to escape through the ends of our domain, meaning that the gradient of the temperature had a discontinuity in the steady state. In two dimensions, we were able to explicitly show cases where the excess heat produced by self-induced temperature gradients could be diffused into a second degree of freedom. Therefore, the system contained one degree of freedom where both the temperature and the probability distribution were continuous and smooth. When considering highly out of equilibrium, two dimensional potentials, we found cases where self-induced temperature gradients actually enhanced the drift of the Brownian system. The reason is because a highly out of equilibrium potential creates a very large steady state current which causes the average temperature of the system to become much higher than the value of the temperature at the boundaries. This elevated temperature then enhances barrier crossing rates and causes the drift of the Brownian system to increase.

By considering self-induced temperature gradients on specially chosen potentials, we were able to realize a heat engine and a heat pump in both one and two dimensions. The heat pumps that we considered used self-induced temperature gradients as a crucial part of their operating mechanism. We were also able to calculate the work done by the engines and their efficiency. Unlike the heat engines and heat pumps considered in [34,39–44], we directly accounted for the effect that heat exchanges had on the temperature of the environment. In order to realize a heat pump or a heat engine in one dimension, we had to consider situations where the temperature was discontinuous. Such a discontinuity is rather difficult to interpret physically. In spite of this, we were able to demonstrate many of the important aspects of heat pumps and heat engines that utilize self-induced temperature gradients. In two dimensions, we were able to obtain a heat pump and a heat engine that did not require discontinuities in the temperature. The two dimensional heat engine and heat pump preserved many of the qualitative features of the one dimensional systems. However, since the two dimensional heat engine and heat pump did not have any discontinuities in the temperature, they are much easier to interpret physically. Experimental realizations of heat engines and heat pumps is currently a very important task [7]. We have provided a widened range of possibilities for experimentalists to pursue by showing how self-induced temperature gradients affect the properties of heat pumps and heat engines.

6.2 Future Work

This thesis achieved many goals and explored many avenues of the theory of Brownian motion with self-induced temperature gradients. As we analyzed this topic, we came up with many questions that are beyond the scope of the thesis, yet highly important.

6.2.1 Inclusion of Inertia (Underdamped Regime)

The heat produced by a Brownian system can be split into two terms. One term considers the heat produced by the change in potential energy of the Brownian system and another term describes the heat produced by the change in kinetic energy of the system. In this thesis, we have been working in the overdamped regime, meaning that we were neglecting the kinetic contribution. Previous authors [31, 34, 41, 43] argue that the heat produced by a Brownian system is dominated by the kinetic contribution. In order to properly model Brownian motion with self-induced temperature gradients in the underdamped regime, we would have to replace Eq. (1.4) with the Fokker Planck equation while explicitly modeling the velocity [54]. This would then alter the heat source term in Eq. (2.1) and would add another parameter to the model to account for the kinetic contribution. Given the claims by these authors, it is important to consider the case where inertia is not neglected.

6.2.2 Modified Equations of Motion for the Temperature

Eq. (2.1) is not the only possible equation of motion for the temperature. In particular, we could slightly modify the equation by considering a non constant thermal diffusivity. In some cases the thermal diffusivity can depend on the temperature. In this case, the heat diffusion term becomes non linear and the equation becomes much more difficult to solve.

Validity of Reduced Description

In App. A, we derived a special form of the heat transfer equation and the Smoluchowski equation that applied under very special assumptions. In particular, we had to assume that the potential was periodic in one direction and an infinite square well in the other direction. We also had to assume that the probability distribution reaches equilibrium in the confining direction and that the temperature is separable. Finding a minimal set of assumptions that still allow one to write a reduced description of the equations is a good direction for future work.

6.2.3 Physical Realizations

This thesis has focused on the theoretical aspects of self-induced temperature gradients both to quantify their affect and because of their important fundamental implications for Brownian motors. It is important, however, to consider regimes in which the system might be physically relevant. In Chap. 2.4, we determined two constants

$$A \equiv \frac{k_B}{\rho c_p} \frac{1}{L^d} \tag{6.1}$$

and

$$B \equiv \frac{\gamma D}{E_0}. \tag{6.2}$$

These dimensionless parameters can be used to describe the regimes of validity of Brownian motion with self-induced temperature gradients. In order to compute the values of A and B, we need to determine each quantity on the right hand side individually. Here we will do so for the case of biological molecular motors. These motors diffuse in water at room temperature ($300\,\mathrm{K}$), where $c_p = 4186\,\mathrm{J}\cdot\mathrm{kg}^{-1}\mathrm{K}^{-1}$ and $D = 1.43 \times 10^{-5}\,\mathrm{m}^2\cdot\mathrm{s}$. For biological motors, the value of the drag coefficient is $\gamma = 10^{-10}\,\mathrm{kg}\cdot\mathrm{s}$ [12]. The typical energy energy barrier for a biological motor is $E_0 = 10 k_B T$ [47], where $T = 300\,\mathrm{K}$, so $E_0 = 4.164 \times 10^{-20}\,\mathrm{J}$. Motor proteins in the cell have a density of 2.32×10^{21} Proteins $\cdot\,\mathrm{m}^{-3}$ [70], so the size of a volume that typically only contains one molecular motor is $L^d = 4.31 \times 10^{-22}\ \mathrm{m}^3$. Putting all of these numbers together, we find that: $A = 1.3 \times 10^{-1}$, $B = 3.45 \times 10^5$ and $\frac{B}{A} = 2.57 \times 10^6$. For these values, self-induced temperature gradients do not have a large impact on molecular motors. Finding physical regimes that can be realized where self-induced temperature gradients are significant could be another important piece of future work.

6.2.4 Additional Analogous Systems

Equation (3.1) is a convection diffusion equation that also applies to a range of physical systems outside the realm of Brownian dynamics. For these systems, we can apply the energetic arguments of Sec. 2.2 to determine an equation of motion for the local environment similar to Eq. (3.2). Exploring the application of our work to other physical systems is an interesting direction of future research. Note, however, that if the quantity evolved in Eq. (3.1) is not a probability distribution, then the Shannon entropy, [Eq. (1.12)] will not hold and Sec. 2.2 will not be valid.

Appendix A

A One Dimensional System Embedded In Two Dimensions

Here we will show the form that the heat transfer equation takes when Ω is a square in two dimensions. We will use a similar approach as the one leading to Eq. 2.27. However, we will eventually reach a slightly different form of the heat equation that applies to time dependent situations as well as the steady state. In order to reach a reduced form of Eqs. (2.1) and (1.4), we have to make some key assumptions about the system. First, we have to assume that the potential forms an infinite square well in the y direction. This means that the Brownian motor is free to move in the y direction, however, it meets an infinite opposing force if it tries to leave the area $y \in [-l,\, l]$. Secondly, we have to assume that the Brownian motor reaches equilibrium in the y direction, so the probability distribution is constant in the y direction and zero outside of $y \in [-l,\, l]$. With this we find that the current does not flow in the y direction and only depends on x. This means that the self-induced temperature gradients produce a heat density that does not depend on y. If we now assume that the temperature is separable in space, then we will be able to integrate both the temperature and the probability distribution to find a one dimensional equation of motion for a two dimensional system. Consider the heat transfer equation:

$$\partial_t T(x,\, t) = -\frac{1}{\rho c_p}\boldsymbol{J}(\boldsymbol{r},\, t)\cdot\nabla V(\boldsymbol{r}) + D\nabla^2 T(\boldsymbol{r},\, t), \tag{A.1}$$

where again, we let $V(x,\, y) = V_0(x,\, y) - fx$ and we make the probability and the temperature periodic in the x direction. As for the temperature, we set $T(x,\, y = \pm l) = T_0(x)$, which corresponds to putting the boundaries at $y = \pm l$ in contact with a reservoir at temperature $T_0(x)$. If we now integrate over a volume Ω and multiply by ρc_p, then we get the following equation:

$$\rho c_p \int_\Omega \partial_t T(\boldsymbol{r},\, t)\,\mathrm{d}\boldsymbol{r} = -\int_\Omega \boldsymbol{J}(\boldsymbol{r},\, t)\cdot\nabla V(\boldsymbol{r})\,\mathrm{d}\boldsymbol{r} + D\rho c_p \oint_{\partial\Omega} \nabla T(\boldsymbol{r},\, t)\cdot\mathrm{d}\boldsymbol{r}. \tag{A.2}$$

The term on the left hand side of the equation is the change in thermal energy inside Ω. On the right hand side, we have the heat being generated inside Ω and the heat escaping through the boundary $\partial\Omega$. If we now define $\widetilde{T}(x,\, t) \equiv \frac{1}{2l}\int_{-l}^{l} \mathrm{d}y\, T(x,\, y,\, t)$, then the left hand side can

be written as $\rho c_p \int_{-l}^{l} \mathrm{d}y\, \partial_t \widetilde{T}(x,\, t)$. As for the heat source, we have:

$$\int_0^L \mathrm{d}x \int_{-l}^{l} \mathrm{d}y\, \boldsymbol{J}(x,\, y,\, t) \cdot \nabla V(x,\, y) = \int_0^L \mathrm{d}x \int_{-l}^{l} \mathrm{d}y\, J^x(x,\, y,\, t)[\partial_x V_0(x,\, y) - f] + J^y(x,\, y,\, t)\partial_y V_0(x,\, y). \tag{A.3}$$

Since the potential does not depend on y for $y \in [-l,\, l]$, we have $\int_{-l}^{l} \mathrm{d}y\, J^y(x,\, y,\, t)\partial_y V_0(x,\, y) = 0$. Putting everything together and defining $\widetilde{J}(x,\, t) = \frac{1}{2l}\int_{-l}^{l} \mathrm{d}y\, J^x(x,\, y,\, t)$, we find that the heat term takes on the following form:

$$\int_0^L \mathrm{d}x \int_{-l}^{l} \mathrm{d}y\, \boldsymbol{J}(x,\, y,\, t) \cdot \nabla V(x,\, y) = 2l[\partial_x V_0(x) - f] \int_0^L \mathrm{d}x\, \widetilde{J}(x,\, t). \tag{A.4}$$

Now we can work on the term representing the heat flowing out of the system.

$$D\rho c_p \oint_{\partial\Omega} \nabla T(\boldsymbol{r},\, t) \cdot \mathrm{d}\boldsymbol{r} = D\rho c_p \left\{ \int_0^L \mathrm{d}x\, \partial_y T(x,\, l,\, t) - \partial_y T(x,\, -l,\, t) + \int_{-l}^{l} \mathrm{d}y\, \partial_x T(L,\, y,\, t) - \partial_x T(0,\, y,\, t) \right\}. \tag{A.5}$$

In order to integrate the first term, we have to assume that the temperature takes on the form

$$T(x,\, y,\, t) = a(x,\, t)g(y,\, t) + b(x,\, t), \tag{A.6}$$

where $g(y,\, t)$ is symmetric in y and $g(0,\, t) = 0$. Upon applying the boundary conditions along the y direction, we find that:

$$T_0(x,\, t) = a(x,\, t)g(l,\, t) + b(x,\, t). \tag{A.7}$$

At the same time, we can get a more precise form for $\widetilde{T}(x,\, t)$, if we define $G(y,\, t)$ to be the antiderivative of $g(y,\, t)$, then:

$$2l\widetilde{T}(x,\, t) = a(x,\, t)2G(l,\, t) + b(x,\, t)2l. \tag{A.8}$$

Combining Eqs. (A.7) and (A.8), we get the following form for the temperature:

$$T(x,\, y,\, t) = \frac{\widetilde{T}(x,\, t) - T_0(x,\, t)}{\frac{G(l,\, t)}{l} - g(l,\, t)} g(y,\, t) + T_0(x,\, t) - \frac{\widetilde{T}(x,\, t) - T_0(x,\, t)}{\frac{G(l,\, t)}{l} - g(l,\, t)}. \tag{A.9}$$

Given this form, we are able to calculate $\partial_y T(x,\, y,\, t)$, which we can use to calculate the first term on the right hand side of Eq. (A.5).

$$D\rho c_p \int_0^L \mathrm{d}x\, \partial_y T(x,\, l,\, t) - \partial_y T(x,\, -l,\, t) = \frac{\widetilde{T}(x,\, t) - T_0(x,\, t)}{\frac{G(l,\, t)}{l} - g(l,\, t)} 2g'(l,\, t). \tag{A.10}$$

The second term of Eq. (A.8) can be found much more directly via the fundamental theorem of calculus:

$$D\rho c_p \int_{-l}^{l} \mathrm{d}y\, \partial_x T(L,\, y,\, t) - \partial_x T(0,\, y,\, t) = D\rho c_p \int_{-l}^{l} \mathrm{d}y \int_0^L \mathrm{d}x\, \partial_x^2 T(x,\, y,\, t),$$
$$= D\rho c_p \int_0^L \mathrm{d}x\, \partial_x^2 \widetilde{T}(x,\, t). \tag{A.11}$$

Now, we can put all of these equations together to find that:

$$\rho c_p \int_0^L \mathrm{d}x\, \partial_t \widetilde{T}(x,\, t) = -2l[\partial_x V_0(x) - f] \int_0^L \mathrm{d}x\, \widetilde{J}(x,\, t) + D\rho c_p \int_0^L \mathrm{d}x\, \partial_x^2 \widetilde{T}(x,\, t)$$
$$+ \frac{\widetilde{T}(x,\, t) - T_0(x,\, t)}{\frac{G(l,\, t)}{l} - g(l,\, t)} 2g'(l,\, t). \tag{A.12}$$

Using the fundamental lemma of the calculus of variations [71], we find that:

$$\rho c_p \partial_t \widetilde{T}(x,\, t) = -2l[\partial_x V_0(x) - f]\widetilde{J}(x,\, t) + D\rho c_p \partial_x^2 \widetilde{T}(x,\, t) + D\rho c_p \frac{\widetilde{T}(x,\, t) - T_0(x,\, t)}{\frac{G(l,\, t)}{l} - g(l,\, t)} 2g'(l,\, t). \tag{A.13}$$

Equation A.13 is an equation of motion for $\widetilde{T}(x,\, t)$ which is similar to Eq. 2.1, except that there is an extra term of the form $\widetilde{T}(x,\, t) - T_0(x,\, t)$ which accounts for the interaction between the system and the heat baths at $y = \pm l$.

Equation A.13 allows us to reduce the dimension of our system by one. It also shows us that in this reduced form, the system interacts with the heat bath by exchanging heat proportional to $\widetilde{T}(x,\, t) - T_0(x,\, t)$. This is very similar to the exchange of heat given by Fourier's law: $\boldsymbol{q} = -k\frac{\mathrm{d}T}{\mathrm{d}x}$. We note however, that for Eq. (A.13) to hold, we have to assume that the temperature can be written in the form $T(x,\, y,\, t) = a(x,\, t)g(y,\, t) + b(x,\, t)$. Furthermore, Eq. (A.13) is not particularly useful unless we have a corresponding reduced form for Eq. (1.4). In general, finding such an equation is very difficult, so instead we will choose to solve the full two dimensional system. However, here we will give the reduced form of Eq. (1.4) in the special case where the potential is an infinite square well in the y direction.

We begin by noting that since the potential is confining in the y direction, we know that $\boldsymbol{J}(x,\, y = \pm l,\, t) \cdot \hat{\boldsymbol{y}} = 0$. Given this, we write $P(x,\, y,\, t) = \mathcal{N} P_x(x,\, t)\psi(y,\, t)$, which allows us to write Eq. (1.4) as:

$$\gamma \partial_t \mathcal{N} P_x(x,\, t)\psi(y,\, t) = \nabla \cdot \{\mathcal{N} P_x(x,\, t)\psi(y,\, t)[\nabla V_0(x,\, y) - f\hat{\boldsymbol{x}}] + k_B T(x,\, y,\, t)\mathcal{N}\partial_x P_x(x,\, t)\psi(y,\, t)\}. \tag{A.14}$$

Now we define $\widetilde{P}(x,\, t) \equiv \frac{P_x(x,\, t)}{2l}\int_{-l}^{l} \mathrm{d}y\, \psi(y,\, t)$ and we integrate Eq. (A.14) over the region Ω in the same way as before to obtain:

$$\gamma 2l \partial_t \int_0^L \mathrm{d}x\, \widetilde{P}(x,\, t) = \int_0^L \mathrm{d}x\, \boldsymbol{J}(x,\, l,\, t) \cdot \hat{\boldsymbol{y}} - \boldsymbol{J}(x,\, -l,\, t) \cdot \hat{\boldsymbol{y}} + \int_{-l}^{l} \mathrm{d}y\, \boldsymbol{J}(L,\, y,\, t) \cdot \hat{\boldsymbol{x}} - \boldsymbol{J}(0,\, y,\, t) \cdot \hat{\boldsymbol{x}}. \tag{A.15}$$

The first term on the right hand side is zero, while the second term evaluates to:

$$\left[-\int_{-l}^{l} \mathrm{d}y\, P_x(x,\, t)\psi(y,\, t)[\partial_x V_0(x,\, y) - f] + k_B T(x,\, y,\, t)\partial_x P_x(x,\, t)\psi(y,\, t) \right]_{x=0}^{x=L}$$
$$= -\left[[\partial_x V_0(x,\, y) - f] 2l\widetilde{P}(x,\, t) + \partial_x P_x(x,\, t) \int_{-l}^{l} \mathrm{d}y\, k_B T(x,\, y,\, t)\psi(y,\, t) \right]_{x=0}^{L}. \tag{A.16}$$

The second term is very difficult to evaluate in general. The other thing to note about this product term is that in general the reduced form of Eq. (1.4) is very different from Eq. (1.4). However, if the potential is an infinite square well in the y direction, then the probability distribution will be constant in the y direction and we find that the reduced form of Eq. (1.4) is:

$$\partial_t \widetilde{P}(x,\, t) = 2l\partial_x \left[[\partial_x V_0(x) - f]\widetilde{P}(x,\, t) + k_B \widetilde{T}(x,\, t)\partial_x \widetilde{P}(x,\, t) \right]. \tag{A.17}$$

Equation (A.17) has the same form as Eq. (1.4). Therefore, as long as we can find the function $g(y,\, l)$, we will be able to reduce a two dimensional problem inside a square well down to a one dimensional problem that has Eq. (A.13) as the equation of motion for the temperature. Also, since the current and the potential are independent of y for $y \in [-l,\, l]$, the heat generated inside the domain will be independent of y. This justifies our assumption that the temperature can be written in the form of Eq. (A.6).

Bibliography

[1] R. P. Feynman, "There's plenty of room at the bottom," *Engineering and science*, vol. 23, no. 5, pp. 22–36, 1960.

[2] R. Phillips and S. R. Quake, "The biological frontier of physics," *Phys. Today*, vol. 59, no. 5, pp. 38–43, 2006.

[3] R. D. Astumian, "Design principles for Brownian molecular machines: how to swim in molasses and walk in a hurricane," *Phys. Chem. Chem. Phys.*, vol. 9, no. 37, pp. 5067–5083, 2007.

[4] S. Leibler and D. A. Huse, "Porters versus rowers: a unified stochastic model of motor proteins.," *J. Cell Biol.*, vol. 121, no. 6, pp. 1357–1368, 1993.

[5] S. Leibler and D. Huse, "A physical model for motor proteins.," *C. R. Acad. Sci.*, vol. 313, no. 1, pp. 27–35, 1991.

[6] M. von Delius, E. M. Geertsema, D. A. Leigh, and D.-T. D. Tang, "Design, synthesis, and operation of small molecules that walk along tracks," *J. Am. Chem. Soc.*, vol. 132, no. 45, pp. 16134–16145, 2010.

[7] I. A. Martínez, É. Roldán, L. Dinis, and R. A. Rica, "Colloidal heat engines: a review," *Soft matter*, vol. 13, no. 1, pp. 22–36, 2017.

[8] Z. Wang, "Bio-inspired track-walking molecular motors (Perspective)," *Biointerphases*, vol. 5, no. 3, pp. FA63–FA68, 2010.

[9] I. A. Martínez, É. Roldán, L. Dinis, D. Petrov, J. M. Parrondo, and R. A. Rica, "Brownian carnot engine," *Nat. Phys.*, vol. 12, no. 1, p. 67, 2016.

[10] P. A. Quinto-Su, "A microscopic steam engine implemented in an optical tweezer," *Nat. Commun.*, vol. 5, p. 5889, 2014.

[11] V. Blickle and C. Bechinger, "Realization of a micrometre-sized stochastic heat engine," *Nat. Phys.*, vol. 8, no. 2, p. 143, 2012.

[12] R. D. Astumian and P. Hanggi, "Brownian Motors," *Phys. Today*, vol. 55, p. 33, 2002.

[13] P. Reimann, "Brownian motors: noisy transport far from equilibrium," *Phys. Rep.*, vol. 361, no. 2, pp. 57–265, 2002.

[14] J. D. Bryngelson and P. G. Wolynes, "Intermediates and barrier crossing in a random energy model (with applications to protein folding)," *J. Phys. Chem.*, vol. 93, no. 19, pp. 6902–6915, 1989.

[15] D. Keller and C. Bustamante, "The mechanochemistry of molecular motors," *Biophys. J.*, vol. 78, no. 2, pp. 541–556, 2000.

[16] M. J. Tyska and D. M. Warshaw, "The myosin power stroke," *Cell Motil. Cytoskeleton*, vol. 51, no. 1, pp. 1–15, 2002.

[17] I. Santamaría-Holek, A. Gadomski, and J. Rubi, "Controlling protein crystal growth rate by means of temperature," *J. Phys. Condens. Matter*, vol. 23, no. 23, p. 235101, 2011.

[18] C. Van den Broeck, N. Kumar, and K. Lindenberg, "Efficiency of isothermal molecular machines at maximum power," *Physical review letters*, vol. 108, no. 21, p. 210602, 2012.

[19] N. Golubeva, A. Imparato, and L. Peliti, "Efficiency of molecular machines with continuous phase space," *EPL (Europhysics Letters)*, vol. 97, no. 6, p. 60005, 2012.

[20] X.-g. Ma, Y. Su, P.-Y. Lai, and P. Tong, "Colloidal dynamics over a tilted periodic potential: Forward and reverse transition probabilities and entropy production in a nonequilibrium steady state," *Phys. Rev. E*, vol. 96, p. 012601, Jul 2017.

[21] Max, von Delius, Geertsema, Edzard M., and Leigh, David A., "A synthetic small molecule that can walk down a track," *Nat. Chem.*, vol. 2, pp. 96–101, feb 2010.

[22] C. J. Myers, M. Celebrano, and M. Krishnan, "Information storage and retrieval in a single levitating colloidal particle," *Nat. Nanotechnol.*, vol. 10, no. 10, pp. 886–891, 2015.

[23] G. E. Uhlenbeck and L. S. Ornstein, "On the Theory of the Brownian Motion," *Phys. Rev.*, vol. 36, pp. 823–841, Sep 1930.

[24] H. Eyring, "The activated complex in chemical reactions," *J. Chem. Phys.*, vol. 3, no. 2, pp. 107–115, 1935.

[25] H. A. Kramers, "Brownian motion in a field of force and the diffusion model of chemical reactions," *Physica*, vol. 7, no. 4, pp. 284–304, 1940.

[26] R. Landauer, "Irreversibility and heat generation in the computing process," *IBM J. Res. Dev.*, vol. 5, no. 3, pp. 183–191, 1961.

[27] R. P. Feynman, R. B. Leighton, and M. Sands, *The Feynman lectures on physics, Vol. I: The new millennium edition: mainly mechanics, radiation, and heat*, vol. 1. Basic books, 2011.

[28] M. Büttiker, "Transport as a consequence of state-dependent diffusion," *Z. Phys. B*, vol. 68, no. 2, pp. 161–167, 1987.

[29] N. van Kampen, "Explicit calculation of a model for diffusion in nonconstant temperature," *J. Math. Phys.*, vol. 29, no. 5, pp. 1220–1224, 1988.

[30] J. M. R. Parrondo and P. Español, "Criticism of Feynman's analysis of the ratchet as an engine," *Am. J. Phys.*, vol. 64, no. 9, pp. 1125–1130, 1996.

[31] K. Sekimoto, "Kinetic characterization of heat bath and the energetics of thermal ratchet models," *J. Phys. Soc. Jpn.*, vol. 66, no. 5, pp. 1234–1237, 1997.

[32] K. Sekimoto, "Langevin equation and thermodynamics," *Prog. Theor. Phys. Suppl.*, vol. 130, pp. 17–27, 1998.

[33] T. Hondou and K. Sekimoto, "Unattainability of Carnot efficiency in the Brownian heat engine," *Phys. Rev. E*, vol. 62, no. 5, p. 6021, 2000.

[34] R. Benjamin and R. Kawai, "Inertial effects in Büttiker-Landauer motor and refrigerator at the overdamped limit," *Phys. Rev. E*, vol. 77, no. 5, p. 051132, 2008.

[35] K. J. Challis and M. W. Jack, "Energy transfer in a molecular motor in the Kramers regime," *Phys. Rev. E*, vol. 88, p. 042114, Oct 2013.

[36] U. Seifert, "Stochastic thermodynamics, fluctuation theorems and molecular machines," *Reports on Progress in Physics*, vol. 75, no. 12, p. 126001, 2012.

[37] D. Cubero and F. Renzoni, *Brownian Ratchets: From Statistical Physics to Bio and Nanomotors*. Cambridge University Press, 2016.

[38] R. Landauer, "Motion out of noisy states," *J. Stat. Phys.*, vol. 53, no. 1, pp. 233–248, 1988.

[39] C. Jarzynski and O. Mazonka, "Feynman's ratchet and pawl: An exactly solvable model," *Phys. Rev. E*, vol. 59, pp. 6448–6459, Jun 1999.

[40] N. Nakagawa and T. S. Komatsu, "A heat pump at a molecular scale controlled by a mechanical force," *Europhys. Lett.*, vol. 75, no. 1, p. 22, 2006.

[41] C. Van den Broeck and R. Kawai, "Brownian Refrigerator," *Phys. Rev. Lett.*, vol. 96, p. 210601, Jun 2006.

[42] M. Hoshina and K. Okuda, "Theoretical and numerical analysis of a heat pump model utilizing Dufour effect," *Eur. Phys. J. B*, vol. 90, no. 4, p. 78, 2017.

[43] M. Das, D. Das, D. Barik, and D. S. Ray, "Landauer's blowtorch effect as a thermodynamic cross process: Brownian cooling," *Phys. Rev. E*, vol. 92, p. 052102, Nov 2015.

[44] M. W. Jack and C. Tumlin, "Intrinsic irreversibility limits the efficiency of multidimensional molecular motors," *Phys. Rev. E*, vol. 93, no. 5, p. 052109, 2016.

[45] X. P. B. P. Ma, "Colloidal transport and diffusion over a tilted periodic potential: dynamics of individual particles," *Soft Matter*, vol. 11, no. 6, pp. 1182–1196, 2015.

[46] H. Wang, "Several issues in modeling molecular motors," *Journal of Computational and Theoretical Nanoscience*, vol. 5, no. 12, pp. 2311–2345, 2008.

[47] F. Jülicher, A. Ajdari, and J. Prost, "Modeling molecular motors," *Reviews of Modern Physics*, vol. 69, no. 4, p. 1269, 1997.

[48] H. C. Berg, "The Rotary Motor of Bacterial Flagella," *Annual Review of Biochemistry*, vol. 72, no. 1, pp. 19–54, 2003. PMID: 12500982.

[49] M. O. Magnasco, "Molecular combustion motors," *Phys. Rev. Lett.*, vol. 72, no. 16, p. 2656, 1994.

[50] C. Bustamante, J. Liphardt, and F. Ritort, "The nonequilibrium thermodynamics of small systems," *Phys. Today*, vol. 58, no. 7, pp. 43–48, 2005.

[51] V. Blickle, T. Speck, L. Helden, U. Seifert, and C. Bechinger, "Thermodynamics of a Colloidal Particle in a Time-Dependent Nonharmonic Potential," *Phys. Rev. Lett.*, vol. 96, p. 070603, Feb 2006.

[52] R. W. H. S. A. H. M. W. D. G. A. M. J. M. B. J. W. S. G. T. M. Joel S. Bader and J. M. Rothberg, "DNA transport by a micromachined Brownian ratchet device," *PNAS*, 1999.

[53] A. Einstein, "On the movement of small particles suspended in stationary liquids required by the molecular-kinetic theory of heat," *Ann. Phys*, vol. 17, pp. 549–560, 1905.

[54] C. Gardiner, *Stochastic methods*, vol. 4. springer Berlin, 2009.

[55] C. Van den Broeck and M. Esposito, "Three faces of the second law. II. Fokker-Planck formulation," *Phys. Rev. E*, vol. 82, p. 011144, Jul 2010.

[56] R. Streater, "Dynamics of Brownian particles in a potential," *J. Math. Phys.*, vol. 38, no. 9, pp. 4570–4575, 1997.

[57] R. Streater, "A gas of Brownian particles in statistical dynamics," *J. Stat. Phys.*, vol. 88, no. 1-2, pp. 447–469, 1997.

[58] R. Streater, "Nonlinear heat equations," *Rep. Math. Phys.*, vol. 40, no. 3, pp. 557–564, 1997.

[59] R. F. Streater, "The Soret and Dufour effects in statistical dynamics," *Proc. R. Soc. London, Ser. A*, vol. 456, no. 1993, pp. 205–221, 2000.

[60] J. Devine and M. W. Jack, "Self-induced temperature gradients in Brownian dynamics," *Phys. Rev. E*, vol. 96, p. 062130, Dec 2017.

[61] J. H. Ferziger and M. Peric, *Computational methods for fluid dynamics*. Springer Science & Business Media, 2012.

[62] W. E. Schiesser, *The numerical method of lines: integration of partial differential equations*. Elsevier, 2012.

[63] J. Bezanson, A. Edelman, S. Karpinski, and V. B. Shah, "Julia: A Fresh Approach to Numerical Computing," *SIAM Rev.*, vol. 59, no. 1, pp. 65–98, 2017.

[64] C. Rackauckas and Q. Nie, "DifferentialEquations. jl–A Performant and Feature-Rich Ecosystem for Solving Differential Equations in Julia," *J. Open Res. Softw.*, vol. 5, no. 1, p. 15, 2017.

[65] I. Dunning, J. Huchette, and M. Lubin, "JuMP: A Modeling Language for Mathematical Optimization," *SIAM Rev.*, vol. 59, no. 2, pp. 295–320, 2017.

[66] A. Wächter and L. T. Biegler, "On the implementation of an interior-point filter line-search algorithm for large-scale nonlinear programming," *Mathematical Programming*, vol. 106, pp. 25–57, Mar 2006.

[67] R. J. LeVeque, *Finite volume methods for hyperbolic problems*, vol. 31. Cambridge university press, 2002.

[68] J. P. Boyd, *Chebyshev and Fourier spectral methods*. Courier Corporation, 2001.

[69] L. N. Trefethen, *Spectral methods in MATLAB*, vol. 10. Siam, 2000.

[70] H. Lodish, A. Berk, S. L. Zipursky, P. Matsudaira, D. Baltimore, and J. Darnell, "Molecular cell biology 4th edition," *National Center for Biotechnology Information, Bookshelf*, 2000.

[71] J. Jost and X. Li-Jost, *Calculus of variations*, vol. 64. Cambridge University Press, 1998.